Progress in Materials Science 74 (2015) 332–400

Contents lists available at ScienceDirect

Progress in Materials Science

journal homepage: www.elsevier.com/locate/pmatsci

Bioinspired engineering of honeycomb structure – Using nature to inspire human innovation

Qiancheng Zhang [a,b,c], Xiaohu Yang [a,b,d], Peng Li [a,b,d], Guoyou Huang [c,e], Shangsheng Feng [a,b], Cheng Shen [a,b], Bin Han [a,b], Xiaohui Zhang [b,c], Feng Jin [a,b], Feng Xu [c,e,*], Tian Jian Lu [a,b,c,*]

[a] State Key Laboratory for Strength and Vibration of Mechanical Structures, Xi'an Jiaotong University, Xi'an 710049, PR China
[b] MOE Key Laboratory for Multifunctional Materials and Structures, Xi'an Jiaotong University, Xi'an 710049, PR China
[c] Bioinspired Engineering and Biomechanics Center (BEBC), Xi'an Jiaotong University, Xi'an 710049, PR China
[d] School of Human Settlements and Civil Engineering, Xi'an Jiaotong University, Xi'an 710049, PR China
[e] MOE Key Laboratory of Biomedical Information Engineering, Xi'an Jiaotong University, Xi'an 710049, PR China

ARTICLE INFO

Article history:
Received 29 October 2014
Received in revised form 12 March 2015
Accepted 5 May 2015
Available online 7 July 2015

Keywords:
Honeycomb structure
Bioinspired materials
Sandwich panel
Material processing
Mechanical behavior
Heat transfer
Acoustics
Optimization design

ABSTRACT

Honeycomb structures, inspired from bee honeycombs, had found widespread applications in various fields, including architecture, transportation, mechanical engineering, chemical engineering, nanofabrication and, recently, biomedicine. A major challenge in this field is to understand the unique properties of honeycomb structures, which depended on their structures, scales and the materials used. In this article, we presented a state-of-the-art review of the interdisciplinary efforts to better understand the design principles for products with honeycomb structures, including their fabrication, performance (e.g., mechanical, thermal and acoustic properties) as well as optimization design. We described how these structural perspectives have led to new insights into the design of honeycomb structures ranging from macro-, micro- to nano-scales. We presented current scientific advances in micro- and nano-technologies that hold great promise for bioinspired honeycomb structures. We also discussed the emerging applications of honeycomb structures in biomedicine such as tissue engineering and regenerative medicine. Understanding the design principles underlying the creation of honeycomb structures

* Corresponding authors at: Bioinspired Engineering and Biomechanics Center (BEBC), Xi'an Jiaotong University, Xi'an 710049, PR China.
E-mail addresses: fengxu@mail.xjtu.edu.cn (F. Xu), tjlu@mail.xjtu.edu.cn (T.J. Lu).

http://dx.doi.org/10.1016/j.pmatsci.2015.05.001

as well as the related scientific discovery and technology development is critical for engineering bioinspired materials and devices designed based on honeycomb structures for a wide range of practical applications.

Contents

1. Introduction

Nature is a great and successful laboratory with a database full of effective solutions to many scientific and technical problems [1–3]. The ideas from nature have inspired mankind with a series of novel designs on high-performance materials and systems that function from macroscale to

nanoscale [4–7]. For instance, one can find a variety of porous structures in nature, which play crucial roles in multifunction realization and system operation in organisms. The majority of artificial designs on porous materials has been inspired by nature or can find their prototypes in nature [8,9], with honeycomb being the most representative example. The honeycomb cellular structure, originating from the natural honeycomb in a nest, consists of uniformly-distributed double-layered hexagonal cells. The materials for constructing cell walls are beeswax and propolis (a kind of plant resin). Studies on the characteristics of honeycomb structures have been going on for literally thousands of years [10–15]. However, honeycomb structures were not incorporated into large-scale applications in human society until about 70 years ago, after which numerous honeycomb structures made from various materials emerged, from papers [16,17], to metals [18], then to ceramics [19] and composites [20]. The technologies used to fabricate honeycomb structures have also been progressively advanced [21–24].

In view of technological invention, the evolution of honeycomb technology may be divided into four stages, i.e., interesting and enlightening stage (60 BC-126), exploratory stage (1638–1901), structure-based application stage (1914–1990), and multi-functional, multi-field and multi-scale rapid development stage (1990–now). During the first stage, people wondered about the hexagonal comb of honeybee for centuries. After experiencing silence for more than 1000 years, the second industrial revolution drove the exploration of porous structures in nature due to increasing demand for lightweight structures, and the invention of microscopes offered a proper tool to explore these magical structures. For example, in 1665, Robert Hook discovered that the natural cellular structure of a cork is similar to that of a hexagonal honeycomb. Hundreds of years of accumulation in understanding the honeycomb structure led to the development of honeycomb technology from a qualitative change in the second stage to a quantitative change in the third stage. In 1914, Höfler and Renyi patented the first structural application of honeycomb structures, initiating the structure-based application stage. Almost 70 years since then, numerous honeycomb related materials emerged in architecture, aviation, space, transportation and many other engineering fields, from papers, to metals, then to composites. The more detailed description of the fatal developments in the history of man-made honeycombs could be found from the open literature, e.g., Bitzer [25,26] and Xiong et al. [25,26].

Since the 1980s, applications of honeycomb structures in engineering fields (Fig. 1A) had expanded significantly into the architecture field, such as the Hex Tower designed by Michel Rojkind in 2005 (Fig. 2A). Besides, new types of honeycomb made from different materials had been designed and manufactured to facilitate specific applications. In particular, over the past two decades, we have witnessed the further expanding of honeycomb structures from engineering fields to nano and biomedical fields (Fig. 1B), such as nanohole arrays in anodized alumina [27], microporous arrays in polymerthin films [28], activated carbon honeycombs [29], and photonic band gap honeycomb structures [30]. Especially in 1999, the conjecture was finally proven by Hales [31] that the way bees build hives is to provide maximum cell space by using a minimal amount of beeswax, indicating that hexagonal honeycomb structure is the most stable for nature. Recently, Karihaloo and his colleagues [32] revealed the mechanism for the transformation of circular honeycomb cells in a natural honeybee comb quickly into rounded hexagonal structures, i.e., the formation of molten viscoelastic wax heated by 'hot' worker bees to flow near the triple junction between neighboring circular cells. This finding witnessed a vigorous continuation of the long-standing debates about whether the honeycomb is an example of blind physics or an exquisite biological engineering.

With the development of electron microscopy technology, new honeycomb structures at micro- and nano-scales in nature have been increasingly discovered. For instance, numerous examples of hexagonal or similar patterns have been found in living tissue [14,33,34], cell aggregates [35] and molecules [36]. In the past several decades, with advances in manufacture technologies, honeycomb structures have been adapted into different applications, ranging from engineering [37–42] to more recently biomedicine [43–45], accumulating a rich store of artificial honeycomb structures at scales varying from macrometer to nanometer. In Fig. 2, we summarized representative applications of the most typical artificial honeycomb structures, which can be divided into three categories depending on scale, i.e., the traditional engineering field, the micro and nanofabrication field, and the biomedicine field [36,44–54]. It can be seen that new applications of honeycomb structures have been

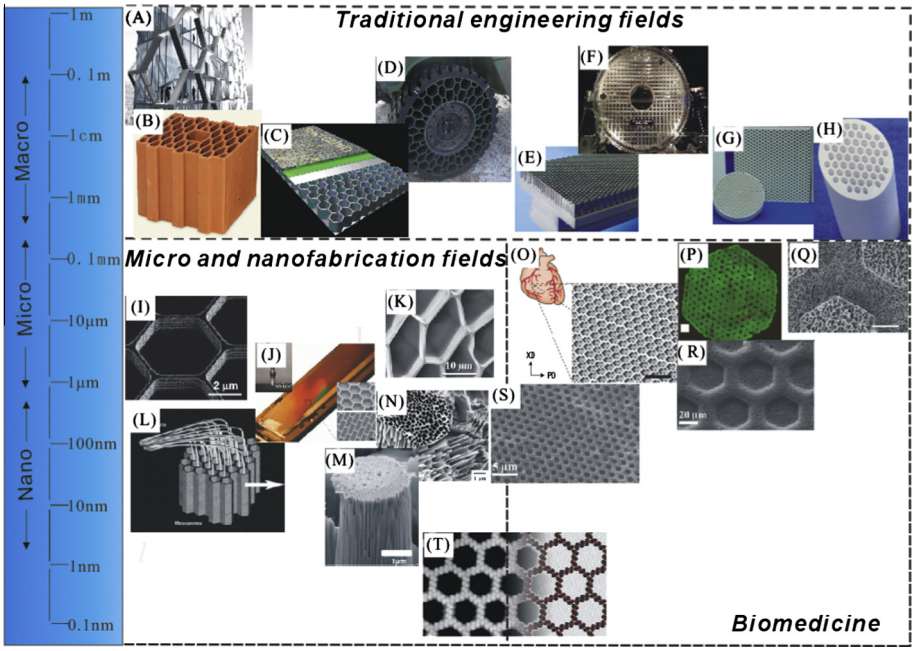

Fig. 1. The most representative honeycomb structures from macro- to nano-scale. (A) Hex tower designed by Michel Rojkind (*Source*: www.minusfive.com); (B) vertically perforated lightweight heat insulation brick (*Source*: www.kudret.com); (C) honeycomb-cored sandwich panel (*Source*: http://www.microthinstone.com); (D) honeycomb-cored airless tire for troop-carrying humvees that prevents thermal damage caused by locally hot spots on the road (*Source*: http://www.resilient-tech.com); (E) turbine honeycomb seal (*Source*: http://jingmengchina.en.made-in-china.com); (F) honeycomb mirror for Hubble space telescope (*Source*: http://en.wikipedia.org/); (G) extruded and sintered ceramic honeycomb (*Source*: http://www.ikts.fraunhofer.de); (H) multi-channel ceramic membrane (*Photo Source*: Membrane Science & Technology Research Center); (I) SEM top view of as-prepared and fully lithiated silicon honeycombs [46]; (J) honeycomb microstructured fluorinated Si surface [47]; (K) channel structure of typical silica microhoneycomb [48]; (L) conceptual scheme where the polyethylene's crystalline fibers grow by means of the mechanisms of mesoporous silica-assisted extrusion polymerization [49]; (M) SEM image: compact structure is sliding above the underneath column with a deformed pillar (2 mm in size) of anodic aluminum oxide nano-honeycomb [50]; (N) SEM image of TiO_2 surface after photoelectrochemical etching under strong (+1.0 V) anodic polarization [51]; (O) schematic illustration of the accordion honeycomb with hexagonal cells consisting of two overlapping squares with a size of 200 × 200 μm [44]; (P) viable honeycomb building unit [45]; (Q) SEM image of cellular morphology on the surface of ice-template-induced scaffold [52]; (R) honeycomb formed in the mesh of a hexagonal grid [53]; (S) SEM image of poly(dimethylsiloxane) star polymer film having honeycomb morphology [53] and (T) honeycomb network of anthraquinone molecules with open pores (diameter 50 angstroms) [36].

constantly launched in the traditional engineering field (e.g., Hex tower designed by Michel Rojkind and airless honeycomb tire), in innovative micro-and nano-scale fabrications (e.g., lithiated silicon honeycombs [46]), as well as in biomedical applications (e.g., scaffold designed with accordion-like honeycomb [44]).

In this article, we reviewed the honeycomb structures, with emphasis on their plentiful morphologies and multifunctional applications, from a multi-scale standpoint. First, we reviewed recent developments in the design concept of topological structure, including the evolution of honeycomb structures, and their structure–property relationships in scales from macrometer to micrometer and nanometer. Then, we summarized the emerging applications of honeycombs as multifunctional nano- and bio-structures and introduced the relevant fabrication methods. Particular focus was paid on the load bearing applications with multi-functionalities, including lightweight, heat dissipation, noise control, catalysis, filtering separation, scaffold, biointerface, and molecular separation. Last, we provided some insights into their challenges and future perspectives.

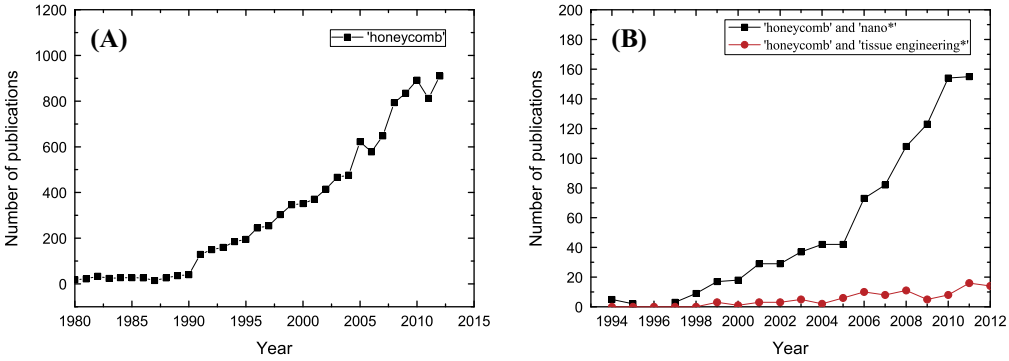

Fig. 2. Number of annual publications on (A) 'honeycomb', (B) 'honeycomb', nano* and tissue engineering*. *Source*: Science Citation Index Expanded [Sci-EXPANDED].

2. The topology and evolution of honeycomb structures

2.1. The topology of honeycomb

Honeycomb structures of interest here are composed of plates or sheets that form the edges of unit cells, with their diameters ranging from tens of micrometers to tens of millimeters. Most honeycombs are closed cell structures. These unit cells are repeated in two dimensions to create a cellular solid. Based on this kind of distribution, the more common honeycomb structures can be arranged to create triangular, square, hexagonal or circular shapes (Table 1). Each of the first three topologies is efficient at supporting structural loads, especially the shear loads encountered in panel bending [38]. These three classes of periodic cellular metals can now be fabricated from a wide variety of structural alloys. Generally speaking, the relative density, which is the ratio between the density of the cellular structure and that of the solid, is an important factor to describe the properties of honeycomb. By identifying a unit cell and deriving the volume fraction occupied by metal, it is very easy to obtain the relative density.

Recent advances in micro-/nano-fabrication and biomedicine have led to the emergence of circular honeycomb topologies (Table 1). Meanwhile, recent advances in topology design and fabrication have led to the emergence of lattice truss structures with open-celled honeycomb topologies, such as diamond textile, diamond collinear lattice, and square collinear lattice. Those structures can be fabricated by a fused deposition modeling process or a wire lay up process followed by transient liquid phase bonding. The fabrication approaches can be found in some review articles [38,55].

2.2. The evolution of honeycomb structures

Honeycomb with hexagonal cells has the most common structure amongst cellular materials, and has been successfully fabricated by using a variety of technologies and materials. In reality, however, to meet the specific needs for different applications, hexagonal honeycomb structures had evolved into many new ones in the man-made world, leading to rapidly increasing diversity from traditional engineering to micro- and nano-fabrication then to biomedicine. Here, we summarized the evolution of honeycomb structures (Fig. 3) to achieve such specific requirements as strengthened performance, simplified process, reduced cost, or enhanced multi-functionality.

In the traditional engineering fields, depending on specific applications, the shape of honeycomb cells had evolved from hexagonal to square [38], triangular [56], columnar [57] or other related shapes [58] (Fig. 3A). For example, honeycombs with rectangular or hexagonal cells are satisfactory configurations for forced convective heat transfer, while triangular honeycomb posses better mechanical performance (in-plane stiffness/strength) over various mechanical loading conditions [59]. Based

upon the two distinct analytical methods, i.e., homogenization theory and discrete network approach, Torquato et al. [60] investigated the effective linear elastic properties of honeycombs with various cell shapes including square, hexagonal and triangular cells. Cross-property bounds relating to bulk modulus and other elastic moduli to thermal conductivity were obtained. To regulate or reinforce superior performance in one aspect, stretching or compressing or shearing of hexagonal microporous arrays

Table 1
Unit cells and relative densities of honeycomb topology structures.

Unit cell shape	Relative density
Hexagonal honeycomb 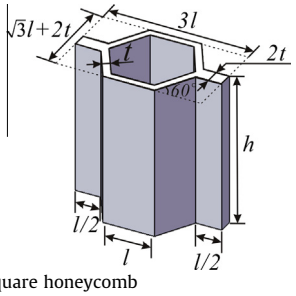	$\rho/\rho_s = \frac{8t}{3(\sqrt{3}l+2t)}$
Square honeycomb 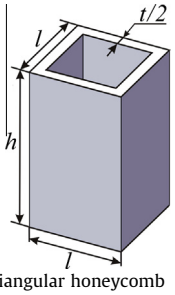	$\rho/\rho_s = \frac{(2l-t)t}{l^2}$
Triangular honeycomb 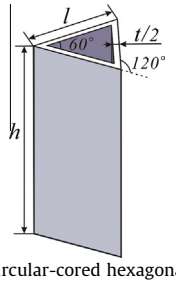	$\rho/\rho_s = \frac{(2\sqrt{3}l-t)t}{l^2}$
Circular-cored hexagonal honeycomb 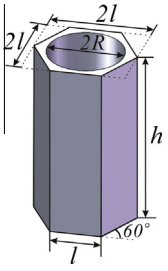	$\rho/\rho_s = 1 - \frac{2\sqrt{3}}{9}\frac{\pi R^2}{l^2}$

(*continued on next page*)

Table 1 (*continued*)

Unit cell shape	Relative density
Circular-cored square honeycomb 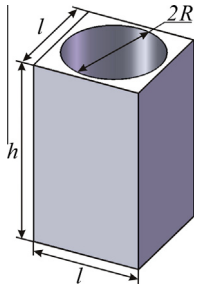	$\rho/\rho_s = 1 - \frac{\pi R^2}{l^2}$

along the K and M axes by a certain factor led to highly over-expanded (OX) [61], rectangular [62], reentrant hexangular [63] and asymmetrical hexangular cells [64,65] (Fig. 3B). The OX cell is obtained based on the standard hexagonal cell via extending along the K direction, resulting in a rectangular cell configuration in the M direction. Relative to hexagonal honeycombs, the OX configuration increases the shear properties in the W direction but decreases the ones in M direction. In addition, combining the above structures generates new structures such as the square supercell constructed by combining squares and triangles [66] and the Kagome cell [67] (Fig. 3C). To provide exceptional formability and low cost, honeycomb structures have been developed from basic cell shapes such as hexagon, square and triangle, to variations such as flex-core [68], double-flex [69] and reinforced hexagonal cells (Fig. 3D). The flex-core cell enables an exceptional formability in compound curvatures due to the anticlastic curvature is reduced and free of buckling the cell walls. Once curvatures were formed very tight radii, the shear strengths for flex-core cell are higher than that for hexagonal cores with equivalent density. Since the flex-core with a unique large cell exhibits desirable formability and relatively higher specific compression properties, the double-flex cell is found to be the most formable configuration.

To enhance multi-functionality, truncated-square [58], reentrant hexangular core [63] and chiral honeycombs [70] were exploited, Fig. 3E. Compared with the macro honeycombs in traditional engineering, a large number of honeycomb structures besides the ones listed in Fig. 3 exist in micro- or nano-fabrication and biomedical fields, partly due to their high sensitivity to manufacturing and handling conditions. Baggetto et al. [46] reported that a regular hexagonal honeycomb structure adopted a striking change, with a wall thickness, height and wall-to-wall spacing respectively of 250 nm, 1.1 μm and 4.8 μm, becoming highly curved as a function of Li contents when at full lithiation (Fig. 4). In nanoscale liquid crystals, the columnar liquid crystals often exhibit a two-dimensional (2D) periodic hexagonal honeycomb configuration designed by self-organizing T-shaped molecules. Sometimes distorted variants also exist, such as rectangular or oblique [71]. Chen et al. [72] reported two topological classes: a periodically-distributed cylinders with identical size and cross-section shape of pentagon and an configuration of cylinders with a ratio in numbers of 2:1 for square and triangular cross-sectional shape. Fig. 5 demonstrates a variety of 2D honeycomb-like structures, most of which are constructed by T-shaped molecules, facial amphiphiles and rod-like molecules.

As microporous films formed from poly(e-caprolactone) or polyacrylamide could be mechanically deformed, it is possible to form various geometric patterns upon mechanical deformation. Nishikawa et al. [73] reported that such geometric patterns as elongated hexagons, rectangles, squares, and triangles could be obtained upon compression or stretching of hexagonal micro polymer films, Fig. 6. The patterning of micromeshes may be applied to fabricate micropatterned soft-materials for cell culture. Wan et al. [74] fabricated microporous honeycomb-patterned films from commercially available polystyrene. Upon increasing the additive content in chloroform solvent, the shape of the pores gradually changed from near-spherical to ellipsoidal (Fig. 7), with interfacial tension of the

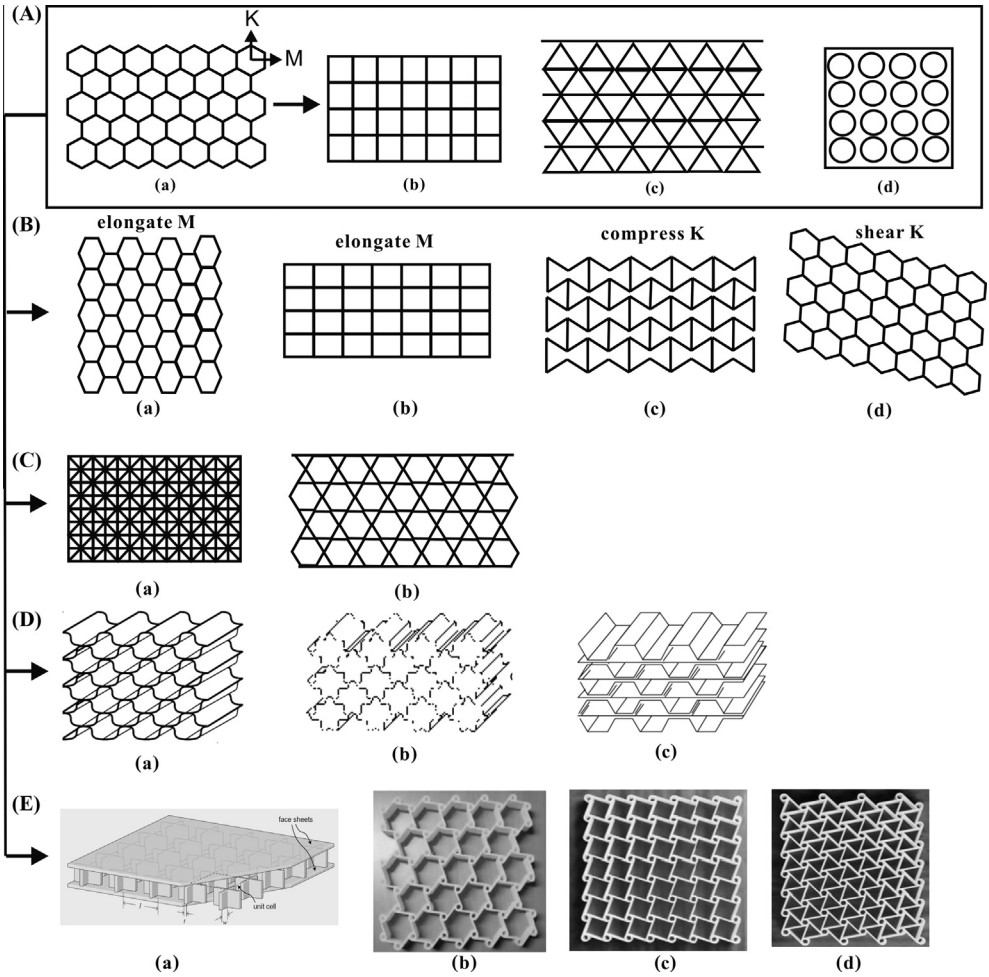

Fig. 3. Periodic honeycombs with various cell shapes. (A-a) Regular hexagonal cell; (A-b) square cell; (A-c) triangular cell; (A-d) columnar cell; (B-a) OX cell [61]; (B-b) rectangular cell [62]; (B-c) reentrant hexangular cell [63]; (B-d) asymmetrical honeycomb [64,65]; (C-a) square supercell constructed from mix of squares and triangles [66]; (C-b) Kagome cell [67]; (D-a) flex-core cell [68]; (D-b) double-flex cell [69]; (D-c) reinforced hexagonal cell (*Source*: http://www.hexcel.com); (E-a) truncated-square cell [58]; (E-b) trichiral cell [70]; (E-c) tetrachiral cell [70] and (E-d) hexachiral cell [70]. K and M denote two arbitrary vector axes in space.

studied system identified as a main factor for pore shape modulation. Four periodic patterns were found in 2D soft materials where uniform circular holes are distributed [75]. As shown in Fig. 8, mechanical instability is observed between expanded and compact periodic configurations.

3. Design principle: structure–property relationships

Through thousands of years of exploration, we have gone beyond the traditional awareness of the exceptionally high mechanical strength as the only characteristic of honeycomb structures, and have gradually deepened our understanding of multifunctional design principle for honeycomb structures. The focus of this section, therefore, is on the relationships between topological structure and the mechanical, thermal and acoustic properties for a variety of honeycomb structures. Other physical, chemical and biological properties of honeycomb structures are closely related to their preparation process and specific applications, and thus are discussed in Section 4.

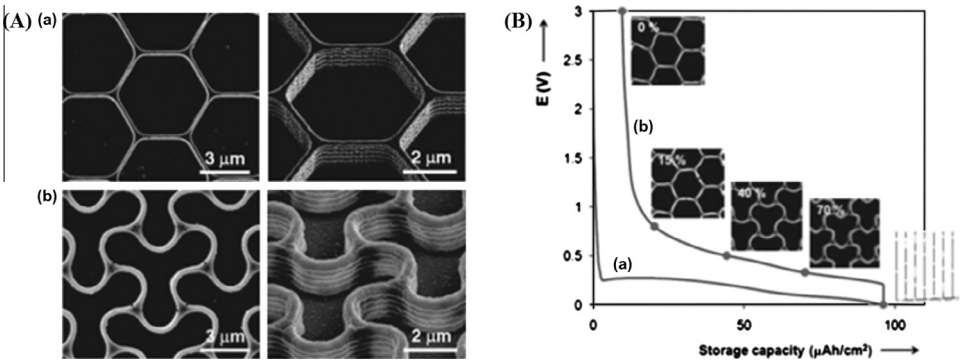

Fig. 4. (A) SEM images in top and tilted view of (a) as-prepared honeycombs before lithiation (as the dashed line depicted) and (b) fully lithiated silicon honeycombs. (B) Morphological changes of the Si honeycomb structure as a function of Li content. The figure depicts the potential profile for Si honeycombs upon lithiation (a) and delithiation (b) measured at 75 μA cm^{-2} during the first cycle [46].

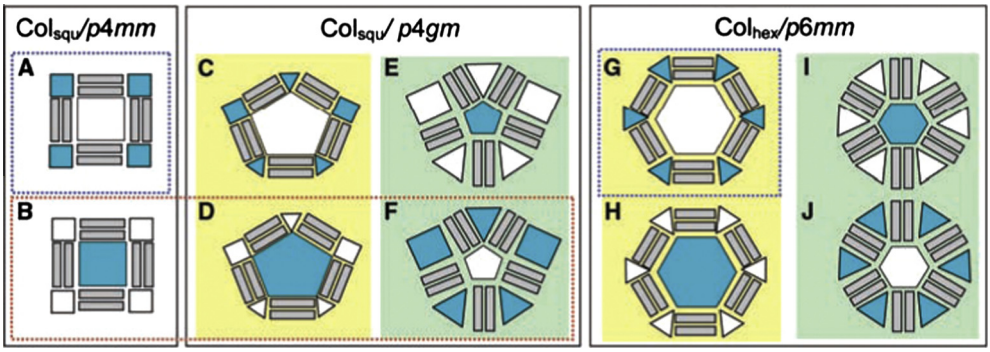

Fig. 5. (A–J) Topological isomers of plane tiling in various honeycomb-like networks forming two groups: lower row is the facial amphiphiles and upper row is the rod-like molecules with two polar end groups and lateral nonpolar chains (bolaamphiphiles) [72].

3.1. Honeycomb conjecture

The mathematical structure of honeycombs has intrigued mankind for thousands of years. The honeycomb conjecture was proposed by Pappus of Alexandria (c. 290–c. 350) with his fifth axiom, which states: "*any partition of the plane into regions of equal area has perimeter at least that of the regular hexagonal grid*". This isoperimetric property of hexagonal honeycombs continues to intrigue mathematicians today. The conjecture was finally proven by Thomas Hales [31,76]. His article "Cannonballs and Honeycombs" [77] described a modern version of the ancient observation in 2D. In three dimensions (3D), not the bee's honeycomb but the Voronoi cells of the body centered cubic is possibly the most efficient design, as shown by FejesTóth and others [78–80].

3.2. Mechanics of honeycomb structures

3.2.1. Mechanics of 2D and 3D macro honeycombs

The in-plane mechanical behaviors of regular hexagonal honeycomb and its derived structures have been intensively investigated as reflected by the large number of research papers on this topic. The main influencing factors such as material [81], structure type [82,83], porosity and relative density

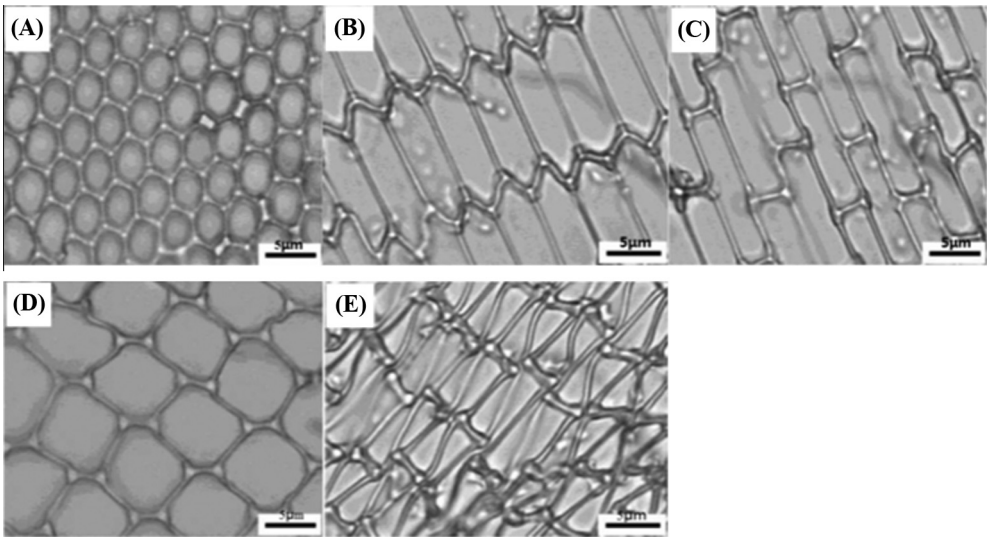

Fig. 6. Topological configurations observed in a stretched microporous film of PCL: (A) hexagonal configuration before stretching; (B) elongated hexagons; (C) rectangular pattern; (D) square-like pattern and (E) triangle-like pattern [73].

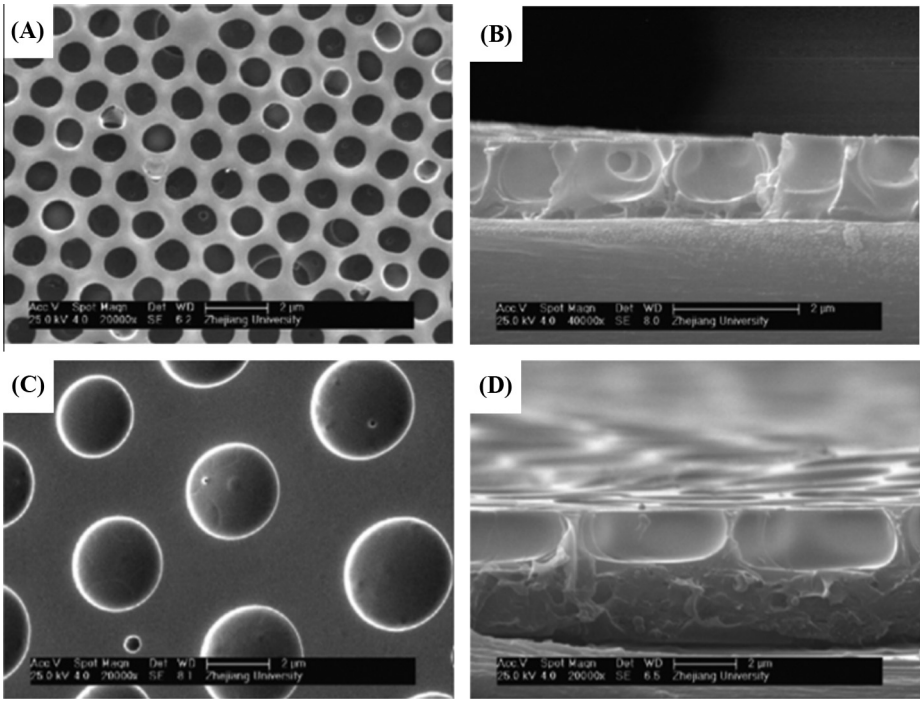

Fig. 7. SEM images of polystyrene/poly(N,N-dimethylaminoethyl methacrylate) films using chloroform (A and B) or tetrahydrofuran (C and D) as solvent: (A and C) top view and (B and D) cross-sectional view [74].

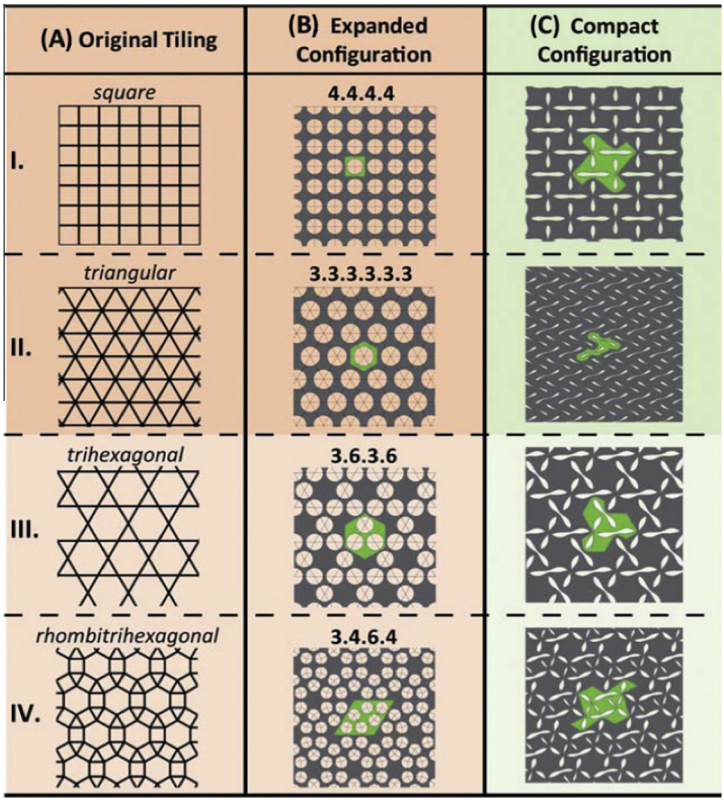

Fig. 8. Three groups (rows) of the arrangement patterns of circular holes for honeycombs, where each row is restricted to four given configurations: (A) tilings; (B) expanded undeformed porous structures (green-shaded regions) and (C) compact (buckled, denoted in green-shaded) porous structures caused by uniaxial compression [75].

[84–86] have been studied. For instance, Zhu and Mills [81] theoretically analyzed in-plane uniaxial compression of regular honeycombs made from a broad range of materials (from polymer to metal), which was found to significantly depend on material type. A deterministic approach was adopted by Fleck and Qiu [82] to predict the fracture response of elastic-brittle 2D lattices, and found that hexagonal honeycombs deform by bar bending while triangular honeycombs deform predominantly by the stretching of the constituent bars due to high nodal connectivity. It has been established that honeycombs having triangular, Kagome, and diamond cells are extension-dominated, beneficial for the design for high modulus; while the design for flexible structures require honeycombs to have the cell shapes of square and hexagonal due to they are bending-dominated [82,83].

Most existing analytical studies assume the mechanics of honeycomb structures to be a 2D problem. Earlier models on metallic hexagonal honeycombs [86] are only suitable for aluminum honeycombs with relative densities less than 0.05, where the dominated failure mode is the elastic buckling. As the relative density exceeds 0.1, yielding and plastic buckling of cell walls become the dominant modes of failure under in-plane compression [84,85]. For honeycomb core sandwich panels, as the core deformation is dictated considerably by thin face sheets, the role of core height and face sheet (skin) and the mechanics of sandwich panel as a 3D problem cannot be ignored [87,88]. Further, with widespread engineering applications (e.g., energy absorption), the stress state involved in practical design often becomes complex, therefore the biaxial in-plane compression and crushing of honeycombs [89,90] have received increasing attention.

To meet the needs of sandwich construction and maximizing its energy absorption capacity in the out-of-plane direction, extensive studies have been performed to investigate the out-of-plane mechanical behavior of honeycomb structures [91]. Again, material, structure type and porosity (relative density) are identified as the main influencing factors [85,92]. Under out-of-plane compression, the most common honeycombs are aluminum foil honeycombs (relative density $\bar{\rho} \leqslant 5\%$) [93] and heavy duty metal honeycombs (relative density $\bar{\rho} > 5\%$) such as those processed via extrusion [23] and square honeycombs made of stainless steel [94,95]. For the former, the honeycomb cells buckle elastically, producing the first deformation at the pressure head end (without face sheet, Fig. 9A) [96] or mid-height (with face sheet, Fig. 9B) [97], and crush by progressive formation of folds. Yang and Qiao [98] proposed a model to predict the corresponding crushing wavelength and core crushing strength. For the latter, the cells exhibit the axial–torsional buckling mode (Fig. 9C), i.e., the vertical nodal axis remains straight, while cell wall segments rotate around this axis [99]. Kim and Christensen [92] compared the mechanical performance of three core types (triangular, hexagonal, and star cell) and found that the triangular core has the same stiffness as the other two cores, but lower compressive and shear buckling strengths. Nevertheless, the highest flexibility is found in the star cell core, beneficial for the engineering design for curved sandwich constructions.

Great attention had also been paid to the mechanical properties of honeycombs when subjected to different types of external loading, including in-plane tension [100], in-plane biaxial compression, out-of-plane transverse shear [101,102], peel [103], uniaxial tension [104], three- and four-point bending [105], combined in-plane compression and shear [106], combined out-of-plane compression and shear [93], creep [107], fatigue [108], dynamic shear and, recently, low- and high-velocity impact [109,110]. Generally, deformation of honeycombs under these loadings can be interpreted by combining three different modes: flexing, stretching and hinging [111]. For the flexure mode, the cell walls act like flexures and are modeled as cantilever beams whose ends are fixed and guided respectively (Fig. 10A). For the stretching mode, cell walls are assumed to be like shock absorbers that only stretch along their length without variation in angle or rotation (Fig. 10B) [111]. With hinging mode, the cell wall does not elongate or bend; the deformation in cells is merely caused by the variation in angle between cell walls. This in mechanism indicates that either global shear or local bending contributes to the hinging mode (Fig. 10C) [111].

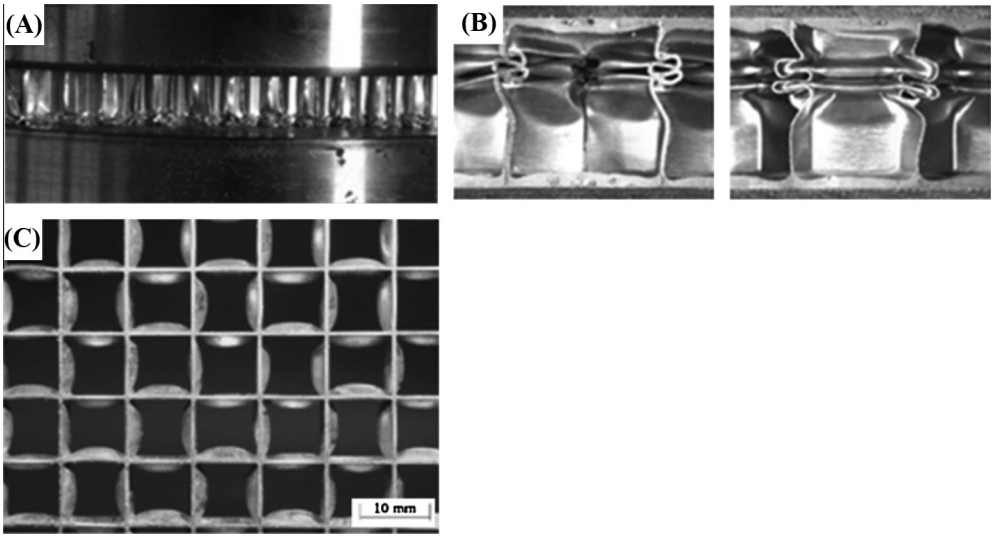

Fig. 9. Out-of-plane compression of metal honeycombs: (A) beginning of deformation in hexagonal honeycomb panel from lower support [96]; (B) honeycomb cells at a certain stage of crushing [97]; (C) axial torsional buckling mode of stainless steel square-honeycomb (viewed from top) [99].

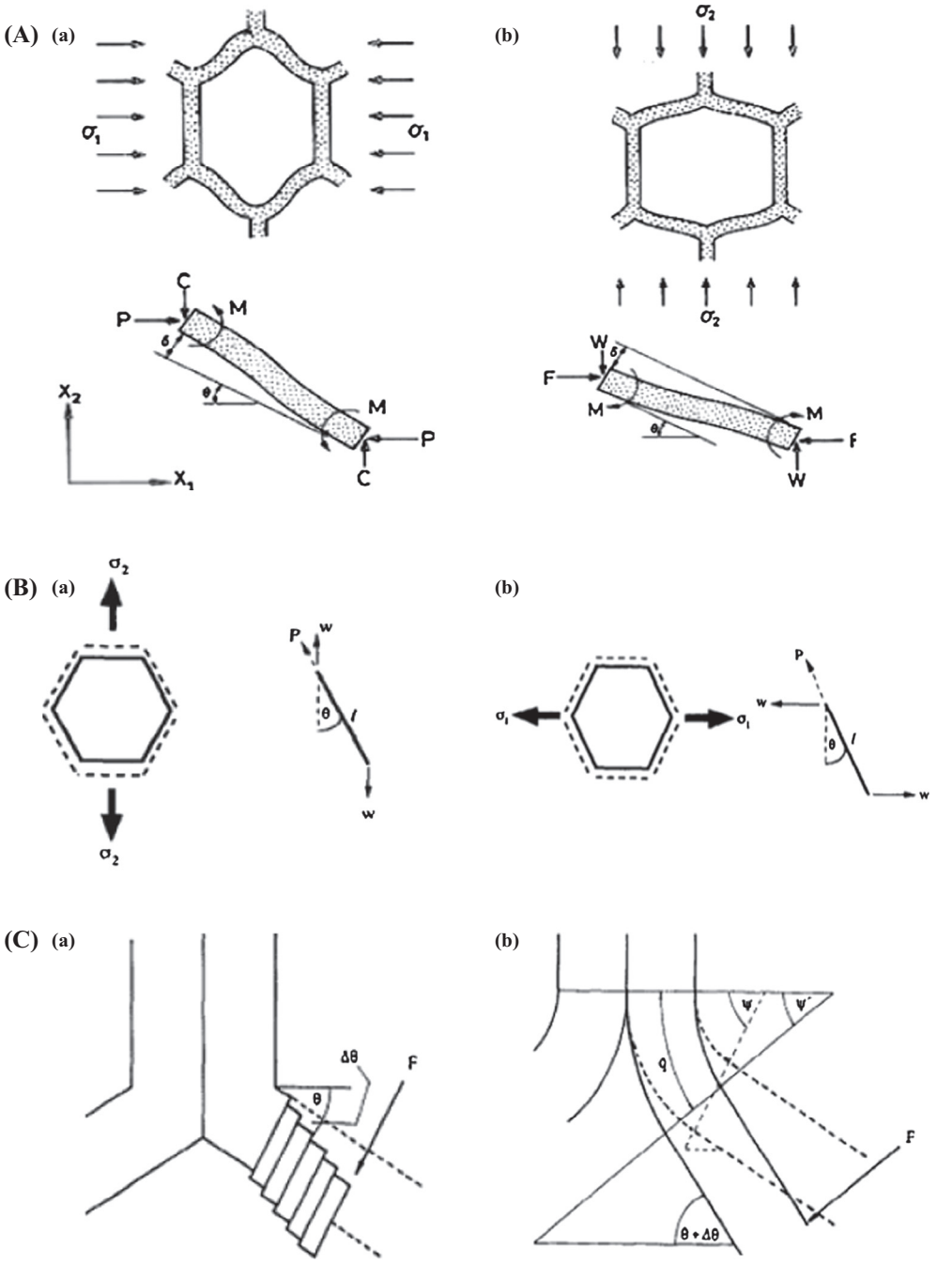

Fig. 10. (A) Deformed honeycomb cell walls with linear-elastic extension or compression; (a and b) bending caused separately by loading in X_1 and X_2 directions [86]. (B) Stretch-resulted deformation in hexagonal cells due to applied tensile load in (a) D2 (direction 2) and (b) D1 (direction 1), where the right side presents the cell wall with applied forces [111]. (C) Hinging-resulted deformation in hexagonal cells: (a) global shear and (b) local bending [111].

Within the density range of 20–300 kg/m^3, honeycombs usually outperform other cellular materials in terms of both stiffness and strength under compression or shear (Fig. 11) [112,113]. Moreover, the superiority of honeycombs also holds in other mechanical properties, including bending resistance [114–116], energy absorption [117], and shock resistance [118]. To further improve the mechanical performance, composite and auxetic honeycomb structures have been exploited. For example, composite structures such as foam filled hexagonal honeycombs [96,119] and honeycomb-filled single and bitubular polygonal tubes [120] have been developed for enhanced energy absorption. Reentrant hexangular cores with negative Poisson ratios [57], as a kind of auxetic honeycombs, exhibit improved mechanical properties, including shear strength, indentation resistance and fracture toughness, compared to conventional honeycombs.

3.2.2. Mechanics of micro- and nano-honeycombs

The advances in nanotechnology have significantly accelerated the development and understanding of honeycomb structures with micro- or nano-sized cells, potentially having widespread

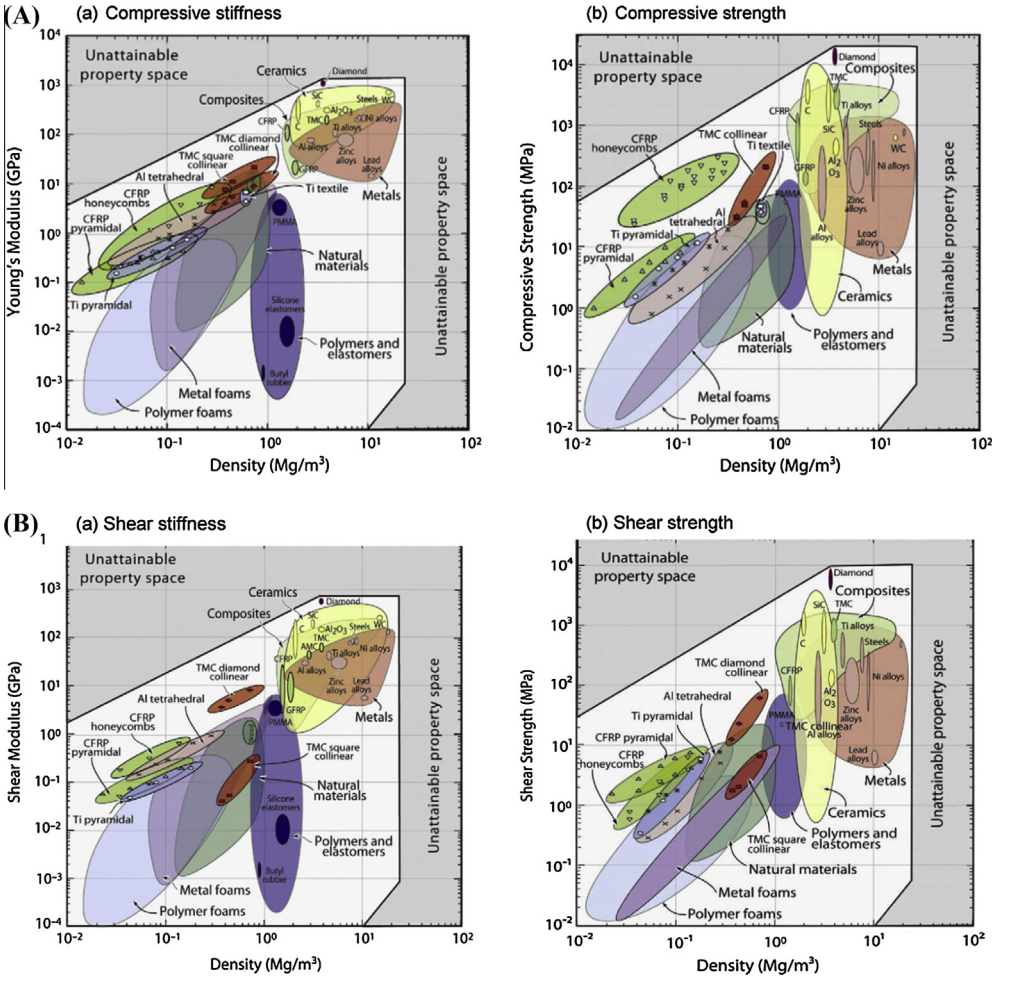

Fig. 11. The relationship between the material density and the mechanical performance of (A) compressive stiffness/strength and (B) shear stiffness/strength summarized by Ashby [112,113].

applications due to large surface area to volume ratio [121]. Balsa wood [122–125] and anodic porous alumina (AAO) [50,126–129] are perhaps the most famous micro- or nano-scale honeycombs.

Balsa wood with a density ranging from 40 to 380 kg/m^3 has a cellular microstructure with approximately hexagonal cross-sections of a typical micro-honeycomb. The micro-honeycomb allows large deformations, leading to high specific energy dissipation capacity. To quantitatively determine the mechanical properties of balsa wood and qualitatively clarify its deformation mechanisms, several uniaxial quasi-static compressive investigations in both longitudinal and transverse directions [122,130–134] have been performed (see Table 2). As a pioneering work, it is found by Easterling et al. [132] that the balsa wood shares the same mechanisms with honeycomb in terms of compressive deformation loaded along and across the grain (analogous to out-of-/in-plane direction in a honeycomb). Further, it is suggested by Gibson [134] that the simple honeycomb model may be sufficient for determine the Young's moduli and compressive strength of woods along and across the grain. Recently, Silva and Kyriakides [122] conducted extensive experiments on the compressive response of balsa wood in axial, radial and tangential directions, and systematically described the macroscopic and microscopic deformation mechanisms (Fig. 12A). The shear [123] and dynamic compression behavior [124,125] of balsa wood have also been investigated (see Table 2).

Anodic porous alumina (AAO) [50,126–129,135], nanoporous silica [136–141], and mesoporous honeycomb-shaped activated carbon [142] were well-known nano-scale honeycombs. To maintain microstructural integrity in practical applications, characterizing their mechanical properties was of great importance. For transversely isotropic nano-honeycombs, five elastic constants were needed, namely, Young's moduli E_{11} and E_{33}, Poisson ratio υ_{13}, and shear moduli G_{12} and G_{13}. However, it was challenging to obtain these properties given the small cell size of nano-honeycombs. Built upon an earlier work [129], Jeon et al. [135] attempted to experimentally determine the mechanical properties of microscopic brittle specimens of transversely isotropic nature by five independent tests using the Nano-UTM and a nano indenter, as shown in Fig. 13. Ng et al. [126] studied AAO honeycomb subjected to nanoindentation along its axial direction and micron-sized pillar of AAO under compression, and observed a unique mode of deformation that the AAO honeycomb is either severely deformed or

Table 2
Mechanical behavior of micro- and nano-honeycomb materials.

Materials	Pore size	Loading methods	Failure mode	Ref.
Balsa wood	30–70 μm	Compression	Buckling and kink band formation	[122,130–134]
Balsa wood	30–70 μm	Shear	Cracks	[123]
Balsa wood	30–70 μm	Modified Kolsky bar	Buckling and kink band formation	[124,125]
–	–	Bending and shear	–	[121,151]
Anodic porous alumina	31 nm	Tensile test in Nano-UTM and flexural testing in AFM	Elastic modulus	[129]
Anodic porous alumina	25–35 nm	Tensile and bending test	Elastic modulus	[135]
Anodic porous alumina	70 nm	Compression	Severe layer distortion at the pillar's head	[50]
Anodic porous alumina	70 nm, 20–80 nm	Nanoindentation	Bilinear and median cracks	[126,127]
Anodic porous alumina	25–35 nm	Bending fatigue	Rectangular fracture shape	[128]
Micelle-templated silicates	35 nm, 80 nm	Compression	Brittle crushing	[136]
Nano-structured glass fibers	3 nm	Simulated nanoindentation	–	[137]
Mesoporous silica	5 nm	Unilateral external pressure	Destroy	[138]
Mesoporous silica	–	Nanoindentation	Elastic modulus, hardness	[139–141]

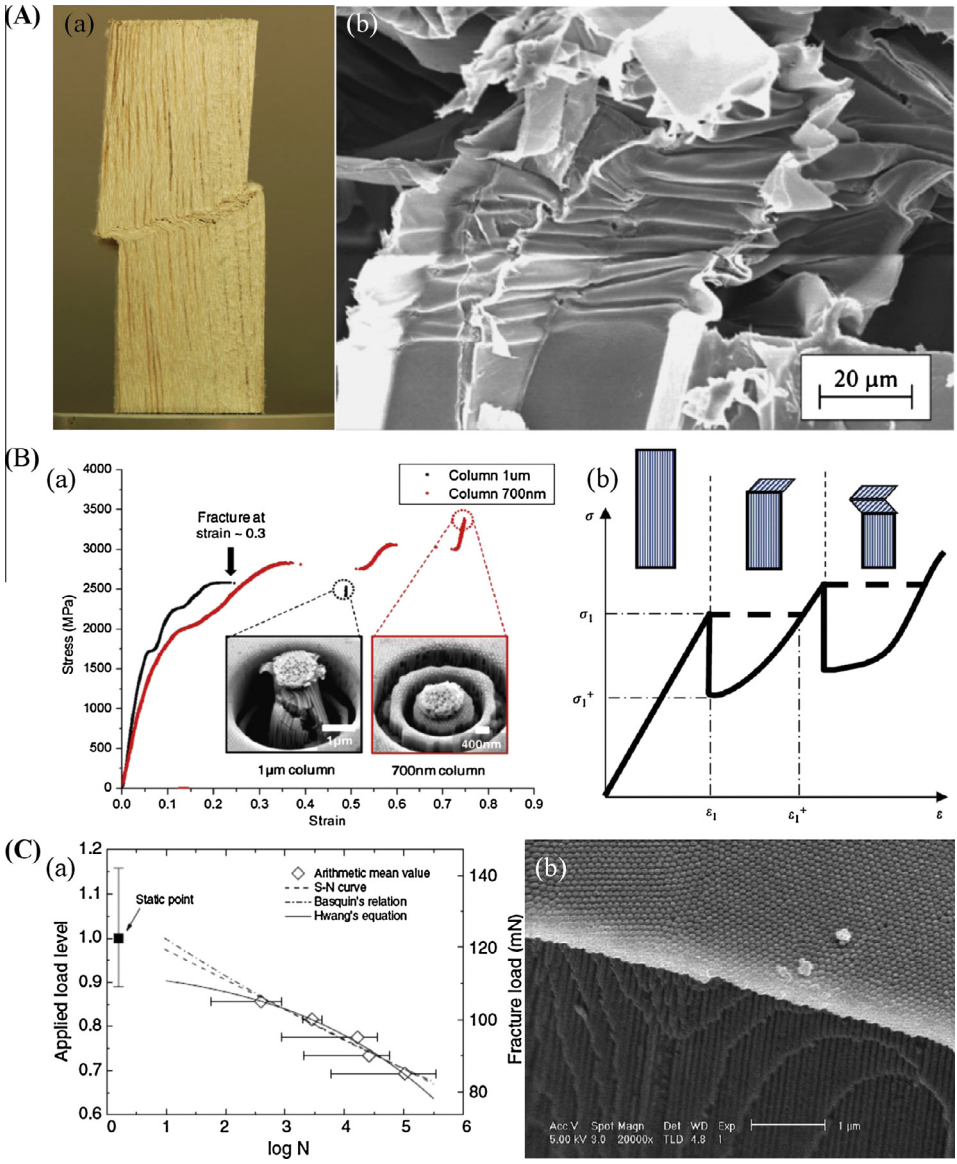

Fig. 12. (A-a) Photograph showing evidence of kink band in balsa wood ($\rho/\rho_s = 0.150$). (A-b) Micrograph of balsa wood showing concertina axial folding of crushed tracheids for $\rho/\rho_s = 0.063$ [122]. (B-a) Comparison of compressive stress–strain responses of a 1 μm column fractured at around 30% strain and a 700 nm column without noticeable facture till 80% strain. (B-b) Schematically demonstration of the stress–strain curve [50]. (C-a) Bending fatigue life data and prediction curves of nanohoneycomb. (C-b) SEM image of fractured surface in anodic porous alumina [128].

remained apparently elastic. The results shown in Fig. 12B demonstrated that AAO is promising as a sacrificial shielding or supporting material in applications involving mechanical contact with other components, e.g., thin film sensors. Nanoindentation was also employed to understand the deformation behavior of AAO honeycombs [126,127]. Further, the fatigue properties of nanohoneycombs were of prime importance in creating stable products for a range of potential applications [128].

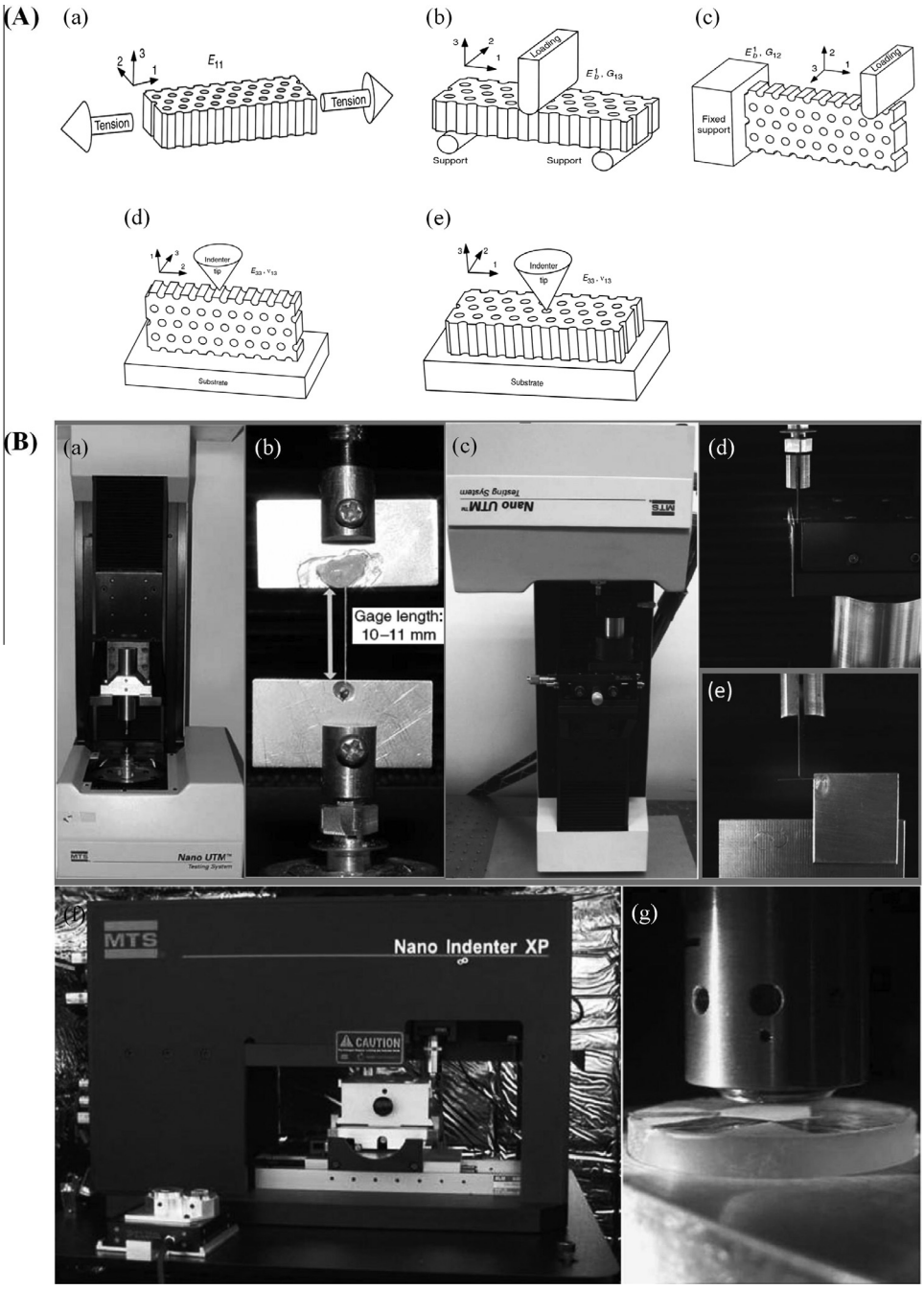

Fig. 13. Schematic display of five independent tests to experimentally determine the mechanical properties of nanohoneycomb specimens: (A-a) tension, (A-b) three-point bending, (A-c) cantilever bending, (A-d) indentation in 1-direction, and (A-e) indentation in 3-direction. Tensile test of nanohoneycomb beam specimen by Nano-UTM: (B-a) general view and (B-b) nanohoneycomb mounted on a metal plate. Bending fixture: (B-c) overall feature, (B-d) three-point bending, and (B-e) cantilever bending. MTS nanoindentation: (B-f) overall view and (B-g) indenter tip holder and sample [135].

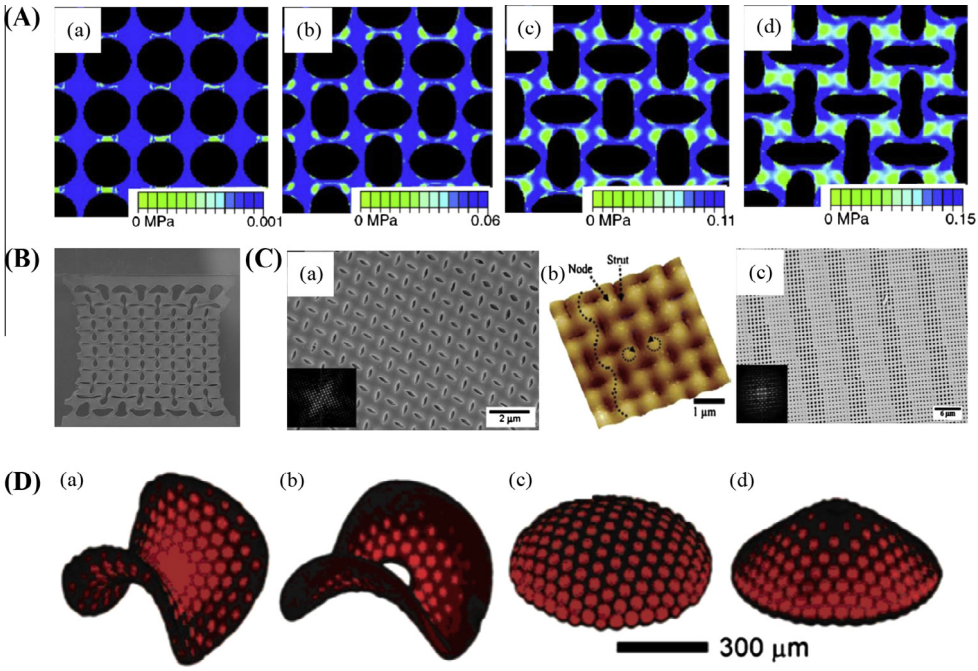

Fig. 14. (A) Experimental images of a square lattice (10.97 mm center-to-center spacing) at different levels of macroscopic compressive strain: (a) 2%, (b) 7%, (c) 8%, and (d) 10% [157]. (B) Experimental images of a porous lattice under compression of $\varepsilon = 0.25$ [152]. (C-a) SEM image of uniform pattern transformation in a square lattice following the polymerized acrylic acid in the pores. (C-b) AFM topographical image of the transformed pattern. (C-c) SEM image show of the regular transformation pattern (inset showed 2D fast Fourier transform) due to large-scale periodic confinement of mechanical instabilities [160]. (D) Halftoned disks with axisymmetric metrics, with patterned sheets programmed to generate (a) a piece of saddle surface, (b) a cone with an excess angle, (c) a spherical cap and (d) a cone with a deficit angle [155].

Concerning ordered mesoporous materials such as silica, many researchers focused on their rigidity and structural stability under stressing [139,143–145]. The mechanical stability of ordered mesoporous silica can be mainly characterized by its elastic modulus, depending on the porous structure and the consolidation extent of silica. The elastic modulus (E_{film}) of thin films with honeycomb-like porous structure has been measured with the technique of nanoindentation [139], while the crushing strength of nanosized hexagonal silica honeycombs with different pore sizes has also been measured. Good agreement has been achieved between experimental measurements and predictions using theoretical model originally for macroscopic hexagonal ceramic honeycombs [136]. Further, higher consolidation has been found to provide a more rigid structure, helpful for eliminating the more hydrothermally sensitive pore surface Si–OH bonds to the benefit of the formation of more hydro-resistive Si–O–Si bonds [146,147]. Several methods have been developed to enhance pore wall consolidation, e.g., surfactant removal processes [140,146], silica nanoparticle [141], salt [148] or alumina additives [149], and humidity treatments [150].

At the micrometer or nanometer scale, the size-dependent effect plays a vital role in the mechanical behavior of honeycombs [121,151]. For example, Zhu [151] found that strain gradient and surface elasticity dominates honeycomb elastic properties at micrometer and nano-meter scale, in respective. Joonho et al. [121] employed the asymptotical expansion framework and the numerical homogenization method to predict the elastic properties of honeycombs in micro and nano scale by introducing the surface elasticity. They found that the mechanical property such as bending stiffness and shear stiffness was dependent upon the size of honeycomb and may attributed to the atomic bonding reconstruction at micro/nano-sized honeycomb surfaces.

3.2.3. Mechanics of polymeric and bio-honeycombs

Owing to the elastic nature of polymeric and bio-honeycomb structures, their mechanical behaviors are significantly different from other honeycomb solids, e.g., the completely reversible transition in buckling instability and the unusual negative Poisson ratio (Fig. 14) [152]. Further, the buckling-based morphological changes induce dramatic change not only in relevant physical properties such as phononic property [153,154], but also in biomedical applications [155]. In tissue engineering, the structure such as 2D or 3D porous structure, micro-/nano-fluidic channels, and microenvironment experienced by cells cultured on the surface of the porous structure can be dynamically tuned by buckling-based reversible changes in morphology.

With subjected to different levels of uniaxial compressive strain, the mechanical instability of porous structures in millimeter-scaled distribution was investigated by Mullin and coworkers [156] (see Fig. 14A). New patterns and super elastic behaviors [75,157] were observed at post-deformation transformation of other lattices with circular voids. Pattern deformation due to buckling instabilities in porous structures with periodically-distributed pores persists at micro-/nano-scales, in a wide range of porous structures with various porous geometries and lattice symmetries. Such pattern deformation can be induced by light [158], solvent swelling [154,159,160] (Fig. 14C), or even temperature [155] (Fig. 14D). For example, Zhang et al. [159] presented pattern deformation in a microporous elastomeric poly(dimethylsiloxane) structure consisted of circular pores (pore diameter varying in the range of 350 nm to 2 mm) distributed in a square array. Such responsive buckled complex surfaces can also be designed as constant Gaussian curvature (spherical cap, saddle and cone) or zero mean curvature (Enneper's surfaces) by using halftone gel lithography [155].

3.3. Heat transfer

Honeycomb structures have attracted significant interest for thermal management applications, either as thermal barriers or heat dissipaters. In general, three fundamental modes of heat transfer are present in honeycombs, namely, conduction, convection (natural and forced convection), and radiation. According to different thermal situations, these modes are usually found to couple with each other.

3.3.1. Conductive heat transfer

In the absence of convection and radiation, heat transport across a honeycomb solid is dominated by solid and gaseous conduction. Prediction of its effective thermal conductivity is, in principle, straightforward by treating the honeycomb as a two-phase material. The effective thermal conductivity in either axial or lateral direction of the honeycomb has been analytically and numerically investigated [161–164]. Considering both solid and gaseous conduction, Groppi and Tronconi [164] derived the effective thermal conductivities of a honeycomb with square cells in both axial ($k_{e,ax}$) and lateral ($k_{e,r}$) directions. For honeycombs made of metal solids, heat conduction through the gas phase is negligible since the gaseous conductivity ($\sim 10^{-2}$ W/mK) is significantly lower than the solid ones ($\sim 10^{2}$ W/mK). Based on this assumption, Lu and Chen [162] obtained a general correlation for the axial and lateral effective thermal conductivities of honeycombs having different cell shapes (Fig. 15), as:

$$K_{eff} = c_k k_s (1 - \varepsilon) \tag{1}$$

where c_k is the coefficient accounting for the tortuous shape of the cell wall. For axial effective thermal conductivity c_k always equal to 1 regardless of the cell shape, whereas c_k is strongly related to cell shape in the lateral direction. Recently, Yang et al. [165] proposed a fully analytical model for effective thermal conductivity of honeycombs, achieving the good prediction for honeycombs with various pore shapes for the full porosity range. They incorporated an analytical expression for shape factor based on the circularity which corrects the deviation caused from the non-circular (or non-spherical) pore inclusion into the Laplace heat conduction equation.

3.3.2. Convective heat transfer

Natural convection. Dating back to 1965, studies had focused on natural convective heat transfer in a honeycomb positioned in the axial direction (Fig. 16A), for its predominant application in flat-plate

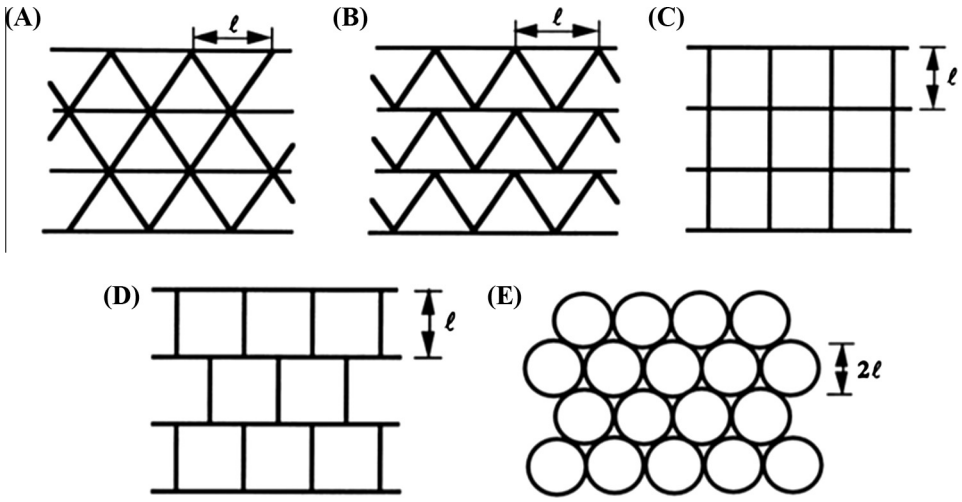

Fig. 15. Honeycomb structures with different cell shapes to study morphology dependent effective thermal conductivity: two packings of equilateral triangles of (A) inline and (B) stagger; two packings of squares of (C) inline and (D) stagger; (E) closely packed circles [161].

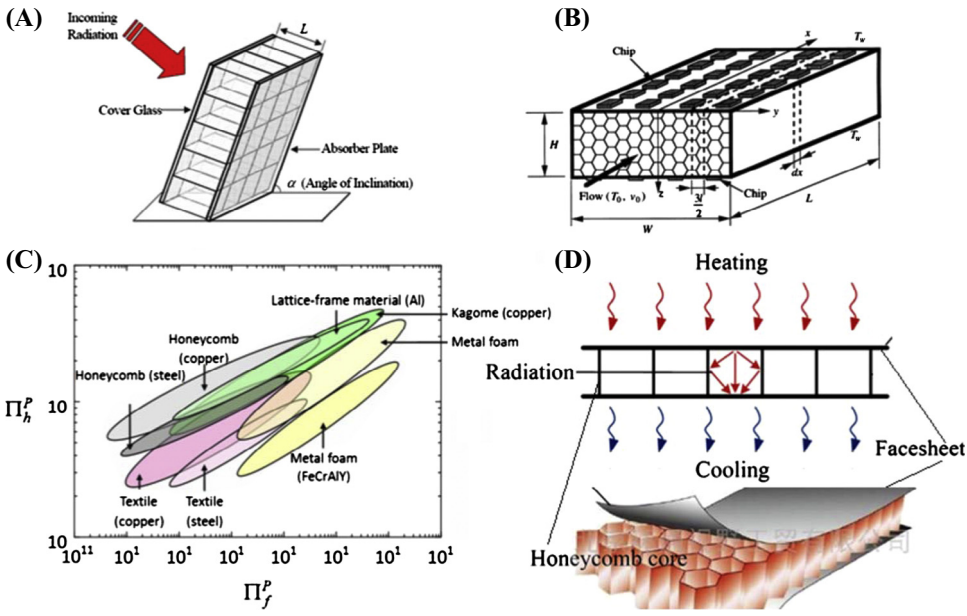

Fig. 16. (A) Illustration of natural convection heat transfer in honeycomb structure in flat-plate solar energy collectors [170]; (B) illustration of forced convection heat transfer in honeycomb structure [171]; (C) comparison of thermal performance between honeycombs with other state-of-the art heat dissipation materials [170], and (D) illustration of radiation heat transfer in honeycomb core sandwich panel.

solar energy collectors. In such applications, honeycombs with low-conducting and thin cell walls are placed the absorber plate and the cover glass to suppress the global natural convection in the chamber. As a result, heat loss from the absorber plate to the cover glass via natural convection is

significantly reduced by introducing the honeycomb. Following the first study of natural convective heat transfer in honeycombs by Hollands [166], numerous experimental and numerical studies [167–170] have demonstrated the high efficiency of honeycombs for reducing the heat loss in flat-plate solar energy collectors.

Forced convection. When positioned in the lateral direction, a honeycomb core sandwich can be used as an efficient heat dissipation material by passing cooling fluid through its continuous open channels (Fig. 16B). In this case, the cell walls of the honeycomb act as fins to dissipate heat deposited at the facesheet of the sandwich. Considering heat conduction in honeycomb solids coupled with forced convection, Lu [171] developed a corrugated wall heat transfer model for honeycomb embedded with cooling fluid flow inside. Using this corrugated wall model, Lu's group studied and optimized various influencing parameters of honeycomb structure with experimental validation [172,173], e.g., cell shape, porosity, surface area density, overall geometrical dimensions, and material properties. It was found that friction factor depends only on surface area density and cell shape of porous structure, whereas heat transfer performance is affected by a variety of parameters including cell shape, surface area density, porosity, thermal conductivity, and overall dimensions.

Besides analytical investigations, McDowell and co-workers developed different numerical methods (finite element and finite difference) for forced convection in honeycomb structures [170]. From a design point of view, their studies mainly concentrated on the optimization of honeycombs with rectangular cells by functionally grading cell size along the height to enhance both structural and thermal performances.

Ideally, a heat dissipation material should attain more heat transfer at the least expense of pumping power to drive the fluid flow. In this regard, both the heat transfer and pressure drop performances are important for a heat dissipation material. The high surface area density of a honeycomb enables superior heat transfer. Meanwhile, the single "easy flow" passage in the honeycomb leads to much lower pressure drop than other heat dissipation materials having high surface area density, e.g., metal foams with stochastic micro-structure [171]. Consequently, under the criteria of given pumping power, honeycomb structures outperform other state-of-the art heat dissipation materials, including metal foam, woven textile and lattice-frame material (Fig. 16C) [170].

3.3.3. Radiative heat transfer

In the 1950s, the employment of sandwich panels with axial honeycomb cellular cores in flight vehicles as outer skins led to great demand in studying the heat transfer through these structures during aerodynamic heating [162,172]. For such high temperature applications, radiation between the facesheets and the honeycomb core is coupled to solid conduction (Fig. 16D). Using numerical simulations, Swann and Pittman [173] obtained a semi-empirical relationship for the effective thermal conductivity of combined radiation/conduction in the honeycomb core as a function of geometric parameters and material properties. Subsequently, this semi-empirical relationship was used throughout the aerospace industry as a standard model for determining combined conductive/radiative heat transfer in panels with axial honeycomb cores. In the combined radiation/conduction heat transfer mode, the contribution of radiation is determined by the exposed surface temperature and the thermal conductivity of cell wall. For instance, Lu and Chen [162] found that for honeycomb cellular metals with hexagonal cells ($k_s > 200$ W/mK), heat transfer is mainly by conduction via solid cell walls, and the influence of thermal radiation was found to be negligible even at a relatively high temperature around 600 K; however, for materials with a thermal conductivity less than 1 W/mK typically involved in thermal insulation applications, even at relatively low temperatures ($\sim$310 K), radiative heat transfer contributes half of the total heat transfer.

3.4. Acoustic property

When a sound wave strikes a structural surface, the total incident sound energy is divided into three parts including scattering sound, absorbed energy and transmitted sound. The transmitted sound is an indication of acoustic performance of the structure as a noise barrier (i.e., sound insulation) between separating spaces. The absorbed energy characterizes the sound absorption capability associated with thermal-viscous effects, resonance dissipation mechanism and so on. Therefore, the

following discussions on the acoustic property of honeycomb structures focus separately on sound insulation and sound absorption.

3.4.1. Sound insulation

Owing to their high stiffness to weight ratio, honeycomb structures are widely used in aerospace industry (e.g., fuselage linings of airplane [174]). Advances in finite element models for complex honeycomb sandwiches have led to the rapid growth of computational requirement due to the increased cells. For this reason, the whole structure is usually regarded as a layered plate medium after homogenization [175]. As a pioneering work, Kurtze and Watters [176] investigated the sound transmission loss (STL) of sandwich structures to design a more quieter wall than the traditional thick single wall. Three types of characteristics governing motion are identified from lower to higher frequency, including bending of whole structure, shear deformation of core and bending of facesheet. As shown in Fig. 17A, the typical STL versus frequency curve of a flat sandwich plate exhibits four different regions controlled separately by stiffness, resonance, mass and coincidence [177]. This indicates that panel stiffness dominates STL curve trend until the start of the lowest order resonance. At about twice the first order resonance frequency, mass inertia begins to play a primary role, ending at the coincidence frequency related to bending stiffness and incidence angle. Compared with one layer flat plate, honeycomb sandwiches have a similar resultant graph but more design variables such as thickness of facesheet or core structure [178]. It is found that the key to design quieter honeycomb sandwiches is to maintain a sub-sonic bending wave speed over as great frequency range as possible [179]. Apart from continuum models, great efforts have also been devoted to investigating honeycomb structures using detailed analytical models [180], finite element method [181], and spectral finite element method [182]. Remarkably, these detailed models are able to reflect discretized and periodic characteristics of the honeycomb, which is especially important for wave propagation analysis rather than STL prediction.

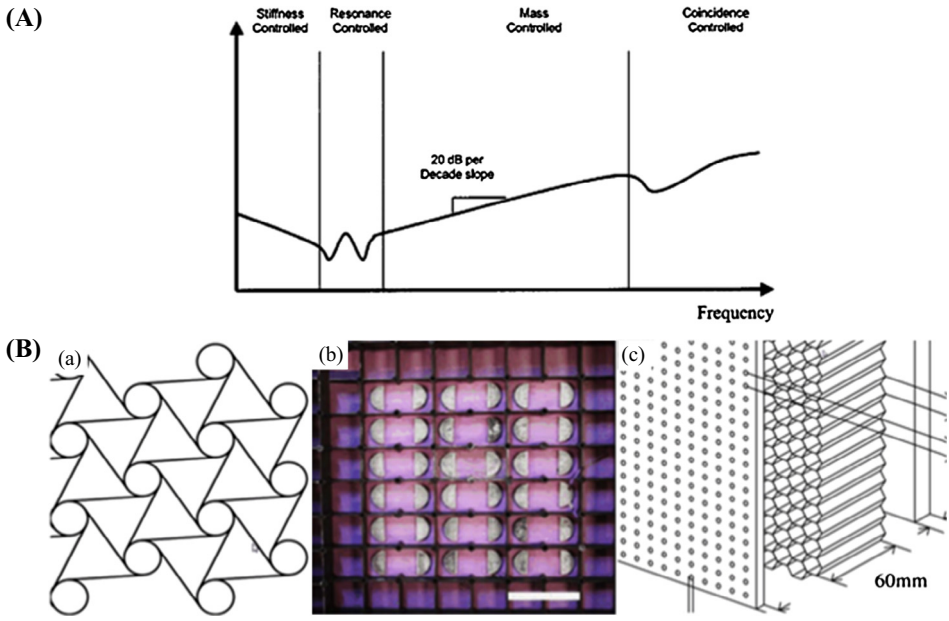

Fig. 17. (A) Typical sound transmission loss (STL) spectrum for a flat plate [177], (B) representative honeycombs with high sound absorption coefficients: (a) hexagonal chiral lattice [186], (b) honeycomb structure with local resonators [194], and (c) schematic of perforated board and honeycomb layer system [198].

In summary, the sound insulation performance of a macro honeycomb structure is related to vibration response of the whole structure, identical to a conventional flat plate for physical mechanism. However, things become different for micro and nano structures [183] since the mechanical properties of these structure turn to be size-dependent. Thus, new constitute relations (e.g., nonlocal elasticity theory [184]) instead of classical continuum models are required to account for the size effect. For example, the wave characteristics of single-walled carbon nanotubes were investigated using nonlocal elasticity [185], which indicated the limitation of applicability of local continuum models. But whether at the macro or micro scale, the main goal to investigate STL of a honeycomb structure is to predict its unitary dynamic response theoretically or numerically as accurate as possible.

3.4.2. Sound absorption

In the past two decades, artificial periodic materials (also known as phononic crystals [186]) have attracted great attention due to the existence of elastic (or acoustic) wave band gaps. For instance, as shown by Ruzzene and Tsopelas [187], a honeycomb sandwich plate with different geometry parameters can generate periodic impedance mismatch to form a bending wave band gap. Phani et al. [188] investigated four planar lattices: hexagonal honeycomb, Kagomme lattice, triangular honeycomb, and square honeycomb. In the high frequency range, the spatial filtering effect due to anisotropy is consistent with geometry symmetry. Generally, the mechanism of band gap formation is attributed to Bragg scattering and localized Mie scattering resulting from periodic elements. For example, Sánchez-Pérez et al. [189] showed that an array of rigid cylinders in air with square lattice configuration generated complete acoustic band gaps in the range of audible frequencies (Fig. 17B-a). Similarly, complete band gaps are achieved with honeycomb water–steel photonic crystals [190]. It is worth noting that the band gap from Bragg scattering mandated the structural periodicity to be on the same order as the incident acoustic (or elastic) wave, thus a low-frequency wave can only be attenuated by acoustic crystals with larger size [191].

Fortunately, another band gap mechanism denoted as a local resonance has been identified [192], offering attractive perspective to realize high STL at low frequencies. For example, a thin membrane-type metamaterial (weight $<3\ kg/m^2$) attached by periodic metal circular disks was designed and fabricated [193]. For such artificial structures, numerical and experimental results demonstrated that an average STL of more than 40 dB could be accomplished from 50 Hz to 1000 Hz. Further, by changing the metal disks to asymmetric rigid platelets, a new kind of metamaterial (as shown in Fig. 17B-b) was proposed recently [194], realizing almost unity sound absorption coefficient. From the existing results, we can anticipate that a honeycomb structure with local resonance cells is promising for sound absorption applications.

Normal honeycomb structures exhibit negligible sound absorption because the damping coefficient of the commonly used materials is small. Nonetheless, honeycomb structures can be transformed into excellent sound absorbers by introducing viscous-thermal dissipation or Helmoholtz resonance mechanisms [195]. One simple and direct way is to fill the honeycomb cavity with polyurethane (PUR) foam [196] or fibrous sound absorptive material [197]. Apparently, the sound absorption coefficient of the whole structure mainly depends on the filled sound absorption materials. Besides the filling materials, the facesheet of honeycomb sandwiches can be replaced by a microperforated board to improve sound absorption [198]. The small ($\sim$1 mm) holes on the facesheet together with the honeycomb structure composed a typical Helmoholtz resonator which could absorb sound energy in a narrow frequency band (Fig. 17B-c). Moreover, if the concept of microperforatation is applied, a wide band absorption may be achieved without using the fibrous or porous filling material [199].

Overall, different from the sound insulation performance, the sound absorption capability of a honeycomb structure is less affected by its overall dynamic response which may be size-dependent for small scale problems. The decisive factor on the final absorption coefficient mainly depends on specific physical mechanisms, e.g., Bragg scattering, local resonance or Helmholtz resonance. Therefore, the critical scientific issues of an acoustic honeycomb structure are related to its mechanical property and absorption mechanism for sound insulation and sound absorption, respectively.

4. Fabrication methods and applications

Naturally-occurring honeycombs have attracted great interests due to their distinct formations studied by scientists for centuries, where advances in engineered (artificial) honeycombs have been largely motivated by their broad applications. For instance, macro-honeycombs have been used not only in sandwich panels [38] but also adopted for many other applications such as energy absorption [57], air directionalization [25], thermal management [171], sound absorption [197], light diffusion [200] and magnetic shielding [201]. In recent years, a wide range of manufacturing processes have also been developed to fabricate micro/nano-honeycomb structures and their evolutional structures that are more affordable and functional for traditional engineering fields as well as emerging biomedicine.

4.1. Fabrication and applications in traditional engineering

Based on thousand years of exploration and the last hundred years of development in engineering, honeycombs have been extensively utilized in various traditional engineering fields (civil engineering, transportation, mechanical engineering, chemical engineering, etc.) because of their multifunctional characteristics including light-weight construction, thermal insulation [170,202,203], and energy absorption [204–206]. The practical applications of man-made honeycombs focus primarily on: (i) ultralight weight design associated with high strength and low density, such as lightweight components used in architectural, automobile and aerospace structures, (ii) high impact energy absorption applications such as armors and helmets, and (iii) high macroscopic shear yield strength applied to non-pneumatic tires. In the following sections, typical examples of these applications are presented.

4.1.1. Architectural engineering

Typical honeycomb structures applied in architectural engineering include honeycomb architecture, construction materials, and building decorations. Honeycomb architecture leads an innovative trend in architectural system, giving the conceptual design of a hexangular tube construction. Honeycomb type buildings with different shapes (Fig. 18A) exhibit superiority in energy-saving, environment-friendly, and earthquake-proof characteristics. Two representative examples of honeycomb architecture are Mexico city-based architect Michel Rojkind's new project and the Metropol Parasol project in Seville, Spain, by Jurgen Mayer H. Architects that is completed in 2009 created a real buzz. Further, two glass towers wrapped in a dramatic honeycomb structure will soon be under construction. There will be the world's largest wooden structure in the city's Santa Fe district; it has 35 stories and can house 180 duplex apartments with a hotel and gardens on the upper floors.

The application of honeycomb structures can be found in such construction materials as honeycomb bricks and transparent insulation (Fig. 18B). Detailed review on the analysis and evaluation of transparent insulation for building applications can be found in Ref. [207]. In addition to honeycomb construction materials, the highly competitive honeycomb transparent insulation is also used in solar collectors [170], roof cover system [208] and integrated collector storage [209], as well as in space heating and day lighting for buildings [210]. Heat transfer takes place through a honeycomb transparent insulation by coupled radiation and conduction.

On closer examination, increasingly more honeycomb elements have been adopted for designing building decorations (Fig. 18C). Sometimes these elements work beyond the ornament function, with the versatile honeycomb-like shelving and Hedler MaxiBrite honeycomb as two examples. Each building unit of a modular honeycomb-like furniture system was made from expanded polypropylene ARPRO, which is in nature a type of plastic foam with high mechanical performance. A box, a seat or a step can be obtained by a single building unit, while putting them together by special clips, multiple building units can be achieved including the shelving units, partitions with built-in storage, and storage boxes. The Hedler MaxiBrite honeycomb is used as a metal reflector due to increased contrast and brilliance b suppressing stray light.

4.1.2. Transportation

With the rapid development of transportation industry, honeycombs have been widely used in this field especially for aerospace and mass transport.

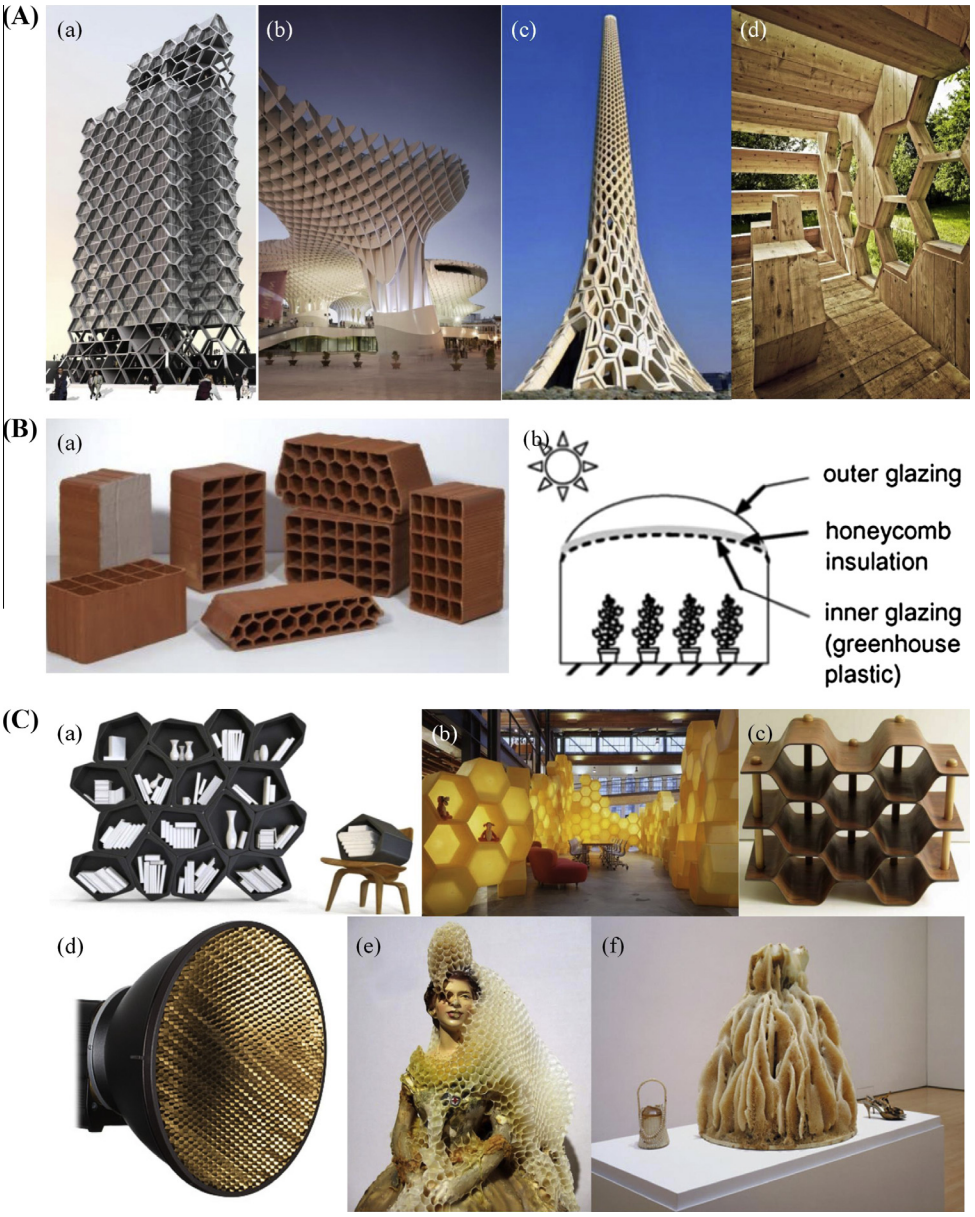

Fig. 18. Representative honeycomb structures in architecture: (A-a) Mexico City-based architect Michel Rojkind's new project; (A-b) Metropol Parasol project; (A-c) KAUST Breakwater Beacon designed by Urban Art Projects; (A-d) versatile honeycomb-like shelving with odd-shaped blocks (http://www.gizmag.com/build-modular-shelving/28349/); (B-a) ClayFix® Heat Isolation Mortar (http://www.kudret.com/eng/products.php); (B-b) typical greenhouse configuration with honeycomb insulation [449]; (C) building decorations with honeycomb design structures: (C-a) versatile honeycomb-like shelving; (C-b) Disney store modular honeycomb design; (C-c) Swedish birch and rosewood wine rack; (C-d) Hedler MaxiBrite honeycomb; (C-e) and (C-f) collectables remixed with real honeycombs.

Honeycomb paulownia surfboard. One of the attractions of honeycomb paulownia surfboards, kayaks and boats is the honeycomb pattern cored out to lighten the board, providing a tight platform for a 1.8 mm 3ply of bamboo to be used as the only deck skin (Fig. 19A). No fiber glass but gum

turpentine and wax is used to seal it, which is the small environmental impact compared to fiber glass products that are associated with pollutants and long decomposition time.

Tires with non-pneumatic honeycomb structure. Pneumatic tires have several disadvantages, including: (i) catastrophic damage caused by flat while driving, (ii) requirement for maintenance of air pressure, (iii) complicated manufacturing processes, and (iv) non-uniform contact pressure distribution [211]. For instance, in Iraq, the explosion of improvised explosive devices (IEDs) can easily blow out the Humvee tires, leading to directly kill the soldiers. That worries the U.S. Army and makes them to look for a novel mode that can prevent tire blew out or keep running after suffering a flat tire. To solve this problem, a company named Resilient Tech recently put forward a new prototype that replaces the key part of a tire with a non-pneumatic honeycomb structure. Besides, several tire engineers also attempted to develop non-pneumatic tires (NPT) through using polygon typed lattice spokes to replace the pneumatic tire (Fig. 19B) [212,213]. Kim et al. [214] explored the structural performance of a NPT with 3D lattice spokes by performing numerical simulation of the contact pressure

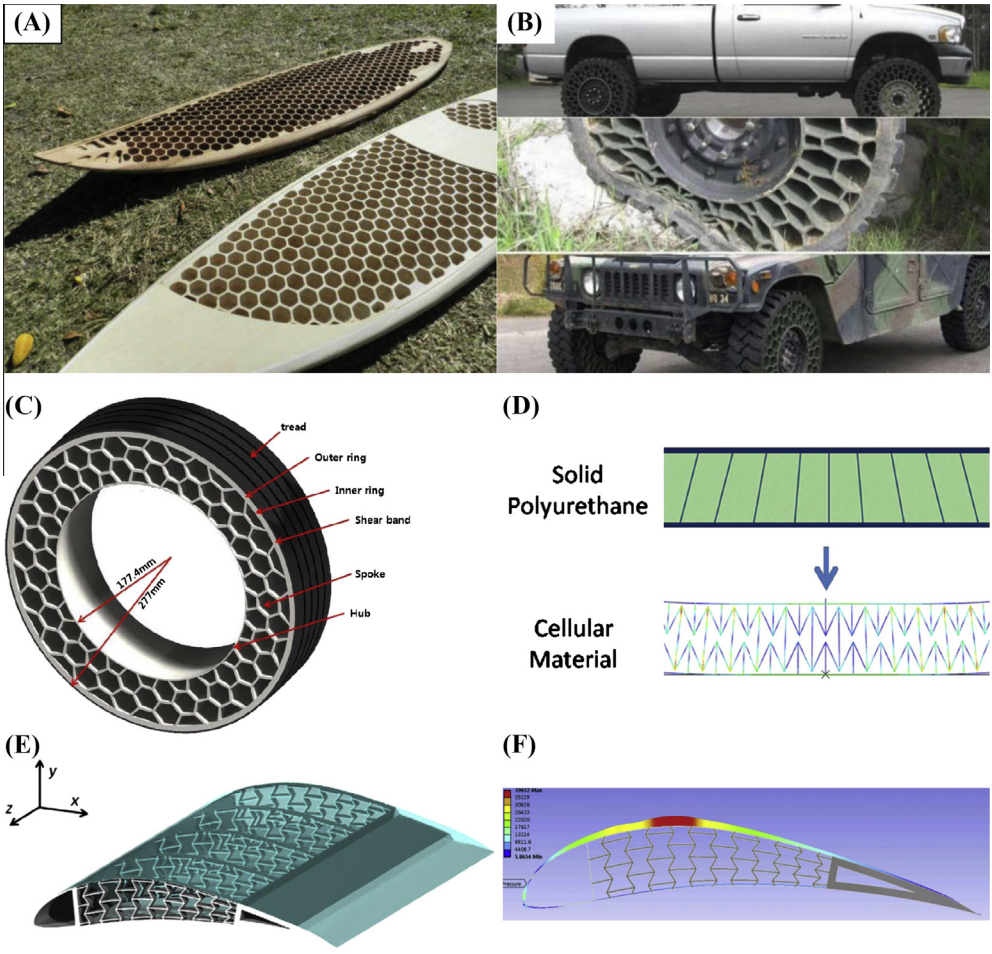

Fig. 19. (A) Honeycomb paulownia surfboard (lightweight surfboard with honeycomb CNC (computer numerical controlled)) routing wooden (http://www.nzffa.org.nz); (B) tire with a non-pneumatic honeycomb structure (http://www.resilient-tech.com); (C) illustration of non-pneumatic tire with hexagonal lattice spokes [214]; (D) replacing homogeneous material with cellular material to reduce hysteretic energy loss; (E) conceptually-designed morphing wing with reentrant hexagonal honeycomb core; and (F) imported pressure load on airfoil with re-entrant honeycomb core [224].

on the NPT and found that 3D hexagonal cellular spokes have a higher out-of-plane stiffness than 2D spokes under targeted load and a lower mass. As demonstrated by the model for determine the in-plane linear elastic behavior for honeycomb, high shear flexure properties could be achieved by properly-designed reentrant hexangular cells with negative Poisson ratios (Fig. 19D) [215]. One of the latest contributions of this study is the design of a non-pneumatic wheel using topology optimization route, with the goal of matching its static stiffness [216].

Honeycomb sandwich as the most prevalent lightweight structure. Honeycomb sandwiches are the most prevalent lightweight structure (Fig. 20). The requirement for lightweight structural materials in transportation industry especially for aerospace and aircraft applications (Table 3) have evoked great need for the development of honeycomb structures [217–225].

A variety of materials have been used as basic materials to fabricate honeycombs, including paperboard, fiberglass, carbon fiber reinforced plastic, nomex reinforced plastic, Kevlar reinforced plastic, polypropylene and metal (usually aluminum). Metal-based honeycombs are conventionally fabricated by the expanded honeycomb manufacturing process and the strip slotting process. Hexagonal honeycombs are typically manufactured from aluminum alloys by an expansion manufacturing process that results in two of the six cell walls having double thickness. This manufacturing method can only produce uniform hexagonal hollow structures with small relative density ($\rho \leqslant 0.03$). Alternatively, Côté et al. [99] and Radford et al. [226] introduced a strip slotting process to manufacture high-density stainless steel square honeycombs with relative density $\rho > 0.03$.

Due to the advantages of cost effective, environmental stability, ease of processing and recycling, polypropylene (PP) becomes a promising candidate material for sandwich constructions. PP honeycomb has the favorable properties [223] such as lightweight, impact resistance, excellent bonding, corrosive resistance, recycling ability and thermal insulation, leading to a more promising utilization

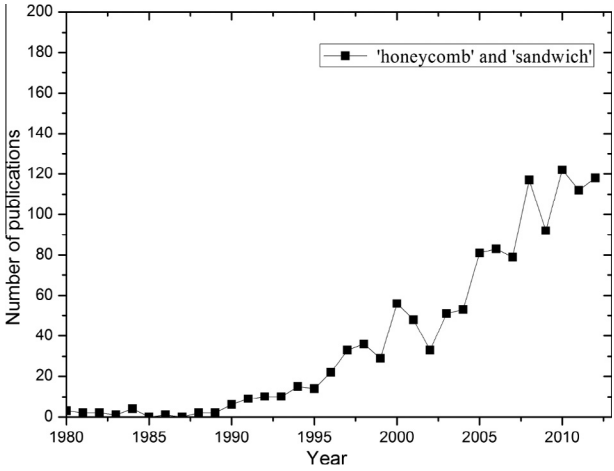

Fig. 20. Number of annual publications on 'honeycomb' and 'sandwich'. *Source*: Science Citation Index Expanded [SCI-EXPANDED].

Table 3
Honeycomb sandwich structures used in transportation industry.

Core material	Product	Ref.
Aluminum F/A-18	Aircraft	[217,218]
Nomex H/C	Aircraft, vehicle	[219,220]
Carbon/epoxy composite	Small aircraft	[221,222]
Polypropylene (PP)	Vehicle	[223]
Carbon/epoxy laminate	Airfoil	[224,225]

in transportation applications compared with honeycombs made from nomex, polypropylene and aluminum, balsa wood and cellular foams. Cabrera et al. [227] reported that 100% PP tubular honeycomb cores sandwiched panels can be fabricated with keeping the mechanical properties of all the PP sheets. Through optimizing the governing factors including environmental temperature, core material and copolymer film under a peel test, the bonding strength where the core joined with the facesheet can be optimized. It is demonstrated that the foam-to-facesheet bond is more homogeneous due to a higher surface contact area [224].

4.1.3. Mechanical engineering

*Lightweight large-scale space-based mirror (*Fig. 21*A and B)*. Refractive optics has been used for space-based optics, where the mirrors must follow strict requirements of functionalities and operations. In addition, they must be lightweight and simultaneously have adequate mechanical strength to withstand a high launch acceleration. The development of lightweight large-scale mirror is essential for the precision performance and efficiency of an optical system. Compared to the mechanically cumbersome solid mirrors, honeycomb designs using lightweight frame as the supporting structure can reduce the mirror weight by 8% [228]. Honeycomb structures with regular hexagonal, square and triangular cells can be fabricated by machine tooling and near net forming processes [57]. Back to the 1980s, metals (e.g., aluminum and beryllium) and glasses (e.g., ULE, Zerodur) were the primary choice of materials to fabricate the space-based mirrors. Since the 1990s, with the development of materials science, the substitute materials such as fused silica, single or multi crystal silicon and silicon carbide have been developed [229,230], prospering the field of manufactory and fabrication.

*Honeycomb seals (*Fig. 21C*)*. Seals are widely used in turbine and compressor construction to enhance aerodynamic efficiency by reducing leakage loss in the gap between the rotating and stationary parts. Since the 1980s, honeycomb seals with hexahedral cellular structure have been frequently used as replacement for the conventional labyrinth seals to ensure a minimum gap loss and increased strength in turbomachinery [231,232]. Among all the geometrical parameters of honeycomb seal, the sealing clearance and honeycomb cell size are the most important factors in the design process [40,233–244]. In particular, the Dresser-Clark company for the first time uses them as end seals for high-pressure centrifugal compressors [245]. In contrast to the labyrinth seals, the tip seals with a honeycomb lands can mitigate the rotor wear while providing a durable interface that enhanced the engine efficiency [232].

Functional honeycomb cores. Over the past few decades, honeycomb cores as functional mechanical components have been used successfully for electromagnetic shielding [61,246,247]; flow directionalization of fluid (typically air and water) flow in a various ducts and channels (typically winder tunnel) [25]; and heat exchange [248]. Metal [248,249], reinforced plastic, Nomex paper and composite or hybrid materials [24,250] are the common materials used in making these honeycombs by expansion, extrusion, extrusion and sintering processes. Aluminum honeycomb is by far the most versatile and widely used. Aluminum honeycombs with properly designed cell sizes and cell depths can attenuate the decibel level in a wide range of sound frequency and thus have been used for radio frequency shielding. In addition, aluminum honeycombs covered by Cr(III) corrosion-resistant coating materials have also been used to directionalize flow. Recently, based on a hierarchical architecture [24], carbon nanotube-reinforced polymer foam has been filled into the cells of aluminum honeycomb to enhance the electromagnetic absorption. This new material is found to be superior to the existed material for electromagnetic absorption in the gigahertz range, setting the stage for multifunctional sandwich panels that has such a mass efficiency to combine high electromagnetic absorption with mechanical stiffness and thermal management.

Intelligent (smart) structures. Honeycomb structures have been used extensively for designing intelligent (smart) structures. For instance, based on the in-plane deformation of the honeycomb with reentrant hexangular cells, Muraoka and Sanada [251] introduced a novel term "honeycomb link mechanism" and according to this link mechanism, a compact design of an efficient displacement amplifier distributed in array for piezoelectric actuators was proposed. Zhang et al. [252] demonstrated a new piezoelectric composite transducer according to the ceramic honeycomb structure, which nearly eliminated the piezoelectric $d(33)$ response of the ceramic and exhibited exceptionally high hydrostatic

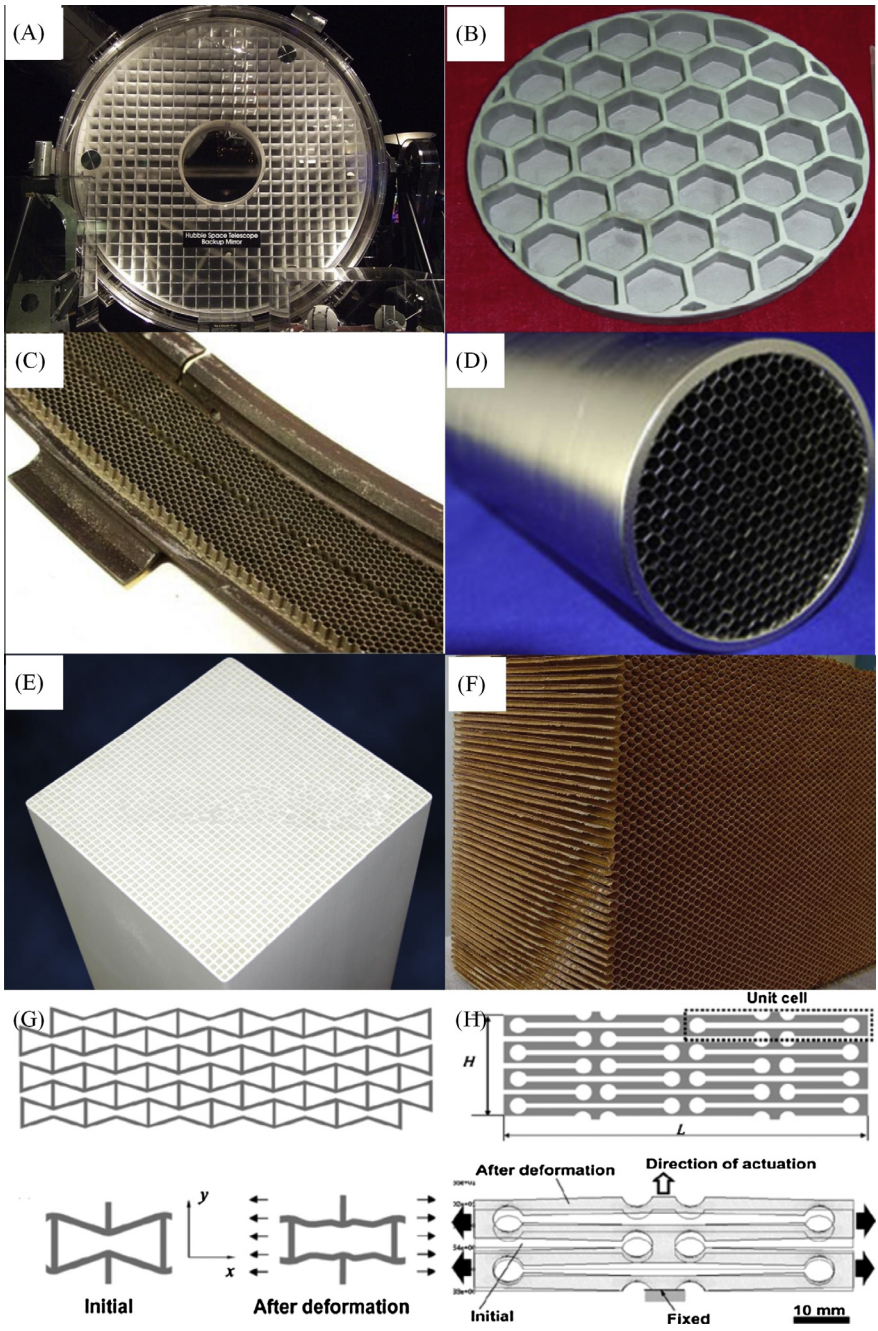

Fig. 21. Photograph of (A) honeycomb-supported core for the backup primary mirror of Hubble space telescope, (B) SiC space-based mirror, and (C) honeycomb seal segment (www.turbineaviation.com). Honeycomb core: (D) stainless steel shielded waveguide vent panel, (E) honeycomb ceramic for catalyst support monolith, and (F) Nomex paper honeycomb. (G) Schematic of honeycomb with a cell shape of reentrant hexagon and in-plane deformation pattern of their single hexangular cell, and (H) patterned honeycomb plate and its finite element analysis to show the deformation with only one end fixed.

piezoelectric response. Hassan et al. [253] illustrated a novel concept of honeycomb structure with hexagonal and auxetic topology. You et al. [254] designed a composite smart antenna structure with high gain and wide bandwidth, and lightweight feature. Here, the honeycomb-cored sandwich construction acted as the basic supporting structure due to its high strength and low density.

4.1.4. Chemical engineering

Honeycombs have been used in a range of chemical engineering applications such as particulate filter [255], concentrator, catalytic combustor [256,257] and catalytic reactor [258] for chemical processes. There exist several excellent reviews on the wide use of ceramic honeycombs as catalyst support, particulate filter for vehicular emission control and other chemical industrial applications such as NOx reduction, effluent concentrator, catalytic combustion and chemical processes [19]. Groppi and Tronconi [259] focused their review on the utilization of novel monolithic catalysts as a substitution of conventional catalyst pellets (packed beds). The high thermal conductivity of the novel monolithic catalysts provides benefits for gas/solid exothermic chemical processes in externally cooled tubular reactors. Recently, their applications touch upon the areas of environmental chemistry such as waste water treatment [260], heat regenerators [261] and solid oxide fuel cell [262].

Typically, ceramic honeycombs (Fig. 22A) possess hexagonal, square and triangle parallel channels. By conventional extrusion processes, the materials exploited to manufacture these ceramic honeycombs are cordierite [263,264], aluminum titanate [257], mullite [265], corundum, zeolite [266], and their compound [265,267]. Compared with conventional ceramics, they have the characteristics of low thermal expansion, high thermal shock resistance, large surface area, and corrosion resistance. Compared to ceramic honeycombs, metallic honeycombs have important metal properties such as good thermal conductivity, electrical conductivity, and fracture toughness. In addition, FeCrAl alloys with excellent oxidation resistance have been used in various applications under temperatures as high as 1200 °C. FeCrAl honeycombs (Fig. 22B) exhibit huge potential to substitute ceramic supports for exhaust gas catalyst and fuel cells [268].

4.2. Fabrication and applications in micro and nanofabrication

With the rapid development of nanotechnology, honeycomb cell structures at the nanometer and micrometer scales have been fabricated using various methods [57]. A review of recent work on ordered porous materials by Davis [269] suggested that ordered porous materials (normally with honeycomb structures) possess exceptional properties, which lead to applications ranging from the traditional catalysts and adsorbents to the emerging fields. Generally, porous materials with pore sizes on the order of 50 nm to 1 mm are of great interest for applications in superhydrophobic surfaces [57], photonics [270,271], optoelectronics [272], and microelectronics [273,274]; while ordered mesoporous solids with a pore size of 2–50 nm are of more importance for fields such as catalysis [275], sensors [276], separation media [277], adsorbents [278], and templates for material synthesis [279]. Molecule-sized porous solids like hexagonal honeycomb lattices with pore sizes smaller than 2 nm are graphene and carbon-nanotubes [280,281], crystalline materials [282], etc. Here we focus our review on typical honeycombs varied by pore size and material type, as well as their emerging applications.

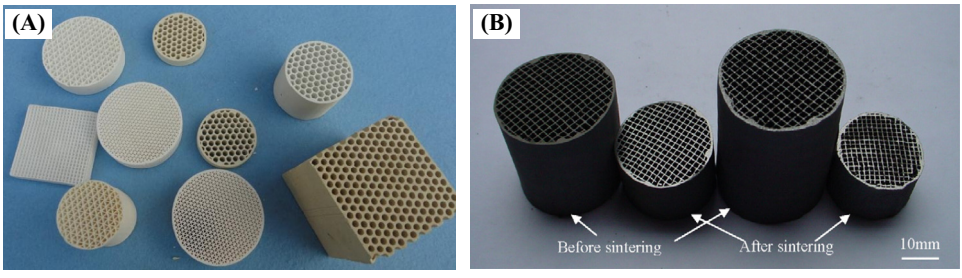

Fig. 22. Topologies of extruded and sintered (A) ceramic honeycombs and (B) FeCrAl honeycombs [249].

4.2.1. Typical micro- and nano-honeycombs

4.2.1.1. Oxide films with micro-/nano-scale pore sizes. Anodic aluminum oxide (AAO) films are the first man-made nanohoneycomb fabricated through a 2-step anodization process (Fig. 23A). The focus of nanoporous AAO has been placed on surface and structural engineering as well as emerging applications as reviewed by Jani et al. [283]. To tailor the surface morphology, Barela et al. [284] developed a complex structure with high aspect ratio by a single-step wet etching of AAO substrate. Because of the ease and low cost in fabrication, AAO films (Fig. 23B-a) have found broader applications in the emerging fields compared to conventional honeycomb structures, such as solar cells [285], magnetic storage devices [286], catalysts [287], carbon nanotubes [288], capacitive humidity sensors [289] and metal nanowires [290,291]. In addition, multifunctional oxide films such as TiO_2 oxide (Fig. 23B-b) and silica oxide (Fig. 23B-c) have been explored to realize certain functionalities. For instance, TiO_2 nano-honeycombs fabricated by a photoetching reaction along the c axes of rutile TiO_2 present regularly ordered quadrangle cells with a few hundred nanometers in width and several micrometers in depth depending on the crystallographic orientation. The topological characteristics of TiO_2 nano-honeycombs including the large area-to-volume ratio and high crystallites enable the utilization in photoelectronic devices such as photocatalysts and dye sensitized solar cells [51].

4.2.1.2. Micro-sized honeycomb-patterned polymer film. In recent years, micro-sized honeycomb films have shown great potential in electronics [292], catalysts [293], photonics [294], superhydrophobic surfaces [295], and optical sensing [296]. Ever since star-shaped polystyrenes (PS) and poly(para-phenylene)-b-PS block copolymers were synthesized in the year of 1994 [297], the breath-figure approach [57] has been widely utilized for the manufacture of polymer films with honeycomb structures. This method is simple, inexpensive and robust in the fabrication of highly ordered honeycomb films compared to other methods such as lithography [298], soft lithography [299], self-assembly [300,301] and transcription [302,303]. Detailed review about the breath-figure

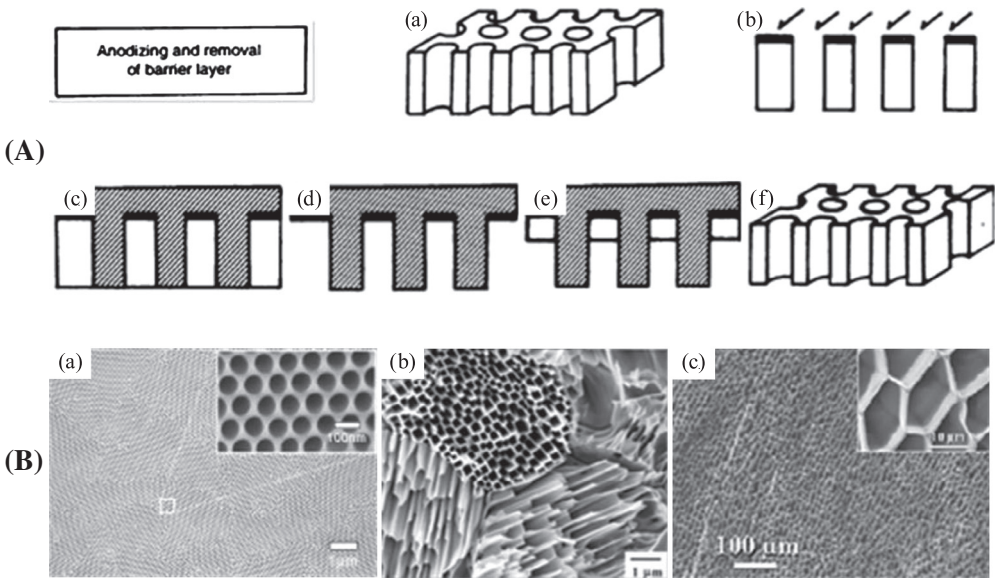

Fig. 23. (A) Schematic of the fabrication process of nanohole array-type metals: (a) honeycomb-like alumina as the parent mode, (b) deposition of metals under vacuum evaporation, (c) injection and polymerization of methylmethacrylate, (d) poly(methyl methacrylate) negative type, (e) electroless metal deposition, and (f) honeycomb-like nano array [27]. (B-a) Morphological images in top and cross-sectional view of the as-prepared AAO film after 10 h processing of second step anodization in 0.3 M oxalic acid [126]. (B-b) SEM image of TiO_2 surface after photoelectrochemical etching under strong (+1.0 V) anodic polarization [51]. (B-c) SEM image of cross-section and channel morphology structure of a typical silica microhoneycomb [48].

formation of self-assembled polymeric- and nanoparticle-based micro- and nanostructures was given by Bunz [304]. Escalé et al. [305] also reviewed recent developments in the preparation of elaborate functional honeycomb polymer films by the processing approach of breath-figure (Fig. 24), and the advances in the design concepts and technologies of functional polymeric surfaces having either stimuli-responsive or super-hydrophobic properties.

4.2.1.3. Mesoporous honeycombs. Mesoporous honeycombs (e.g., mesoporous honeycomb membrane and mesoporous silica nanoparticle) are classified based on cell shape: columnar cells (low porosity) and hexagonal cells (high porosity). Ordered mesoporous silica films are typical columnar honeycombs, attracting great attention for their superior low-dielectric property. A great number of studies have focused on enhancing their mechanical properties to fulfill the need for broad applications [57]. For example, Jung et al. [306] found that the mechanical properties of such films are affected by pore ordering and film density. For a film with random pore geometry, the elastic modulus is positively correlated to film density. While for a modified mesoporous silica film with periodic pore distribution, a negative correlation is observed within a certain density range, which can be advantageous to low-*k* materials. The interests in ordered mesoporous materials with hexagonal honeycomb structures arouse due to their uniform pores, large surface-area-to-volume ratio, particularly attractive as catalysts for the synthesis of crystalline linear polyethylene nanofibers [54] and hydrodesulfurization of petroleum resides [307]. Representative mesoporous materials include siliceous hexagonal SBA-15 and MCM-41, cubic MCM-48 and KIT-6 (with lamellar (MCM-50) well-defined structure) (Table 4). The mesoporous silica SBA-15 template from a tri-block copolymer in strong acidic media has been intensively studied in view of its good hydrothermal stability and well-defined geometry. Particularly, the pore width of SBA-15 can be adjusted from 5 to 30 nm according to the synthesis route, given the accommodation of the bulky reactants and products within a reaction.

4.2.1.4. Molecule-sized honeycombs. Honeycomb patterns at molecule levels maximize net intermolecular separation while preserving the molecular rows, thus holding great potential in catalytic, electronic, mechanical and biological applications. The mechanism for molecule assembly into

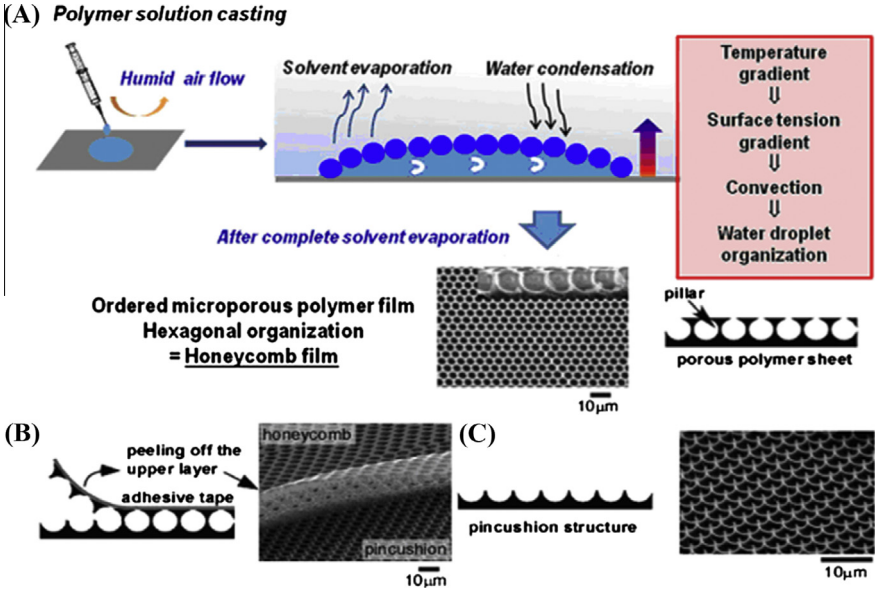

Fig. 24. Schematic illustration and SEM image of (A) the breath figure method and the honeycomb film, (B) the peeling processing, and (C) the pincushion structure [305].

Table 4
Mesoporous honeycomb structures.

Mesoporous solid	Space group	Pore diameter (nm)	Structure	Ref.
MCM-41	*P6mm*	2–5	Hexagonal 1D channel	[277]
MCM-48	*Ia3d*	2–5	Bicontinuous 3D	
SBA-15	*P6mm*	5–10	Hexagonal 1D channel	
SBA-16	*Im3m*	Min 1–6; max 4–9	Body center arrangement of cages	
SBA-1	*Pm3n*	2–4		
SBA-3	*P6mm*	2–4	Cubic 3D	
MSU	*P6mm*	2–5	2D hexagonal	
HMS	*P6mm*	2–5	2D hexagonal Hexagonal	

honeycomb patterns is attributed to the molecular structure and intermolecular bonding characteristics (Fig. 25A) [36]. Trimesic acid is one of the typical assembling molecules that has been extensively studied to form ordered 2D honeycomb networks. Ye et al. [308] summarized 1.1-nm pore diameter hexagonal and other derivative porous networks (Fig. 25B) generated by assembling trimesic acid, and gave a unified unit cell model describing the whole family of its assembling structures. Crystalline structures with the introduction of metal–organic framework contained honeycomb pores of 1.0–2.0 nm in diameter (Fig. 25C) (Table 5) and surface areas up to 3000 $m^2 g^{-1}$ [282,309]. Such materials with exceptionally high surface areas are of critical importance, addressing one of the biggest challenges involving porous media and holding great potential for various applications related to catalysis in chemical engineering, separation technologies and the development and utilization of gas storage [57].

4.2.1.5. Low-dimensional porous materials with honeycomb structures. Typical low-dimensional honeycomb-structured materials include photonic crystal fibers [57], self-assembled honeycomb polyurethane nanofibers [310], nanohoneycomb-structured glass fibers [137,310], hexagonal nanotubes and nanorods, and grapheme and its allotropes [311]. For example, the photonic band gap structures of photonic crystal fibers improve the optical properties of conventional materials through the method of wavelength-scale morphological microstructuring. Knight et al. [312] fabricated a photonic crystal fiber with extra air holes in an otherwise regular honeycomb pattern of holes (Fig. 26A-a), and demonstrated that its guided modes with extraordinary properties are supported by the waveguide. Coffey [313] also demonstrated new types of microstructured optical fibers such as multicore, multimode and hollow core endowed by high porosity honeycomb-spatial properties, targeting next-generation systems with better fiber capacity (Fig. 26A-b). Kievsky and Sokolov [314] found that microscale silica fibers fabricated using self-assembly technique have a nanohoneycomb-structured glass fiber, with a hexagonal cross-section of 2 μm and a length of 5 μm (Fig. 26C). These new fibers can be used as self-healing composite [137,310], chromatography, drug delivery, manufacturing nanowires, and nanoreactors for "1D" chemistry. In addition, there is densely-packed graphene in a honeycomb crystal lattice; and the graphene serves as the basic structural element of graphite, charcoal, carbon nanotubes and fullerenes [311,315]. Through various techniques such as wrapping, rolling and stacking, the graphene can be fabricated into 0D buckyballs, 1D nanotubes and 3D graphite (Fig. 26D) [311], respectively.

4.2.2. Emerging applications

4.2.2.1. Super-hydrophobic surfaces. Super-hydrophobic surfaces endowed by unique porous micro- or nano-structures possess high contact angles and extremely low flow resistance, which is promising for a broad range of engineering applications such as self-cleaning [5], deicing [316,317], corrosion resistance [318], and resistance on current conduction [319]. Cassie and Baxter [320] proposed that hydrophobic or even super-hydrophobic surface can be achieved by constructing topographic structures, where honeycomb and its derived structures have received much attention. Li et al. [321] proposed the possibility of fabricating honeycomb-like aligned carbon nanotube (ACNT) films with a hierarchical structure (Fig. 27A and B) through capillary effects. Mishchenko et al. [316]

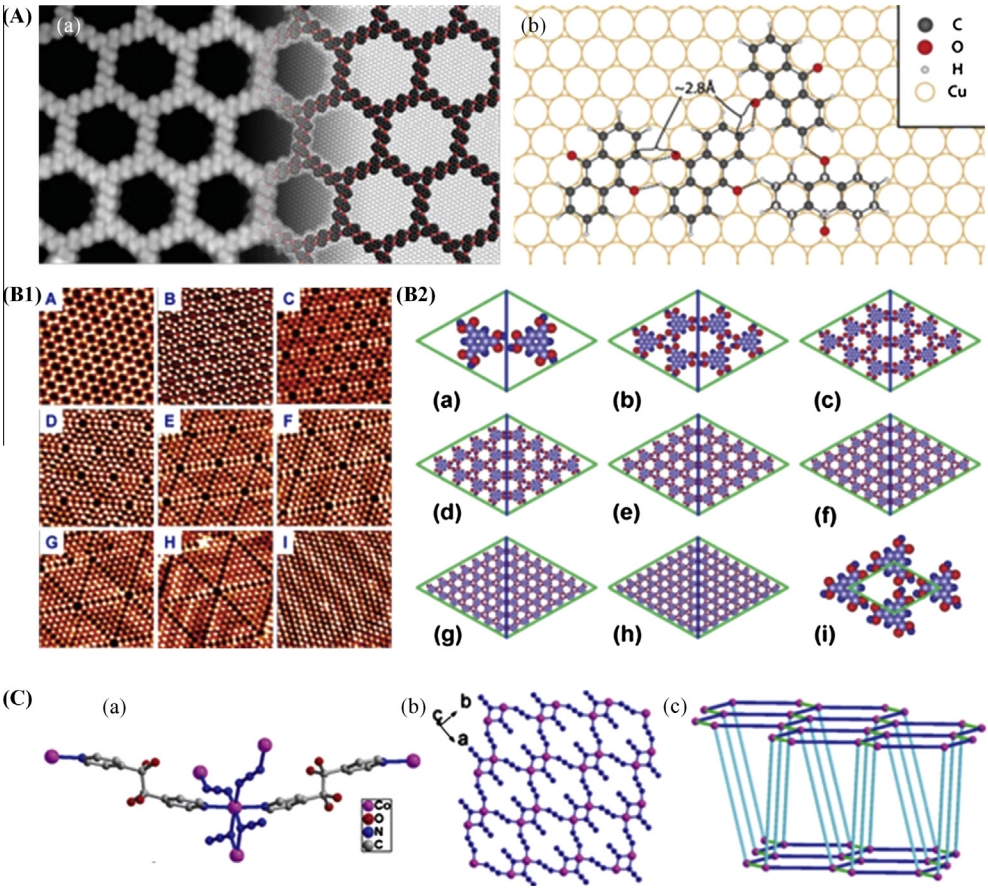

Fig. 25. Some typical molecule-sized honeycomb structures. (A-a) (Left) STM image of the anthraquinone molecules assembled in a honeycomb network on a Cu(1 1 1) surface. (Right) Model of the $(\sqrt{304} \times \sqrt{304})R23^{\circ}$ unit cell. (A-b) A row (left) and a vertex (right) assembly of anthraquinone molecules [36]. (B1) STM images of coverage-induced evolution of the $H_{TMA\text{-}n}$ (n = 1–8 and ∞) self-assembling structures. (B2) Corresponding unit cell models for experimentally observed assembling structures in (B1) [308]. (C-a) Local environment of Co^{2+}; (C-b) azide-bridged (EE and EO) honeycomb layer; and (C-c) Bpg-bridged 3D structure [282].

Table 5
Representative crystalline materials with honeycomb structures.

Material	Main framework composition	Structure	Pore size (nm)	Ref.
Co(N3)2(bpg).S*n*	*meso*-R,â-bi(4-pyridyl) glycol (bpg) ligands	Square, honeycomb, and Kagome	1.36	[282]
Zn4O(1,3,5-benzenetribenzoate)2	MOF-177	Six-membered rings	1.08	[309]

fabricated a silicon membrane with honeycomb-shaped pores (Fig. 27C and D) by reactive ion etching, overcoated with a nanonail architecture of a 7.4-μm-thick organic self-assembled monolayer or fluoropolymer. These super-hydrophobic surfaces can avoid ice accumulation on aircrafts or other structures, which may cause danger and require extra deicing procedures that are expensive and environmentally unfriendly.

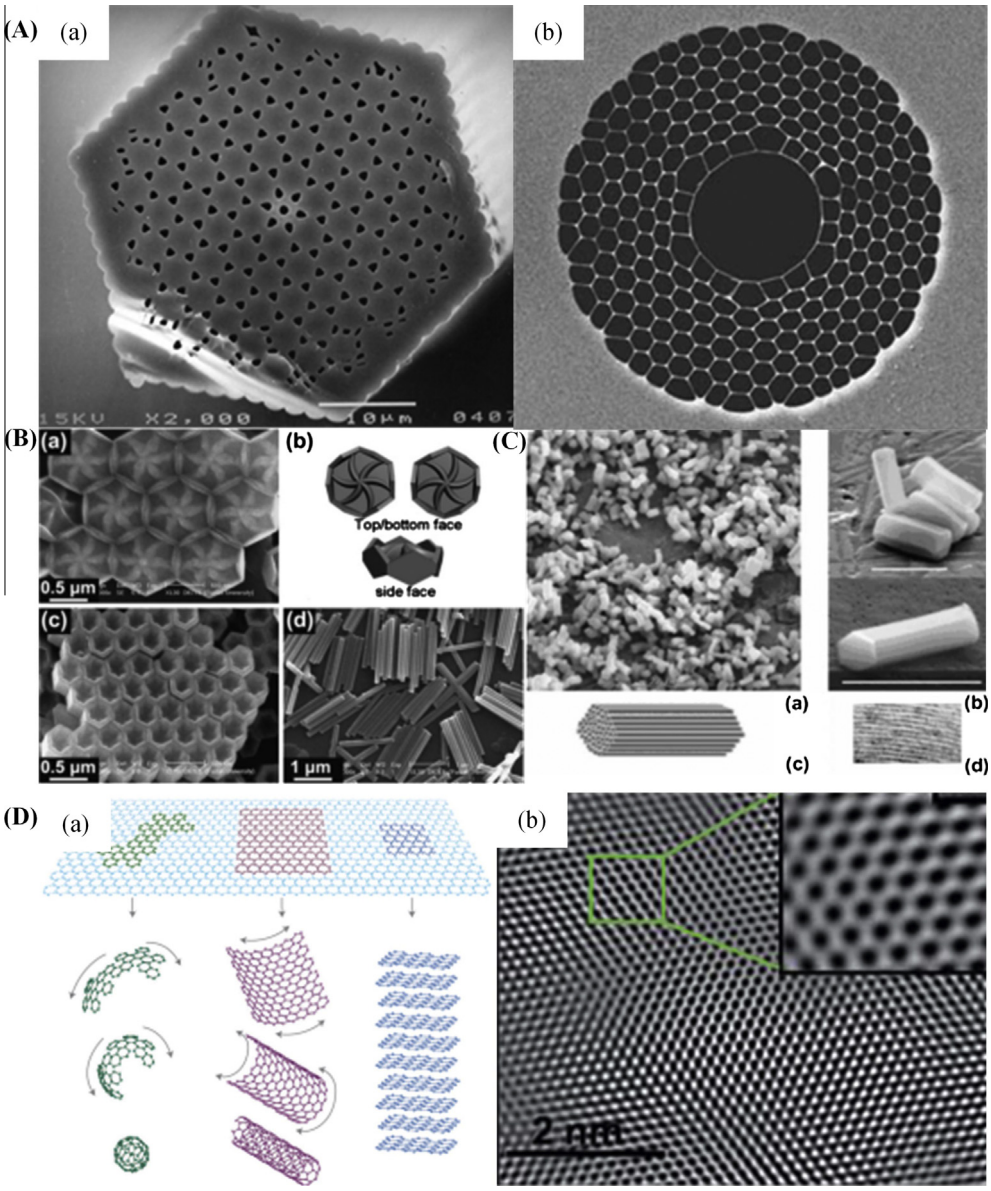

Fig. 26. (A-a) Cross-section of photonic crystal fiber with close-packed hexagonal pattern [312]; (A-b) SEM image of Hollow-core photonic bandgap fiber [313]; (B-a) SEM image of array of flower-patterned hexagonal disk of b-NaYF4. (B-b) SEM images of the top- and side-view of the disk. (B-c) and (B-d) SEM image of array of b-NaYF4 hexagonal nanotube and nanorods, respectively [317]. (C) Self-assembly synthesized glass fibers: (a) large-area SEM image (bar size 22 μm); (b) zoomed image (bar size 5 μm); (c) schematic show of nano configuration within the fiber; and (d) TEM image showing a 3 nm periodicity distribution near the fiber edge. (D-a) Graphene as mother of all graphitic forms such as buckyballs, nanotubes and graphite [311]; and (D-b) High resolution TEM image of graphene [315].

4.2.2.2. Energy conversion. To develop micro honeycomb structures with excellent mechanical properties and high specific surface area has become the focus of 3D design of lithium-ion batteries and efficient solar harvesting devices [322,323], including cathode [46], electrolyte [324], and anode

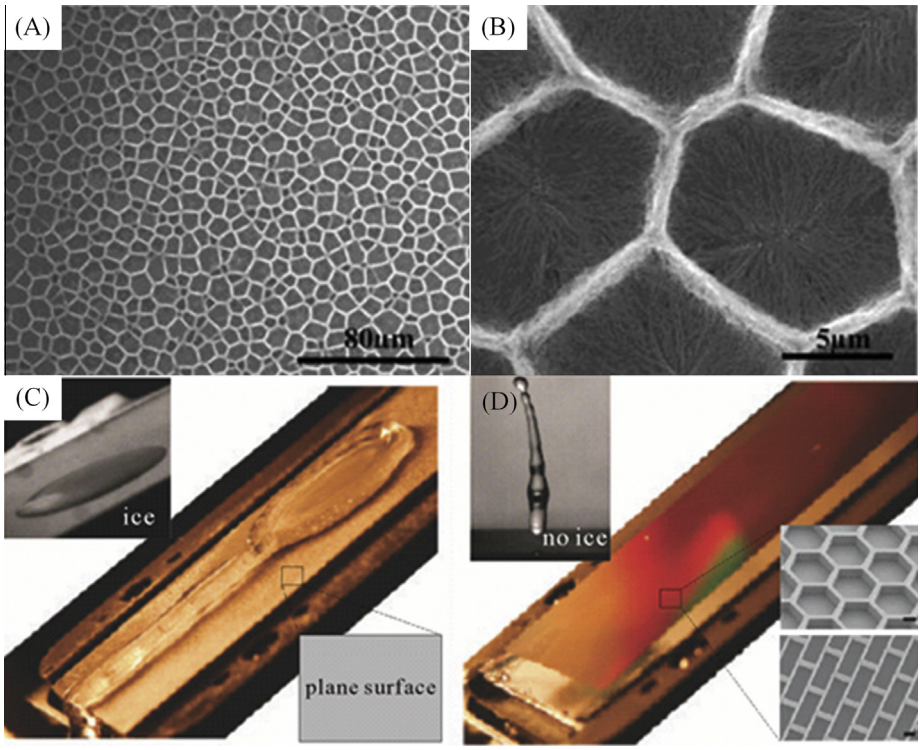

Fig. 27. (A) SEM image of large-area near-honeycomb pattern aligned carbon nanotubes, consisting of hexagonal honeycomb. (B) Higher magnification SEM image of typical honeycomb-like pattern. Ice accumulation on (C) flat aluminum and (D) honeycomb microstructured fluorinated Si surface.

[325]. To improve the storage capacity of Si negative electrode materials and cycling life of Li-ion micro-batteries, Si honeycombs on micro- and nanometer scales are fabricated by photolithography and etching (Fig. 4), which can undergo striking mechanical deformations, achieve higher cycling life and reduce wall cracking by tailoring the thickness and length of cell walls [46]. Kotobuki et al. [324] employed the sol–gel method to fabricate a 3D battery using ceramic electrolyte with two types of LLT ($Li_{0.35}La_{0.55}TiO_3$) honeycomb structure (Fig. 28). This structure reduces internal cell resistance and improves the discharge capacity to 7.3 μA h cm^{-2} operated at 1.1 V. Li et al. [325] prepared honeycomb graphitic-carbon films containing an array of 75 nm diameter pores, and found that these honeycomb carbon films dramatically improve rate capabilities relative to thin carbon films used as Li^+-insertion anodes. In addition, a porous material with hierarchical pore sizes at micro-, meso- and macrometer scales has been proposed to be ideal for overall performance enhancement [48]. For this, "ice templating" method was employed to synthesize nanoporous materials with micro-honeycombs (Fig. 28B), where the ice crystals grow within the precursor and act as a template during the freezing of their parent hydrosols or hydrogels unidirectionally.

Recently, Yin et al. [322] reported is a fundamentally new strategy for the design of next-generation high-power energy storage devices. Based on the principle of "breath figure" method [297,326], they successfully developed a scalable self-assembly strategy to create bioinspired hierarchical structures (microscale honeycomb structure, see Fig. 29D) composed of functionalized graphene sheets, optimizing ion transport and increasing the reversible capacity up to 1600 mA h/g (the highest level ever reported for the pure carbon materials, see Fig. 29F and G). Besides, Yin et al. [323] applied a novel approach to create free-standing hierarchical porous graphene structures, which show a large area of uniform honeycomb structure and favor holding functional nanoparticles

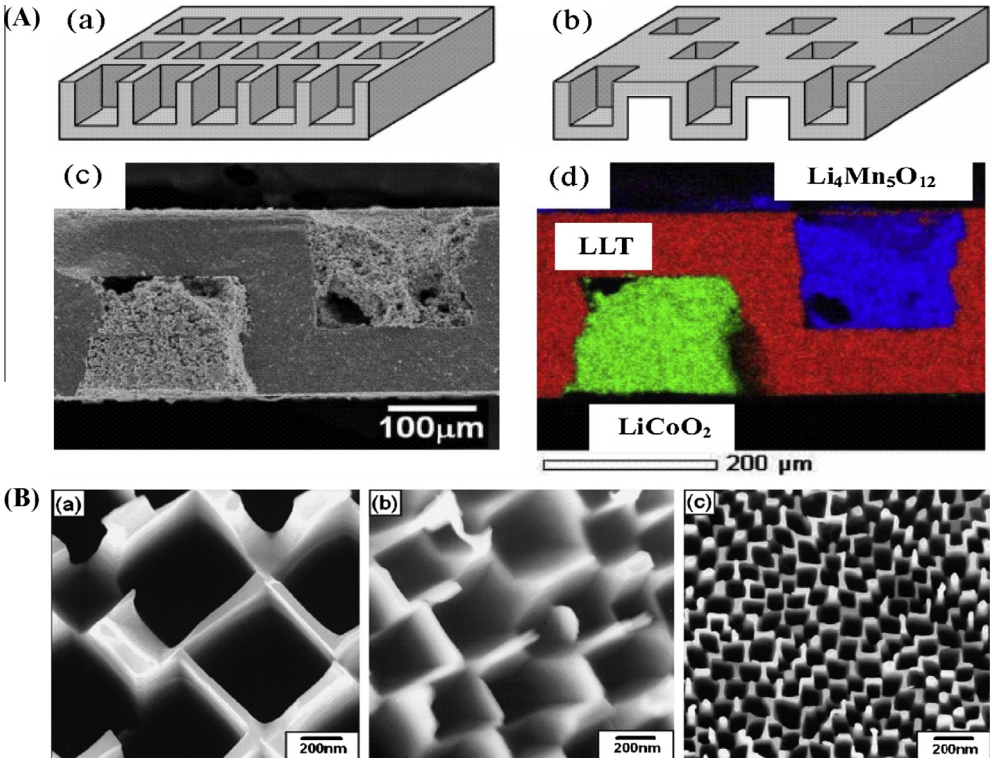

Fig. 28. (A) The honeycomb structure of LLT membrane: (a) half honeycomb with 400 holes on one side and (b) full honeycomb with 200 holes on each side; the hole size was 180 μm × 180 μm × 180 μm. Cross-sectional (c) SEM and (d) EDS images of $LiCoO_2$/LLT/$Li_4Mn_5O_{12}$ cell [324]. (B) SEM image of single crystal TiO_2 electrode prepared by reduction at: (a) 650 °C for 4 h, (b) 700 °C for 4 h, and (c) 1000 °C for 1 h [327].

to form multi-functional composites. Via utilizing such kind of multi-functional composites (combination of the graphene-based free-standing films with TiO_2 nanoparticles), they successfully solved one of the bottlenecks to increase the conversion efficiency in photovoltaic devices, leading to increasing the efficiency of light conversion in solar energy conversion applications.

4.2.2.3. Photonics. Typical photonic band-gap materials had 2D photonic lattice structures, usually represented by honeycomb nano-structures [270], honeycomb photonic bandgap fibers [30], and artificial compound-eye-like structures with honeycomb-shaped microlenses [328]. The search for photonic band-gap materials evoked considerable efforts in the past several years. For example, Meade et al. [329] showed through theoretical modeling that a honeycomb nano-structure of air cylinders in dielectric provided a photonic band gap for all directions normal to the cylinders. Gourley et al. [270] experimentally demonstrated that through the fabricating method of electron beam lithography using Al and Ga, honeycomb nano-structures are capable of possessing stable structures and nonradiative surface recombination; besides, they found that the resonant coupling of light into/out of the lattice occured at selected wavelengths satisfying the Bragg condition. Inspired by insect eyes, Liu et al. [328] explored a simple method to fabricate honeycomb-shaped microlenses on curvilinear surfaces by the femto-second laser microfabrication and the thermomechanical bending process (Fig. 30). Over 7600 hexagonal-shaped microlenses with a diameter of 50 μm were fabricated on a hemispherical poly(methyl methacrylate) shell. The wide field-of-view imaging using the microlens array reached up to 162°.

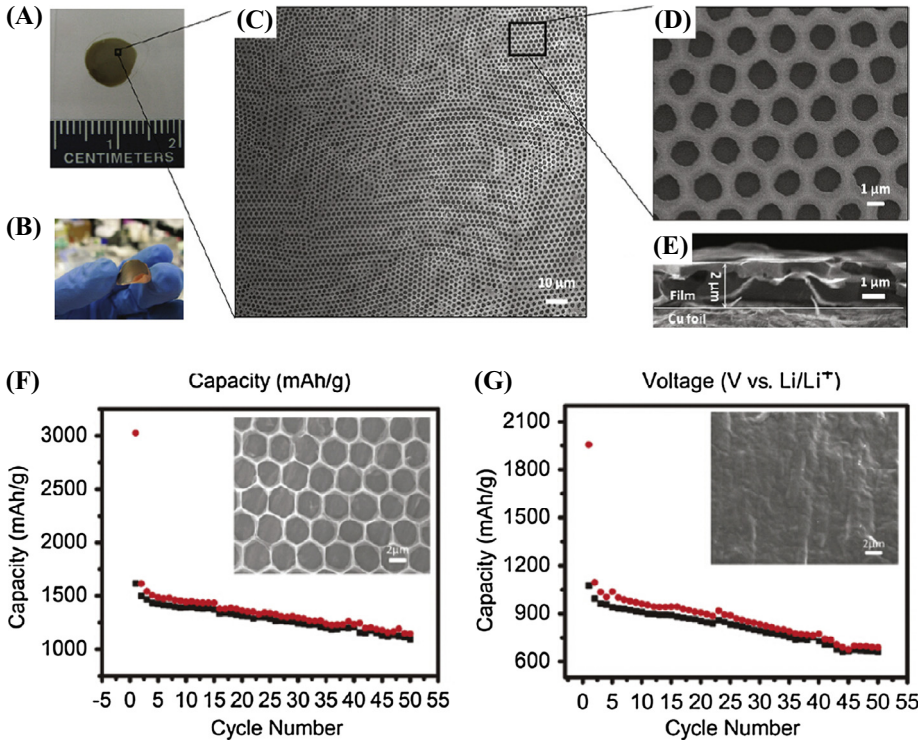

Fig. 29. Configuration and electrochemical properties of the honeycomb structures: (A and B) photograph of the honeycomb film/honeycomb-patterned on the glass/copper foil; (C and D) SEM images of honeycomb-patterned film prepared from 1 mg/mL of the GO/DODA complex on the silicon wafer; (E) cross-sectional SEM image of the honeycomb-patterned film on the copper foil; (F and G) capacity versus cycle number for the honeycomb film and non-patterned film at a current density of 50 mA/g showing charge (square, black) and discharge (circle, red) (the insets are the corresponding SEM images) [322].

4.2.2.4. Microelectronics. Honeycombs are widely found in microelectronic devices typically made from semiconductor materials, such as transistors [330], capacitors [331], inductors [332], resistors, diodes, insulators, and conductors. Zhang et al. [333] successfully synthesized a 2D NiO nano-honeycomb by thermal annealing of Ni thin film deposited onto a silicon substrate for micro-electronics and micro-systems. This opened the door for the integration of nano-honeycombs and micro-systems, leading to nano-scale functional devices. Sazio et al. [334] utilized a hybrid technology to fabricate a large-air-fraction fiber with honeycomb-structure holes to a germanium-filled honeycomb MOF (microstructured optical fiber) by chemical vapor deposition (Fig. 31).

4.2.2.5. Micro/nano sensors. A micro- or nano-sensor is an extremely small element that is capable of picking up and relaying environmental information of biological, thermal, chemical [335], and other forms of signals [336], which are subsequently sent to a processor. Nanotechnology enables designing sensors that are much smaller, have less power consumption, and are more sensitive than the current macrosensors. Nano sensors work by sensing the interaction of molecules, processing and transmitting the data with electrons, and storing the information in nanoscale structures. A variety of honeycomb-structured materials have been explored as substrates for sensor applications. For example, Chen et al. [337] designed a Phenylboronic acid segregated honeycomb-patterned porous film for glucose sensing. Kumeria et al. [338] employed nanoporous anodic aluminum oxide to design interferometric micro-sensor to detect volatile sulfur compounds and hydrogen sulfide gas. Walt and co-workers [339,340] proposed the design of optical multisensor arrays based on optical fibers, where

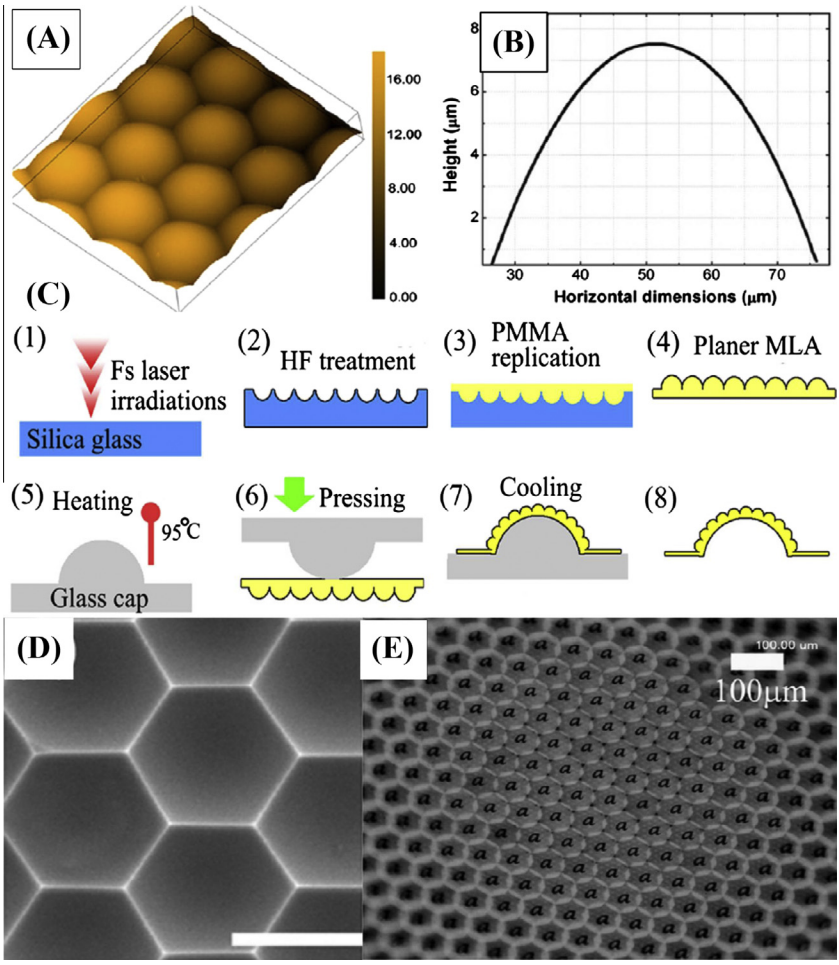

Fig. 30. (A) 3D profile of microlenses on top of hemispherical shell, obtained using a laser confocal microscope. (B) Cross-sectional profile of a microlens shown in (a). (C) Schematic of fabrication process. (D) SEM observation of the morphology of the molding template; the scale bar was 50 μm. (E) Imaging performance of microlens array, obtained via a 5× objective lens [328].

bundles of optical fibers with terminal parts covered with fluorescent polymeric dyes (Fig. 32) were employed to collect signals from the multi-sensor. Upon the interaction with many types of gases, the polymers changed their structure, causing wavelength shifts of emitted light. Graphene, composed of a single layer of carbon atoms packed into a 2D honeycomb lattice, has been recently found to be promising as a low electrical noise material [341], prospering the field of ultra-sensitive and ultra-fast electronic sensors. With a single atom thick, graphene indirectly contacts with the substrate, making the interface state govern the sensing. Nano-sensors designed based on this principle have shown promise in detecting external deposited agents with ultra high resolution [57].

4.2.2.6. Environmental engineering. Free-standing, three-dimensional (3D) ordered porous graphene structure e.g., honeycomb-patterned layer makes an essential step in utilizing the advantages of graphene nanosheets for macroscopic applications, especially the environmentally engineering applications such as antibacterial applications and water treatment [342,343]. Yin et al. [323] introduce a low-cost facile, simple, environmentally-friendly strategy to create free-standing hierarchical porous

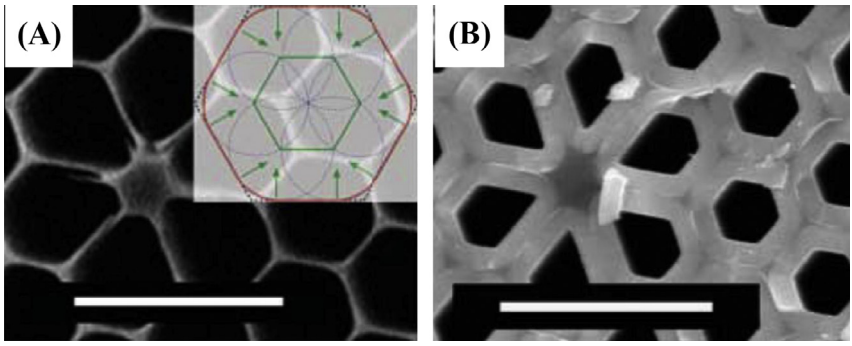

Fig. 31. (A) Unfilled honeycomb MOF template (scale bar, 5 μm); (inset) schematic show of inward surface growing at a uniform rate normal to the local side (green arrows). (B) Honeycomb template after germanium deposition (scale bar, 5 μm) [334].

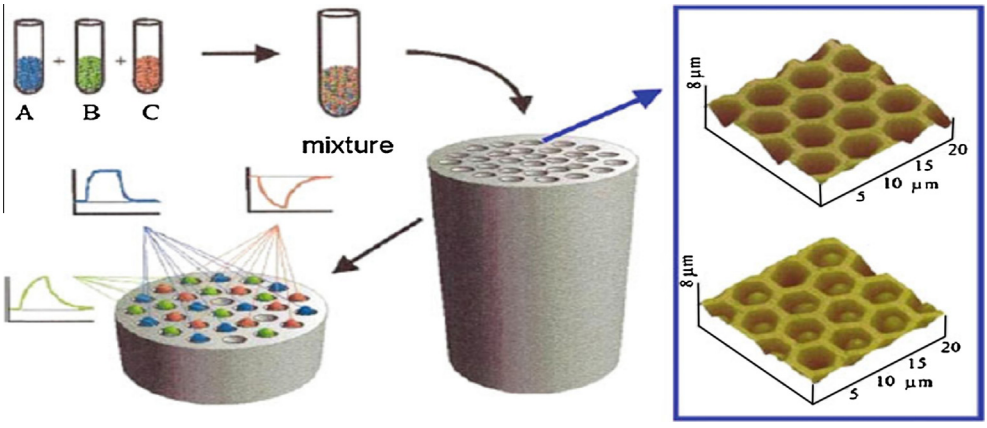

Fig. 32. Schematic of fabricating the matrix of gas-sensitive fluorescent polymer microspheres at the end of an optical waveguide. Inset: micrograph of "honeycomb" structure of the butt-end surface of the waveguide before and after application of polymeric microspheres [339,340].

graphene with uniform honeycomb structures via an "on water spreading" method [344]. They experimentally proved such free-standing hierarchical honeycomb film to be antibacterial without any additional antibacterial agent (see Fig. 33). The fabricated honeycomb film does not contaminate the surrounding environment and is capable of avoiding the possible leaks. The advantage of flexibility, mechanical stiffness and especially antibacterial property of free-standing hierarchical honeycomb film makes it essential potential for environmentally-friendly water treatment.

4.3. Fabrication and applications in biomedicine

Honeycomb structures are also commonly found in biological fields (Table 6). Taking DNA structures as an example, there are two types of unpredictable DNA–lipid complex: the spaghetti-like bilayer-coated DNA complex and the densely packed honeycomb complex. May and Ben-Shaul [345] demonstrated that the spaghetti-like bilayer-coated DNA complex is only marginally stable while the densely packed honeycomb complex is stable over a wide range of composition structures. For cell/tissue morphogenesis, microscope studies have shown that the orderly packing retinal pigment epithelium cells form a layer in the back of the eye behind the retina, representing

characteristic honeycomb-like structure [34]. Recently, the emerging applications of honeycombs in biomedicine have encouraged further research activities although most were preliminary applications in biomedicine [34,35,345–348]. In this section, we review these applications, with focus on tissue engineering and regenerative medicine, biosensors and bioelectronics, bioadsorption and biocatalysis, and drug release.

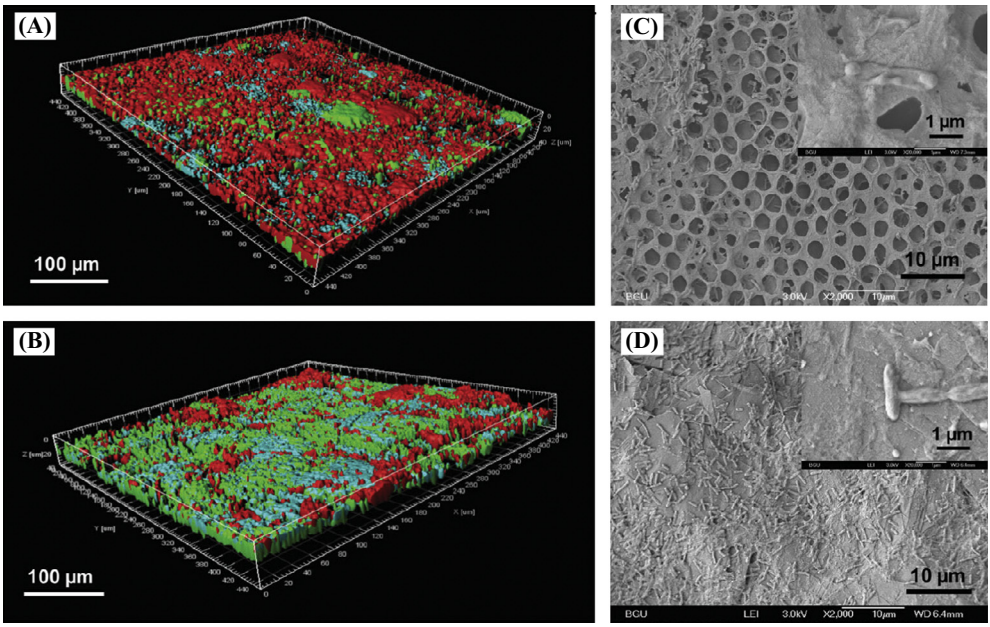

Fig. 33. Antibacterial properties of the free-standing honeycomb film: (A and B) Laser scanning confocal microscopy images of green fluorescent protein labeled *Pseudomonas aeruginosa* PAO1 biofilm on (A) graphene honeycomb film and (B) graphite surface after 48 h incubation; the green, red and blue spot represent live, dead and EPS kit, respectively; SEM images of green fluorescent protein labeled *Pseudomonas aeruginosa* PAO1 biofilm on (C) graphene honeycomb film and (D) graphite surface after 48 h incubation [323].

Table 6
Typical applications of honeycombs in biomedicine.

	Methods	Material	Cells	Applications	Ref.
Film scaffold	Surfactant-free water templating	PLGA	Osteoblast-like MG63	Cell culture	
Surface	–	Nanoculture plate	MPCs	3D cell culture	[375]
Building blocks	Directed self-assembly	NHF, KGN	NHF, KGN	Tissue engineering	[45]
3D scaffold	Direct-write assembly	pHEMA	Primary rat hippocampal neurons	Cell culture	[374]
	Ionotropic gelation	Alginate	ECs, HSMCs	Co-culture	

pHEMA = poly(2-hydroxyethyl methacrylate).
PLGA = poly(lactide-co-glycolide).
MPCs = human bone marrow-derived mesenchymal stem/progenitor cells.
NHF = normal human fibroblasts.
KGN = human granulosa cells.
ECs = endothelial cells.
HSMCs = human smooth muscle cells.

4.3.1. 2D honeycomb-patterned substrates

Mesoscopically honeycomb-patterned porous 2D substrates (e.g., honeycomb films), with submicron to micron pore sizes, are of particular interest for biomedical application as biointerface [349], cell culture substrates [350–353], separation membranes for blood cells [354], immobilization of biomolecules [355], dialyzer [356,357] and oxygenator membranes [349]. To design honeycomb substrates for biomedical applications, great efforts have been devoted to developing grafting and cross-linking honeycomb films [351]. For example, Connal and Qiao [53] reported preparation of hierarchically porous poly(dimethylsiloxane)-based honeycombs by forming honeycomb-structured porous polymer films on non-flat honeycomb grid surfaces (Fig. 34A). Zhang et al. [358] developed a highly efficient breath figure approach that enables the fabrication of highly ordered honeycomb films prepared over large non-planar honeycomb grid surfaces, which may facilitate commercial utilization of the micro-fabrication technique for a variety of surfaces. Further, it has been found that the more important factor for affecting the occurrence of cracking during the formation of honeycomb film is not the glass transition temperature but the Young's modulus of a polymer (Fig. 34B).

Honeycomb-patterned substrates have been employed in an early stage for cell culture [352,353]. To explore the effect of honeycomb pattern on cell behavior, hepatocytes were cultured on polymer subtracts with various honeycomb patterns fabricated by self-organization technique [57]. The hepatocytes are flattened with cultured on a flat film, where actin filaments spreading around the regions (Fig. 35A and B); while hepatocytes form spheroids when cultured on a honeycomb film with actin filaments located inside the edge of the spheroid pattern (Fig. 35C and D). However, endothelial cells cultured on the honeycomb films exhibit greater spreading and flattening capabilities (Fig. 35E and F) [359]. Besides honeycomb patterns, the texture of the substrate also plays an important role in cell behavior. For instance, Fukuhira et al. [360] demonstrated that NIH3T3 fibroblasts cultured on honeycomb patterned poly(D,L-lactide) film fabricated with dioleoylphosphatidylethanolamine show better cell proliferation compared those that on film fabricated with copolymer of dodecylacrylamide and o-carboxyhexylacrylamide. Sunami et al. [57] reported that the honeycomb film with site-selectively adsorbed fibronectin plays a key role in cell adhesion and proliferation. These findings reveal that honeycomb-patterned films are suitable to act as 2D substrate for cell culture or 2D scaffold with enhanced cell adhesion and proliferation.

4.3.2. 3D honeycomb scaffolds

Today, tissue engineers are attempting to engineer virtually every human tissue, including cartilage, bone, heart valves, nerves, muscle, bladder, liver, etc. Besides, due to the complex cell microenvironments with different physical and biochemical properties, there is no surprise that cell behaviors in 3D culture are unexpectedly different as compared to those in 2D culture [361–363]. In particular, to understand the effect of organized 3D cell microenvironments on neuronal cell development, engineering of 3D cell microenvironments is needed to imitate neuronal cells and mimic their surrounding native microenvironment. New tissue engineering strategies mainly aim on designing 3D porous biomaterial scaffolds to provide a 3D structure to enhance nutrient delivery, as well as mechanical support for cell behaviors (e.g., attachment, proliferation and differentiation), and their architecture defines the ultimate shape of the newly grown soft or hard tissue [364,365]. Among various 3D porous biomaterial scaffolds, 3D honeycomb scaffolds have attracted great attention due to their high porosity and good mechanical performance, which render them great potential as 3D porous scaffolds for tissue engineering and regenerative medicine.

Early scaffolds were not fabricated with precise porous architecture. Hutmacher [55,366] gave the first report on various honeycomb scaffold architectures manufactured by a promising rapid prototyping (RP) technology – fused deposition modeling (FDM) for tissue engineering applications (Fig. 36A). The research results show that these highly reproducible and economical honeycomb scaffolds have good mechanical properties [367,368], as well as excellent biocompatibility with human fibroblast and periosteal cell culture systems [367]. FDM has attracted wide attention [369], and made an enormous influence on the extending development of such honeycomb rapid prototyping technique series as extrusion-based RP techniques, three dimensional printing, selective laser sintering, stereolithography, microstereolithograph, electron beam melting, and selective laser melting [370,371]. Recently, Fratzl group made an important impact, and the theoretical and experimental study of

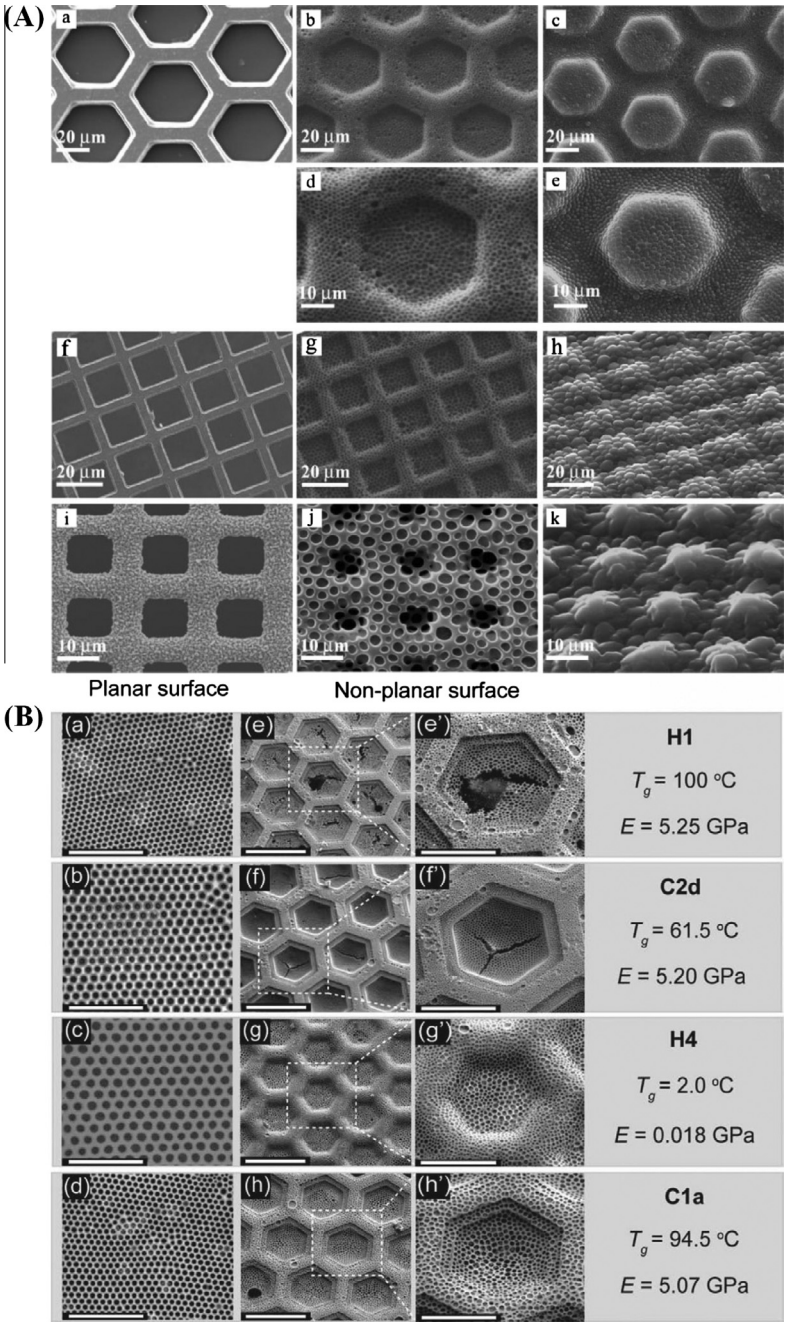

Fig. 34. (A) SEM image of the honeycomb morphology for: (a) honeycomb grid with hexagonal cells in the scale of 600 mesh; (b) honeycomb with hexagonal cells formed on surface in the scale of 600 mesh; (c) image of replica-molding honeycomb (b) is the parent mode); (f) 1000 mesh square honeycomb grid; (g) surface-embossed honeycomb with 1000 mesh square; (h) image of replica-molding honeycomb (g) is the parent mode; (i) 2000 mesh square honeycomb grid; (j) surface-embossed honeycomb with 2000 mesh square; (k) image of replica-molding honeycomb (j) is the parent mode [53]. (B) SEM image of polymer film with honeycomb morphology prepared from star polymer on (a–d) planar and (e–h and e′–h′) non-planar honeycomb grid substrates. Scale bars: (a–d) 10 μm, (e–h) 100 μm, (e′–h′) 50 μm [358].

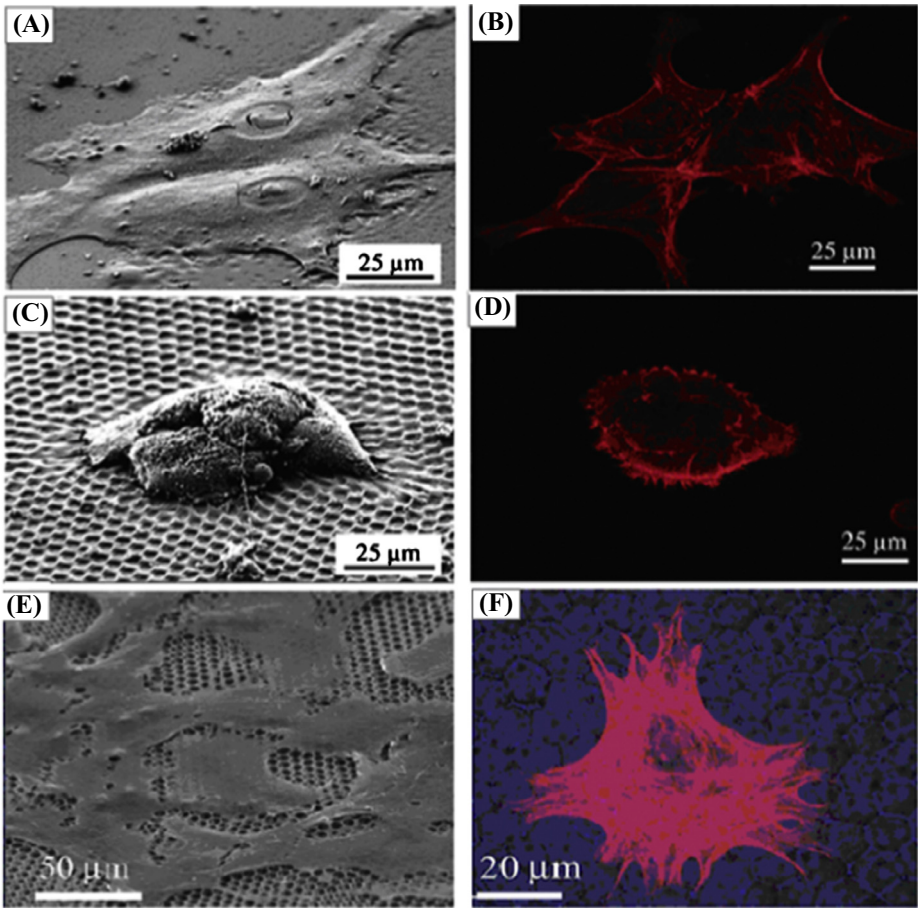

Fig. 35. SEM image of hepatocytes and CLSM image of actin localization in adhered hepatocytes at 72 h after culture on (A and B) flat film and (C and D) honeycomb film where approximate 100 μm spheroids was spread. There were not deformation and detachment of spheroids from honeycomb film could be observed [346]. (E) SEM and (F) CLSM image of vascular endothelial cell on honeycomb film [359].

cross- and square-shaped honeycomb hydroxyapatite scaffolds supports that the pore shape of scaffolds also contributes significantly to control the kinetics of tissue deposition [372,373]. These results suggest that the optimization of pore shapes may improve the speed of ingrowth of bone tissue into porous scaffolds (Fig. 36B).

High performance honeycomb scaffolds provide important material basis on tissue engineers and regenerative medicine. In addition to Hutmacher and Fratzl groups' outstanding contribution to honeycomb application on biomedical engineering, other related applications are introduced as follows. Shepherd et al. [374] fabricated 3D micro-periodic square honeycomb scaffolds by direct-writing assembly of photopolymerizable poly(2-hydroxyethyl methacrylate) hydrogel ink. The hydrogel honeycomb scaffolds is a preferred culture system with kind of robust and biocompatibility for primary hippocampal neurons, facilitating 3D in vitro studies of hippocampal neurons and other sensitive cell types. For cancer study, 3D cell culture improved the prospect of treating cancer with gene therapy [361]. Miyagawa et al. [375] used a micro-fabricated honeycomb scaffold with diameter of approximately 2–3 μm to induce spheroid formation of human bone marrow-derived mesenchymal progenitor cells and promote efficient adipogenic differentiation. For myocardial repair

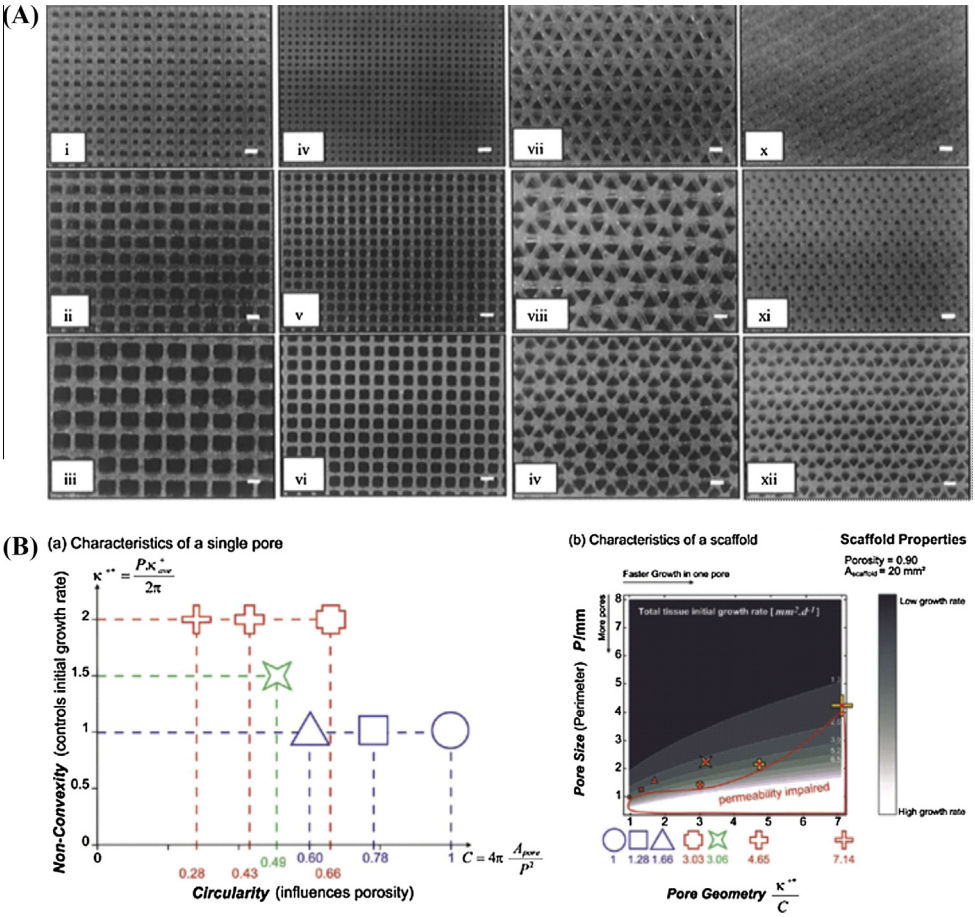

Fig. 36. (A) Cross-sectional view of various 3D honeycomb scaffold systems fabricated by FDM. Scale bar represents 1 mm. (i)–(iii) lay-down pattern: 0/90°; nozzle tip: 0.016″; porosity: 50, 68, 75%; (iv)–(vi) 0/90°; 0.010″; 50, 68, 75%; (vii)–(viii) 0/60/120°; 0.016″; 68, 75%; (ix) 0/60/120°; 0.010″; 80%; (x)–(xii) 0/60/120°; 0.010″; 50, 68, 75%. (B-a) Pore shapes can be classified using the "non-convexity" which determines tissue growth rate in the pore and the "circularity" which influences the number of pores fitting in a scaffold. (b) Contour plot representing the influence of pore geometry and pore size on the total tissue growth rate in a 20 mm^2 scaffold with a porosity of 0.9.

by tissue-engineered grafts, present scaffolds such as non-woven poly(glycolic acid) (PGA) mesh and collagen foam are structurally incompatible with the anisotropy features of recapitulating cardiac. Novel microfabrication techniques have thus been developed to create porous, elastomeric 3D scaffolds with accordion-like honeycomb microstructure [376]. Due to its controllable stiffness and anisotropy, accordion-like honeycomb is able to sustain the structural–mechanical limitations of prevalent scaffolds, beneficial for the grafts with aligned heart cells and mechanical properties that more closely resemble native myocardium (Fig. 37). Subsequently, through the approach of laser ablation and oxygen plasma-mediated lamination, Park et al. [377] successfully controlled the pore microarchitecture on the multi-layered elastomeric PGS scaffolds. The results suggest that multi-layered PGS scaffolds are found to be suitable for myocardial repair applications that require mechanical support, cell delivery and active implant contractility. For bone repair, Schantz et al. [378] fabricated 3D polycaprolactone (PCL)–hydroxylapatite (HA) honeycomb-like scaffolds. Mineralized matrix deposition and calcification of tissue as well as irregular osteoid formation can

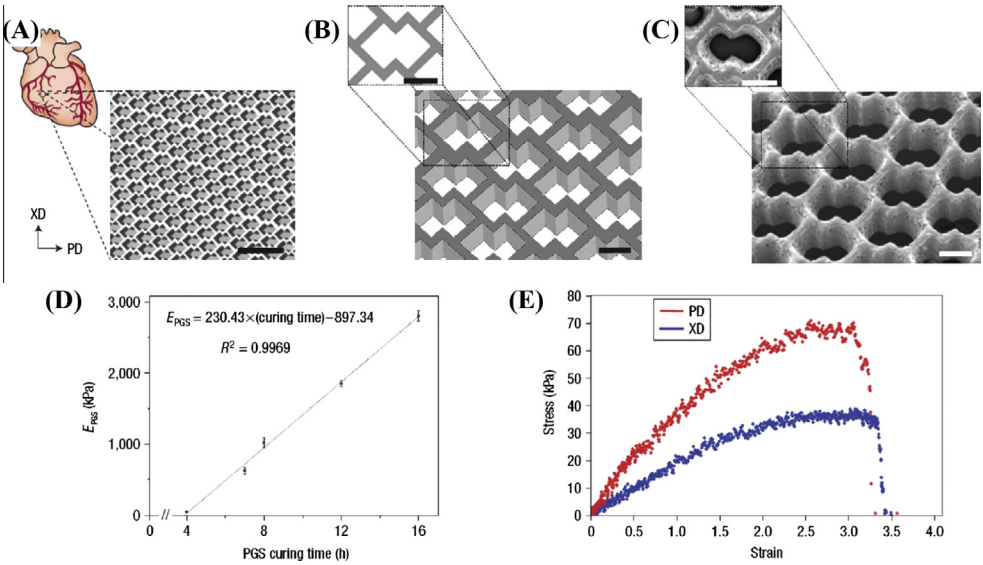

Fig. 37. Accordion-like honeycomb scaffolds. (A and B) Schematic show of accordion-like honeycomb with diamonds overlapped design. Preferred (PD) and orthogonal cross-preferred (XD) material directions, corresponding separately to circumferential and longitudinal axes of the heart, were indicated. (C) SEM image of the fidelity of excimer laser microablation in rendering an accordion-like honeycomb design in PGS. Scale bar: (A) 1 mm, (B) 200 μm and (C) 200 μm. (D) PGS curing time was systematically varied, yielding a linear dependence of PGS effective stiffness (EPGS) on curing time within the tested range. (E) Representative uniaxial stress–strain plots for accordion-like honeycomb scaffolds with cultured neonatal rat heart cells (scaffolds fabricated from PGS membranes cured for 7.5 h at 160 °C; neonatal rat heart cells cultured for 1 week) [376].

be observed in explants. From colloidal crystal templates, 3D honeycomb-structured periodic hydrogel scaffolds with a 3D honeycomb-like structure have been fabricated with tunable internal dimensions and adjustable gel stiffness down to that of soft tissues [379]. These findings demonstrate the possibility of using 3D honeycomb scaffolds to investigate, in realistic 3D tissue models, the mechanisms that influence cell migration and other cell functions (e.g., screening compound libraries aimed at preventing tissue invasion during cancer metastasis).

4.3.3. Cell encapsulated honeycomb cellular constructs

By allowing inclusion of such bioactive components as growth factors, cells and drugs, cell encapsulated cellular construct systems offer new opportunities in tissue engineering and regenerative medicine [380–382]. Hutmacher et al. [383] present a milestone in scaffold fabrication by developing solvent-free and aqueous-based systems in which cells can be encapsulated into the scaffolds during the fabrication process. For instance, Zhang et al. [384,385] developed a novel method based on robotic micro-assembly to fabricate honeycomb scaffold with truncated-square cell and encapsulated cells for a variety of tissue-engineering applications.

In addition, 3D honeycomb-structured hydrogels have recently used to encapsulate and culture cells for tissue engineering and regenerative medicine, which possess improved properties for mechanical supporting and efficient nutrient delivery [386,387]. For example, Xu et al. [388] recently fabricated 3D tissue constriction structures by assembling square honeycomb building blocks with magnetic field [388], acoustic field [389] and electrical interaction [390] (Fig. 38A). To fabricate large living tissues, Tejavibulya et al. [45] used the approach of cell-to-cell adhesion and directed self-assembly to successfully fabricate the honeycomb building blocks with scaffold-free multi-cellular structure (Fig. 38B). To maintain cell viability, a critical diffusion distance is required, which restricts the size of spheroid building blocks. This kind of fabrication routine, however, unlimited the overall size of the honeycomb [388]. In addition, the emerging bioprinting technologies,

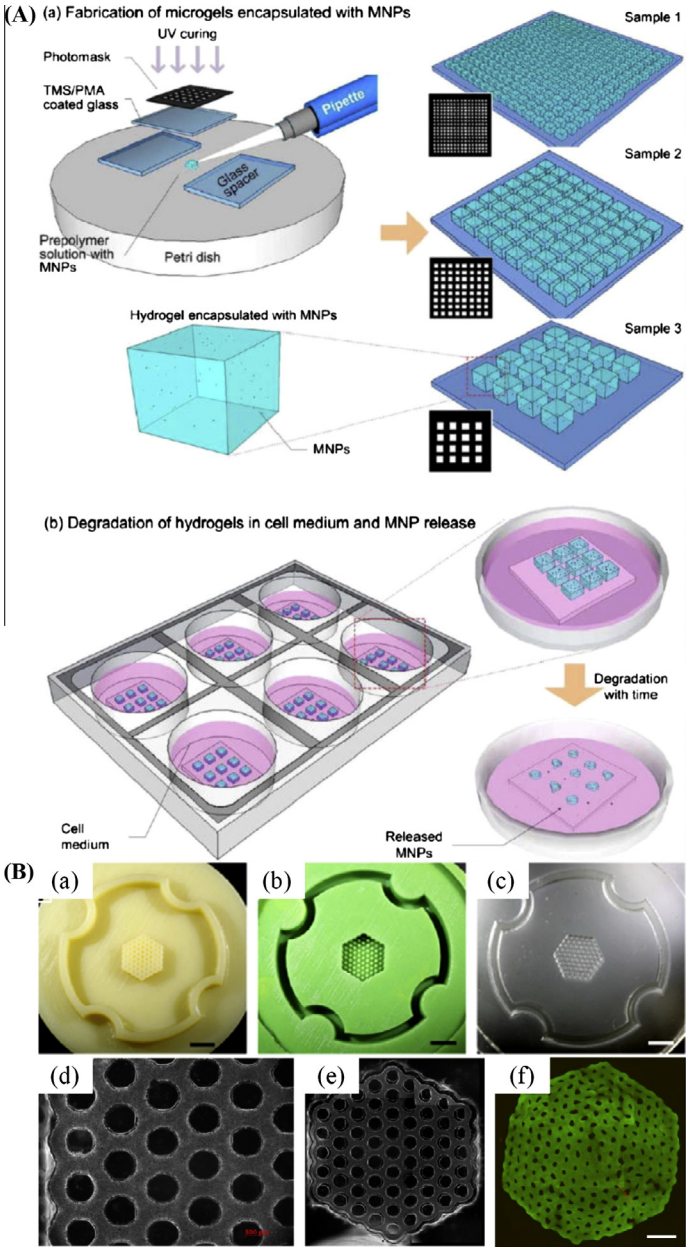

Fig. 38. (A) Schematic show of magnetic nanoparticle (MNP) encapsulation and release from hydrogels. (A-a) Fabrication of cell encapsulating hydrogels with MNPs. (A-b) Degradation of hydrogels and release of encapsulated MNPs. Wax prototypes and replicates of two honeycomb designs [388]. (B) Photographs of wax prototypes produced by a ThermoJet® rapid prototyping machine from CAD design of a four-orbital (B-a) honeycomb. Positive Reprorubber replicates of the four-orbital (B-b) honeycomb design. Negative PDMS replicates of the four-orbital (B-c) honeycomb design. Large multi-cellular honeycombs. NHF (B-d and B-e) cells were seeded onto a hydrogel micro-mold where they self-assembled into a single four-orbital multi-cellular honeycomb microtissue. The eight-orbital honeycomb of NHF (6×106 cells) formed in an agarose micro-mold was stained for viability with a live/dead assay after 24 h of culture. (B-f) The merged fluorescent images joined together from nine locations were shown. Scale bar: 1800 μm [45].

with the advantages for depositing cell-encapsulated droplets in a controlled and high-throughput manner, may greatly promote the development and application of cell encapsulated honeycomb cellular constructs [391–393].

4.3.4. Biosensors and bioelectronics

Besides tissue engineering and regenerative medicine, honeycomb structures with high specific surface area as electrodes have also been applied in biosensors and bioelectronics fields [394]. Fulati et al. [395] found that the nano-honeycomb flake ZnO material provided 1.8 times higher sensitivity than previously used ZnO nanorods under the same conditions. Also microsensors have been used in various applications involving the detection and measurement of the environmental and atmospheric hazardous chemicals as well as body glucose. Suneesh et al. [396] reported an electrochemically anodized Ta_2O_5 honeycomb nanostructure as the non-enzymatic glucose sensor. Morphological studies proved that the nanopores were highly uniform with an average diameter of 30 ± 2 nm, and the pore size was reduced to 24 nm and 18 nm during subsequent electrodeposition of Pt and CuO inside the nanopores. The non-enzymatic glucose sensor with high specific surface area has high sensitivity (response time <3 s), selectivity, specificity (free of interfering from ascorbic acid, uric acid, dopamine and acetaminophen), and wide range of detection (and a low detection limit of 1 μM; linear response to glucose up to 31 mM) (Fig. 39) [396]. Similarly, fourfold and threefold greater activity have been found in the fibers with mesoporous honeycomb structure than conventional non-templated silica samples and horseradish peroxidase immobilized silica powders, in respective [397]. It is worth noting that honeycomb-derived graphenes as emerging bioelectronic platform have huge

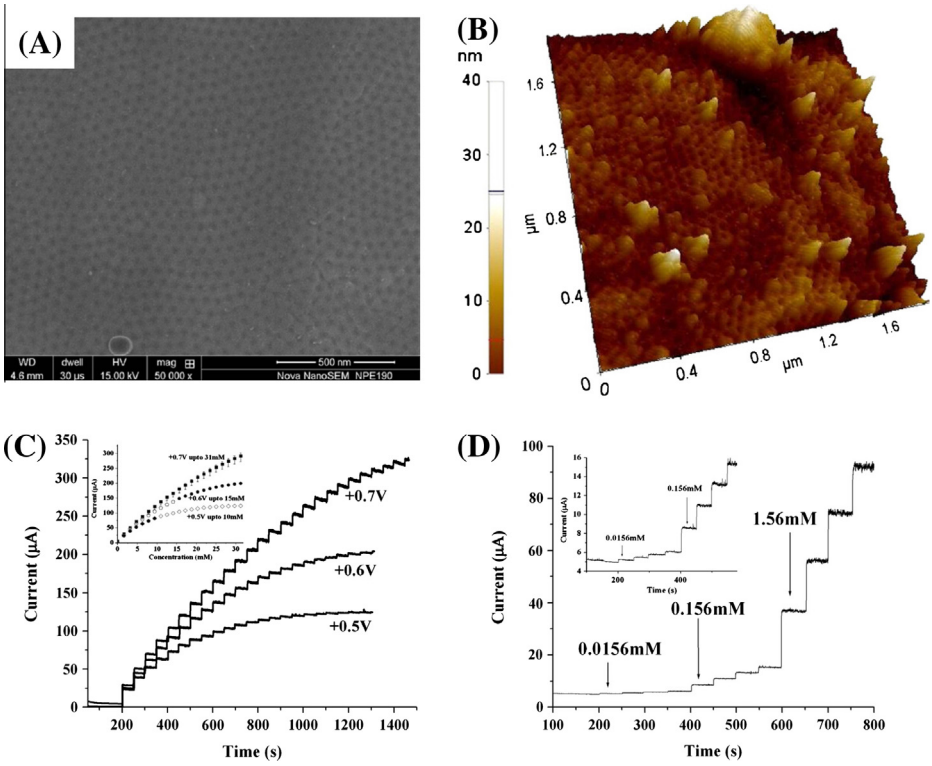

Fig. 39. High resolution SEM image of CuO/Pt/tantalum oxide honeycomb nanostructure (A) and corresponding AFM image (B). Steady state response current recorded on sensor electrode at different potentials in a constantly stirred solution of 0.1 M NaOH with repeated additions of 1.5 mM glucose (C) and different glucose concentrations (D) [396].

potentials for next-generation biosensors due to its chemical robustness and sensitivity to electromagnetic environment changes [398,399].

4.3.5. Bioadsorption and biocatalysis

Adsorption and biocatalysis of small biomolecules has great impact on basic and applied research in biomedicine. For example, protein adsorption can cause blood clotting and heart disease [400]. What's worse, even a small amount of deposited proteins may lead to subsequent adsorption of fibrous proteins [401]. Hence, over the past few years, encapsulation of enzymes and other proteins into inorganic host materials for bioadsorption and biocatalysts applications have attracted considerable attention. Nano-honeycomb structures and materials play an important role in bioadsorption and biocatalysis, such as adsorption of small biological molecules. Hartmann [402] summarized the adsorption of biologically interesting compounds over twenty different kinds of ordered mesoporous silica (MCM-41, MCM-48, FSM-16, SBA-15, etc.) and carbon molecular sieves (CMK-1, CMK-3). Although the latter can solve the stability of mesoporous silicas upon prolonged exposure to aqueous solutions, the absorption amount (e.g., of lysozyme) is significantly lower than that for the former in spite of similar trends with respect to solution pH, pore volume, and pore diameter as observed. Popat et al. [403] indicated that research interests are directing toward the synthesis and evaluation of highly ordered, small size and ultra large pore size (20–50 nm) MSNs (mesoporous silica nanoparticles), which will facilitate immobilization of a broader range of enzymes and increase the application of these materials in bioadsorption and biocatalysis areas. Protein enzymes play a vital role in biocatalysis. They are the main carrier for chemical transformations on organic compounds. Because pure mesoporous media is neutral in charge and offers only mild acidity, not pure but dopant (i.e., trivalent metal ions M3+) incorporated ordered mesoporous media acted as a carrier for protein enzymes. For instance, Yue et al. [404] and Vinu et al. [405] reported direct synthesis of AlSBA-15 and found that AlSBA-15 had a higher catalytic activity in cumene cracking and tert-butylation of phenol, compared with AlMCM-41. Vinu et al. [405] directly synthesized AlSBA-15 with high aluminum content and controllable pore diameters by simply adjusting the molar water to hydrochloric acid ratio (nH$_2$O/nHCl).

4.3.6. Drug release

Nano-honeycomb structures and materials including mesoporous silica-based media and mesoporous carbons have been widely used in drug delivery research for nanomedicine applications, especially as drug carrier due to their ordered pore network, high porosity and high surface area [406,407]. Since MCM-41 was first proposed as drug-delivery system in the year of 2001 [408], the mesoporous silica-based media (MCM-41, MCM-48, and SBA-15) have been successfully employed

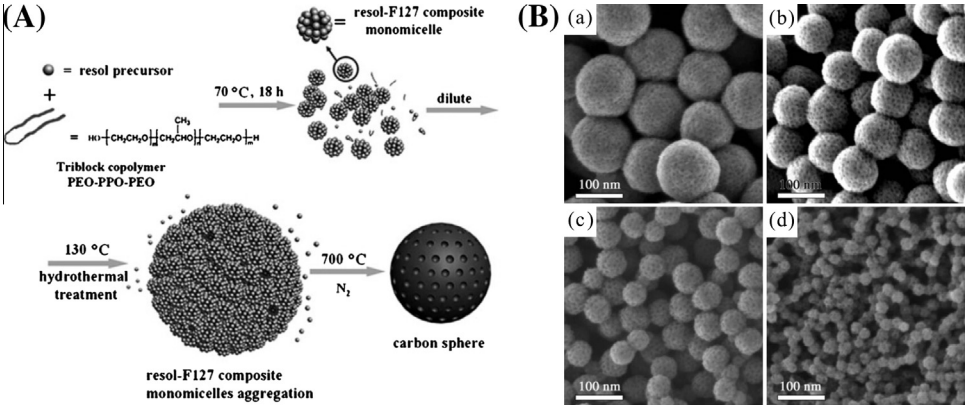

Fig. 40. (A) Formation of uniform ordered mesoporous carbon nanospheres. (B) HRSEM images of ordered mesoporous carbon nanospheres prepared by a low-concentration hydrothermal method at 130 °C: (a) MCN-140, diameter 140 nm; (b) MCN-90, diameter 90 nm; (c) MCN-50, diameter 50 nm; and (d) MCN-20, diameter 20 nm [347].

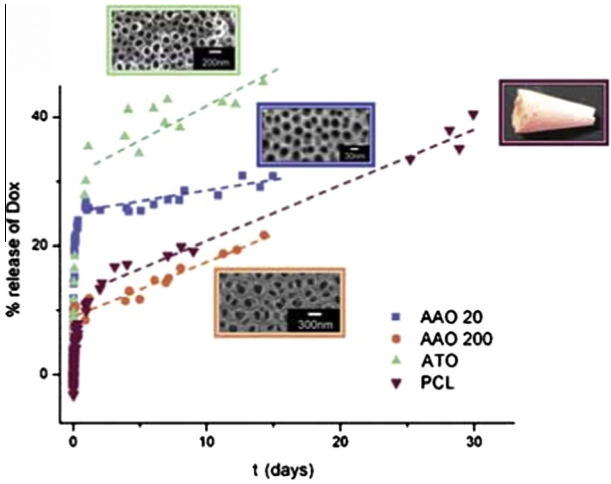

Fig. 41. Representative curves for the percentage of Dox released from such platforms as anodic aluminum oxide (AAO-20 with 20 nm pore diameter and AAO-200 with 200 nm pore diameter), anodic titanium oxide (ATO), and biodegradable polycaprolactone (PCL) [422].

as carrier for a multitude of drugs such as antipyrine [409], amoxicillin [410], alendronate [411], captopril [57], erythromycin [412], gentamicin [413], ibuprofen [414], naproxen [415], nimodipine [416], sertraline [57], taxol [417], and vancomycin [418]. However, the potential issue of possessing some sign of toxicity limits the universal use of silica-based mesoporous materials as drug carrier [57]. Nontoxic mesoporous carbon can be used as a new drug delivery medium. Surfactant templating techniques have been successfully employed to synthesize mesoporous carbons by using precursors such as phenol [57], phloroglucinol [57], resorcinol [419], and hexaphenol [420]. Fig. 40 showed a schematic of surfactant-templated synthesis of a mesoporous carbon and a high-resolution SEM (HRSEM) image of mesoporous carbon nanospheres with honeycomb-like structure fabricated by the hydrothermal method of low-concentration [57].

Nano-honeycomb structures and materials are intended for both systemic-delivery systems and implantable local-delivery devices in medical implants [421]. Those materials are usually loaded with therapeutic agents to reduce infections, enhancing implant bonding and preventing restenosis in cardiovascular stents. For instance, Gultepe et al. [422] found that nonerodible (biocompatible nanoporous coatings) as alternatives to polymeric systems, such as anodic aluminum oxide (AAO), are suitable for sustained drug release up to weeks from implants for a variety of therapeutic situations (Fig. 41).

5. Conclusions and future perspectives

Ancient honeycombs, both familiar and strange to us, are still vigorous. Relevant researches have exceeded their original areas of honeycomb, starting from the aesthetic to mechanical properties, and have extended from single function design awareness to hierarchical/hybrid and multi-functional structure design, especially with significant advances in nano- and bio-technologies. At the same time, honeycomb structures used in traditional fields are constantly developed, including new decorative design with honeycombs, magnetic shielding structure of composite honeycombs, and corrugated structure filled with honeycombs (Fig. 42) [424]. Even research on old honeybee combs is still increasing [57]. Current scientific advances in: (i) the design principles for products with honeycomb structures, including their fabrication, performance (e.g., mechanical, thermal and acoustic properties) as well as optimization design; (ii) micro- and nano-technologies that hold great promise for bioinspired honeycomb structures and the related emerging applications are summarized as follows. Further, the current challenges and future perspectives for honeycomb structures are also discussed.

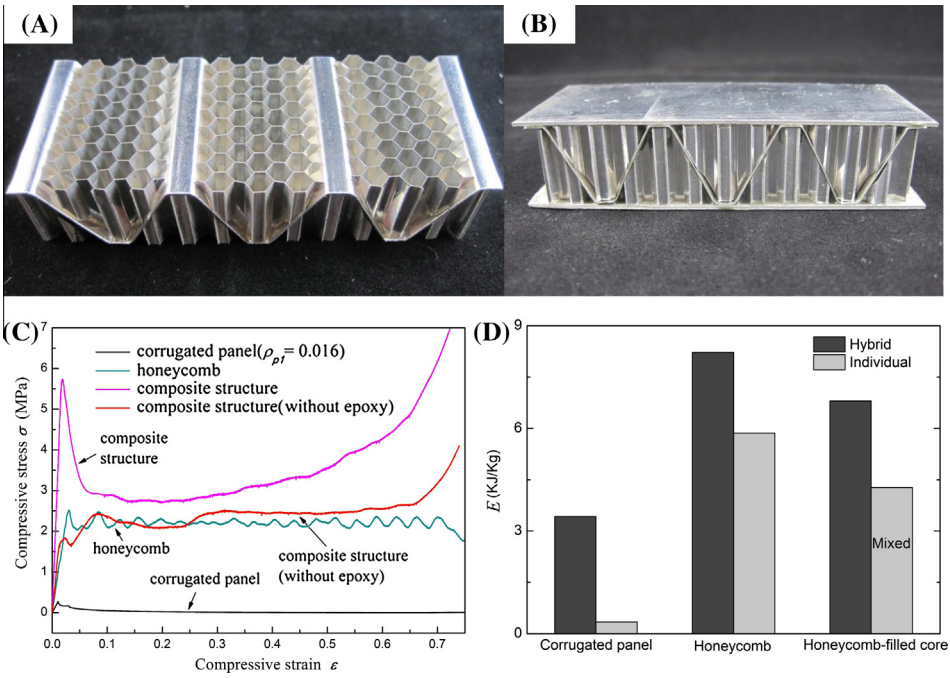

Fig. 42. Honeycomb-corrugation hybrid structure for enhanced mechanical performance [424]: (A) top view; (B) sandwich panel; (C) quasi-static compression stress versus strain curve of corrugated core sandwich, honeycomb core sandwich and hybrid-core sandwich; and (D) energy absorption per unit mass of honeycomb-corrugation hybrid core and its constituents up to nominal compressive strain of 0.30.

5.1. Design and fabrication of hierarchical/hybrid structure

While natural honeybee comb is a paradigm for engineering cellular porous structures fascinated long by engineers, mathematicians, physicists and biologists [57,423], it is not well known hitherto the reason why the bees build the combs out of hexagonal cells with sophisticated and hierarchical structure. It is surprising that nature produces microstructural sophistication of honeybee comb without complicated tools and powerful computers as used by engineers. Thus far, the detailed in situ microscopic and macroscopic physical properties of cell walls [425], wax, silk [57] of the honeybee combs, and their implications for biomimetic designs have been partly explored.

- The hierarchical structure and the mechanical properties of fresh and old natural honeycombs at distinct scales were imaged and measured by optical microscope, environmental SEM, nano/microindentation, and by tension and shear tests, respectively (Fig. 43) [426].
- With hierarchically functional adaptation, their mechanical properties are superior to convectional materials. The microstructures of these biomaterials provide a desirable route to the synthesis of artificial composites [57,427]. For instance, hierarchical structures in nature can lead to breakthroughs to conceptually designing new materials [428,429]. In addition, the design of structure and material is related to micro, nano and biological systems, whereas in synthetic materials there is often a disciplinary separation between materials (material engineers) and structures (civil/mechanical engineers).
- Honeycomb structures have attracted significant interest for thermal management applications, either as thermal barriers or heat dissipaters. With high surface area density and single "easy flow" passage, under the criteria of given pumping power, honeycomb structures outperform other state-of-the art heat dissipation materials, including metal foam, woven textile and lattice-frame material.

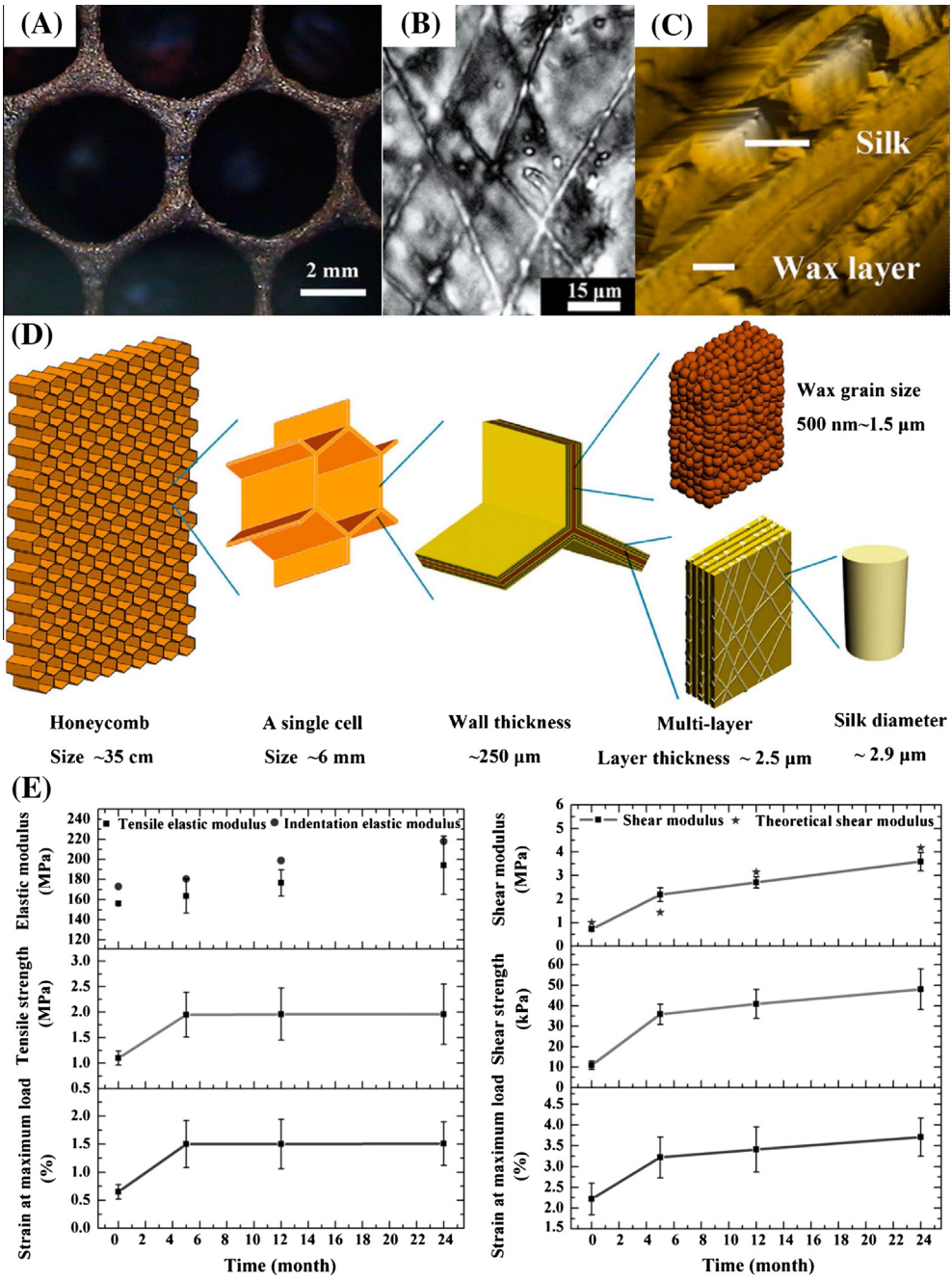

Fig. 43. Structural and mechanical properties of one-year-old honeycomb at different scales: (A) top view; (B) optical image of the surface of a peeled layer; (C) 3D microstructure of cell wall cross-section; (D) hierarchical structure of one-year-old honeycomb at macro-, micro- and nanoscales [426]; and (E) variation of mechanical properties of the wall and comb with age.

- The sound insulation performance of a macro honeycomb structure is related to vibration response of the whole structure, identical to a conventional flat plate for physical mechanism. New constitute relations (e.g., nonlocal elasticity theory [184]) instead of classical continuum models are required to account for the size effect for micro and nano structures [183]. Different from the sound insulation performance, the sound absorption capability of a honeycomb structure is less affected by its overall dynamic response that may be size-dependent for small scale problems. The decisive factor on the final absorption coefficient mainly depends on specific physical mechanisms, e.g., Bragg scattering, local resonance or Helmholtz resonance.

People spare no effort to search various bioinspired materials and structures. Due to limitations of current technologies, most man-made honeycombs designed and manufactured by engineers only mimic the macroscopic geometry of natural honeycombs with features of single material, single scale and single function. Conventional synthetic materials and traditional design methodologies, have been used to design hierarchical materials, e.g., the formation of mesoporous honeycombed carbon coatings based on unsmooth surface of preformed honeycomb cordierite (Fig. 44). New frontiers reside in the synthesis of bioinspired materials through two main groups:

(1) Processes imitating biological systems, involving nanoscale self-assembly of components and fabrication of hierarchical structures [430];

The man-made counterparts out of such kind of materials are typically obtained under some extreme conditions, but their sophisticated structures are created under common temperature and pressure. Manufacturing techniques inspired biomimetic nature may lead to technical evolution of the way to manufacturing. The current research frontier in the investigations of bio-inspired materials goes beyond the situation of just copying the structures. It starts with genetically engineered proteins at the nanometer level; it also sought to form a structure by component self-assembly techniques. This enormous potential research field is not well developed and just in infancy.

(2) Emerging 3D printing technologies for producing hierarchical complexity of porous structures [431].

3D printing technologies have attracted significantly increasing attention. Compton and Lewis [431] developed a novel epoxy-based ink enabling 3D printing of lightweight cellular composites. Particularly, they successfully 3D printed a hierarchical honeycomb structure with multi-scale, high aspect ratio fiber reinforcement. Its Young's modulus is up to 10 times higher than existing polymers fabricated by commercially 3D-printer. Bauer et al. [432] demonstrated that micro-truss and -shell structures in alumina–polymer composite can be produced and characterized by applying 3D laser lithography (Fig. 45A–E). Through this fabrication routine, alumina shells showed size-dependent strengthening characteristics, particularly with a thickness below 100 nm. A Young's modulus of

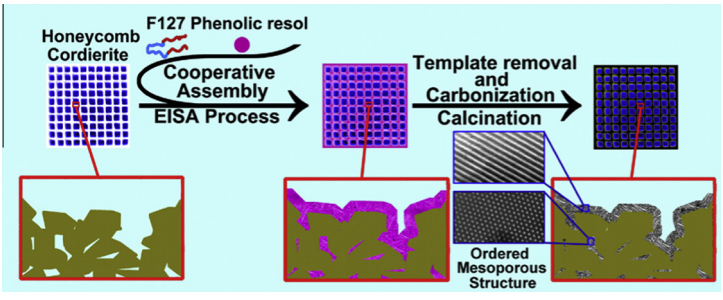

Fig. 44. Schematic formation of ordered mesoporous carbon coatings on unsmooth surface of cordierite [429].

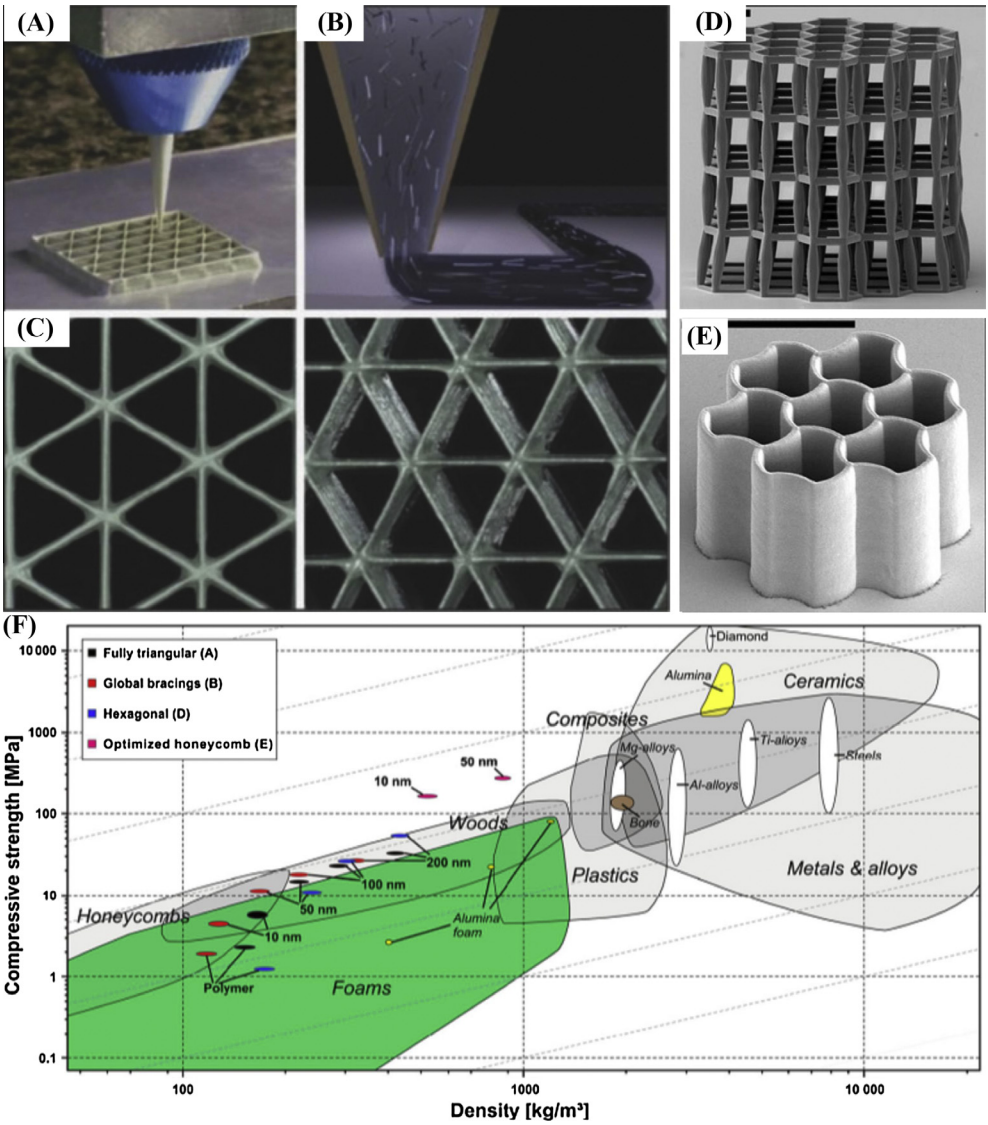

Fig. 45. (A) Optical image of 3D printing of a triangular honeycomb composite and (B) schematic illustration of the progressive alignment of high aspect ratio fillers within the nozzle during composite ink deposition. Optical images of (C) triangular honeycomb structures composed of SiC-filled epoxy. SEM images of cellular microarchitectures such as (D) hexagonal truss structure and (E) shape-optimized honeycomb design (scale bar: 10 μm). (F) Compressive strength versus density chart showing cellular ceramic composite materials compared with other materials (CES EduPack, Granta Design Ltd.) [432].

280 MPa can be obtained by the optimization of honeycomb shape (with a density of 810 kg/m^3) (Fig. 45F), which exceeds all materials in nature and engineering with a density below 1000 kg/m^3.

5.2. Multi-functional design and fabrication approaches

Nowadays, multi-functionality is a pursuit for engineers. Innovative materials incorporated with lightweight, well-defined mechanical properties and cost effectiveness have been more and more

attractive. The multiscale honeycomb as a storage of honey and pollen is an important clue to recognize the nestmate [433,434] and to understand the evolution of honeybees (e.g., honeybee growth and brood survivorship) [435,436]. Similarly, most biological materials exhibit inherent multifunctional integration due to porous and multiscale structures (Table 7) [437–440]. For artificially-made multifunctional honeycombs, their functional properties should be understood as their mechanical properties to better meet the requirements. The current progress in multi-functional design of multiscale honeycomb and related emerging applications are broadly summarized as:

- To enhance multi-functionality ability, standard hexagonal honeycombs have been developed from the basic cell shapes to variations of truncated-square [58], reentrant hexangular core [63] and chiral honeycombs [70], favoring the combined mechanical and thermal characteristics on both efficient structural load supports and thermal management [58]. Particularly, the reentrant hexangular core has negative Poisson ratios or auxetic characteristics, which not only increase its in-plane mechanical properties [441] and undergo synclastic curvature when subjected to out-of-plane bending [442], but also yield appropriate permittivity properties [61].
- Biological porous materials with multiscale structures exhibit inherent multifunctional integration, which inspires scientists and engineers alike to inherit multiscale structured materials for multifunctional integration by using biological mineralization technologies. Multiscale and multi-dimensional structure of natural creatures have been used as template for fabricating hierarchically delicate structure of the creature, passing on its conformation and physical structure, mutating its chemical composition, and compounding new materials and new material structures, with the aim to realize the design and synthesis of function–structure integration and orientation [443]. Another significant progress in using external laser irradiation to create programmable and adaptable nano biosystems was made by Miyako et al. [440]. CNT-functionalized Morpho butterfly wing (Fig. 46) serves as template for the assembly of honeycomb-shaped carbon nanotube (CNT) networks, leading to inherent functions of Morpho butterfly wings with combination of the powerful photothermal characteristics and high electroconductivity of CNTs, such as laser-triggered remote heating, high electrical conductivity and repetitive DNA amplification.
- With exceptional properties, nano- and micro-scaled ordered porous materials (normally with honeycomb structures) have great potential in emerging applications ranging from 2 nm to 1 mm. For the pore size of less than 2 nm, typical graphene, carbon-nanotubes [280,281] and their assemblies [322] would be favorable for the accessibility of the electrolyte, rapid diffusion of the lithium ions, fast transport of electrons and host uptake, leading to enhance the energy capacity, power density and recharge time of high performance energy storage devices. For the ordered mesoporous solids with a pore size of 2–50 nm are of more importance for catalysis [275], sensors

Table 7
Multifunctional characteristics of selected biological materials with porous and multi-scale structures.

Biological material	Functionalities	Ref.
Honeycomb	Structural support for larvae storage of honey and pollen	[435,436]
Bone	Structural support Protect for body and blood cell formation Minerals storage	[437]
Red-bellied woodpecker beak	Structural support Amazingly efficient shock energy absorption	[438]
Tree trunk and root	Structural support Anchoring Nutrient transport	[439]
Butterfly wing	Structural support Structural color Superhydrophobicity Self-cleaning properties Directional adhesive functions Chemical sensing capabilities	[440]

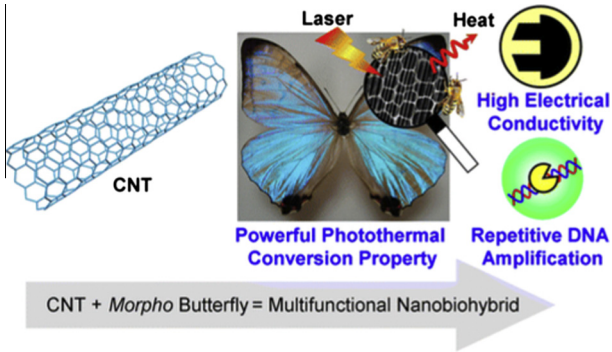

Fig. 46. Structural characterization of CNT_butterfly wing composite [440].

[276], separation media [277], adsorbents [278], and templates for material synthesis [279]. For the pore size range of 50 nm to 1 mm, great interest is emerging for applications in superhydrophobic surfaces [57], photonics [270,271], optoelectronics [272], and microelectronics [273,274].

- In biomedicine, the honeycomb structures also hold great potential in addressing major challenges in tissue engineering and regenerative medicine. One of the most challenging goals in tissue engineering is to design scaffolds as guidance for tissue regeneration, especially for 3D artificial thick living tissues and even organs. 3D scaffold-based tissue engineering is mainly based on seeding cells on scaffold surface, followed by inducing cell to grow into the scaffold [55,366,367]. Starting from the pioneering work by Hutmacher [55], honeycomb structures are continually explored in micro-/nano-biotechnologies, such as ice templates [52], computer aided design (CAD) based intricate 3D honeycomb tissue scaffolds [444] and bottom-up design based 3D bioprinting [445].
- Recently, cyto-compatible hydrogels capable of 3D cell encapsulation have attracted increasing attention due to their biocompatibility, biodegradability, processability, and advanced properties that mimic nature extracellular matrix. Directed self-assembly of honeycomb cell-laden microgels is used as building blocks to create large living tissues [45]. Besides, bottom-up approaches are newly developed to create 3D tissue constructs by assembling honeycomb cell-laden microgels with magnetic [446], acoustic [389] and electrostatic forces [447], which holds great potential for overcoming diffusion limitation ($\sim$200 μm) that is usually encountered in traditional top-down approaches [448].
- Honeycomb structures with high specific surface area as electrodes have also been applied in the field of biosensors, bioadsorption, biocatalysis and drug release. Microsensors composed of nano-honeycomb flake ZnO [395] or electrochemically anodized Ta_2O_5 honeycomb nanostructure [57] have been used in various applications involving the detection and measurement of the environmental and atmospheric hazardous chemicals as well as body glucose. Nano-honeycomb structures and materials play an important role in bioadsorption and biocatalysis, such as adsorption of small biological molecules. Ordered mesoporous silica (MCM-41, MCM-48, FSM-16, SBA-15, etc.) and carbon molecular sieves (CMK-1, CMK-3) are the main carrier for chemical transformations on organic compounds [402]. Nano-honeycomb structures and materials including mesoporous silica-based media (such as MCM-41, MCM-48, and SBA-15) have been successfully employed as carrier for a multitude of drugs (antipyrine [409], amoxicillin [410], alendronate [411], captopril [57], etc.). To unfreeze the limits of some sign of toxicity during the use of silica-based mesoporous materials as drug carrier [57], Nontoxic mesoporous carbon, synthesized by surfactant templating techniques can be used as a new drug delivery medium [57].
- The design and fabrication of multiscaled honeycomb structures is the future developing trend for research and applications, especially the emerging applications associated with biological medicine, tissue engineering, energy conversion for high efficiency storage battery, multi-functional

environmental friendly materials. Understanding the design principles underlying the creation of honeycomb structures as well as the related scientific discovery and technology development is critical for engineering bioinspired materials and devices designed based on honeycomb structures for a wide range of practical applications. The trends of these prospective are summarized as follows: Multifunctional designs on artificial honeycombs have involved 3D printing and biological mineralization.

- Energy conversion and environmental engineering: The bioinspired hierarchical structures (microscale honeycomb structure) [322] and the free-standing hierarchical porous structures composed of functionalized graphene sheets, especially those multi-functional composites (hierarchical porous combined functional nanoparticles) [323] show great potential in high performance energy capacitors, water treatment and solar energy conversion.
- 3D scaffold-based tissue engineering: the main challenge associated with this strategy is to construct thick and complex tissues/organs: (i) good mechanical properties to maintain structural integrity; (ii) sufficient nutrient supply; and (iii) controlled 3D cell distribution and micro environmental cues (both physical and biochemical) in 3D scaffolds.
- Special sensing characteristics: honeycomb-derived graphenes as emerging bioelectronic platform have huge potentials for next-generation biosensors due to its chemical robustness and sensitivity to electromagnetic, mechanical environment changes [449-452].

Acknowledgements

This work was supported by the National Basic Research Program of China (2011CB610305), the National Natural Science Foundation of China (11321062, 11472209, 11102152, 10825210, 31050110125, 11372243 and 81000453), the Major International Joint Research Program of China (11120101002), International Science & Technology Cooperation Program of China (2013DFG02930), the Fundamental Research Funds for Xi'an Jiaotong University (xjj2015102), and the National 111 Project of China (B06024). FX was also partially supported by the China Young 1000-Talent Program and Program for New Century Excellent Talents in University (NCET-12-0437).

References

[1] Liljas A. Function is structure. Science 1999;285:2077–8.
[2] Bonderer LJ, Studart AR, Gauckler LJ. Bioinspired design and assembly of platelet reinforced polymer films. Science 2008;319:1069–73.
[3] Fan TX, Chow SK, Di Z. Biomorphic mineralization: from biology to materials. Prog Mater Sci 2009;54:542–659.
[4] Bhushan B. Biomimetics: lessons from nature – an overview. Philos Trans R Soc A: Math Phys Eng Sci 2009;367:1445–86.
[5] Feng L, Li S, Li Y, Li H, Zhang L, Zhai J, et al. Super-hydrophobic surfaces: from natural to artificial. Adv Mater 2002;14:1857–60.
[6] Sarikaya M, Tamerler C, Jen AKY, Schulten K, Baneyx F. Molecular biomimetics: nanotechnology through biology. Nat Mater 2003;2:577–85.
[7] Chen PY, McKittrick J, Meyers MA. Biological materials: functional adaptations and bioinspired designs. Prog Mater Sci 2012;57:1492–704.
[8] Evans AG, Hutchinson JW, Ashby MF. Multifunctionality of cellular metal systems. Prog Mater Sci 1998;43:171–221.
[9] Zhou H, Fan TX, Li XF, Zhang D, Guo QX, Ogawa H. Biomimetic photocatalyst system derived from the natural prototype in leaves for efficient visible-light-driven catalysis. J Mater Chem 2009;19:2695–703.
[10] Zhang K, Duan H, Karihaloo BL, Wang J. Hierarchical, multilayered cell walls reinforced by recycled silk cocoons enhance the structural integrity of honeybee combs. Proc Natl Acad Sci 2010;107:9502.
[11] Mackenzie D. Mathematics – proving the perfection of the honeycomb. Science 1999;285:1338–9.
[12] Szpiro G. Mathematics: does the proof stack up? Nature 2003;424:12–3.
[13] Galilei G. Discorsi e dimostrazioni matematiche intorno a due nuove scienze (Leiden, 1638), 98. Retour.
[14] Hooke R, Gunther RT. Micrographia, 1665. Dawsons of Pall Mall; 1968.
[15] Siculus D, Geer RM. Library of history, vol. X. Cambridge, Massachusetts: Harvard University Press; 1954.
[16] Fahey DJ, Dunlap M, Seidl RJ, Laboratory FP. Thermal conductivity of paper honeycomb cores and sound absorption of sandwich panels. Wisconsin, Uo: USDA, Forest Service, Forest Products Laboratory; 1953.
[17] Moore J, Sturgeon D. High modulus organic fibre composites in aircraft applications. Composites 1973;4:34–8.
[18] Herbert TA. Method of making stainless steel honeycomb panels. Google Patents; 1960.
[19] Bardhan P. Ceramic honeycomb filters and catalysts. Curr Opin Solid State Mater Sci 1997;2:577–83.
[20] Vinson JR. Optimum design of composite honeycomb sandwich panels subjected to uniaxial compression. AIAA J 1986;24:1690–6.

[21] Long Z, Qing Z, Hualin F, Fengnian J. Hierarchical composite honeycombs. Mater Des 2012;40:124–9.
[22] Du Y, Yan N, Kortschot MT. Light-weight honeycomb core sandwich panels containing biofiber-reinforced thermoset polymer composite skins: fabrication and evaluation. Compos B: Eng 2012;43:2875–82.
[23] Dempsey BM, Eisele S, McDowell DL. Heat sink applications of extruded metal honeycombs. Int J Heat Mass Transfer 2005;48:527–35.
[24] Huynen I, Quiévy N, Bailly C, Bollen P, Detrembleur C, Eggermont S, et al. Multifunctional hybrids for electromagnetic absorption. Acta Mater 2011;59:3255–66.
[25] Bitzer T. Honeycomb technology: materials, design, manufacturing, applications and testing. Chapman & Hall; 1997.
[26] Xiong XP, Lin MF, Zou WW. Honeycomb structured porous films prepared by the method of breath figure: history and development. Curr Org Chem 2011;15:3706–18.
[27] Masuda H, Fukuda K. Ordered metal nanohole arrays made by a 2-step replication of honeycomb structures of anodic alumina. Science 1995;268:1466–8.
[28] Yabu H, Takebayashi M, Tanaka M, Shimomura M. Superhydrophobic and lipophobic properties of self-organized honeycomb and pincushion structures. Langmuir 2005;21:3235–7.
[29] Gadkaree KP. Carbon honeycomb structures for adsorption applications. Carbon 1998;36:981–9.
[30] Broeng J, Barkou SE, Bjarklev A, Knight JC, Birks TA, Russell PS. Highly increased photonic band gaps in silica/air structures. Opt Commun 1998;156:240–4.
[31] Hales TC. The honeycomb conjecture. Discrete Comput Geom 2001;25:1–22.
[32] Karihaloo B, Zhang K, Wang J. Honeybee combs: how the circular cells transform into rounded hexagons. J R Soc Interface 2013;10:20130299.
[33] Uraki Y, Tamai Y, Hirai T, Koda K, Yabu H, Shimomura M. Fabrication of honeycomb-patterned cellulose material that mimics wood cell wall formation processes. Mater Sci Eng 2011;31:1201–8.
[34] Marmorstein AD, Bonilha VL, Chiflet S, Neill JM, Rodriguez-Boulan E. The polarity of the plasma membrane protein RET-PE2 in retinal pigment epithelium is developmentally regulated. J Cell Sci 1996;109:3025–34.
[35] Lecuit T, Lenne PF. Cell surface mechanics and the control of cell shape, tissue patterns and morphogenesis. Nat Rev Mol Cell Biol 2007;8:633–44.
[36] Pawin G, Wong KL, Kwon KY, Bartels L. A homomolecular porous network at a Cu(1 1 1) surface. Science 2006;313:961–2.
[37] Seepersad CC, Dempsey BM, Allen JK, Mistree F, McDowell DL. Design of multifunctional honeycomb materials. AIAA J 2004;42:1025–33.
[38] Wadley HNG. Multifunctional periodic cellular metals. Philos Trans R Soc A 2006;364:31–68.
[39] Davalos JF, Qiao PZ, Xu XF, Robinson J, Barth KE. Modeling and characterization of fiber-reinforced plastic honeycomb sandwich panels for highway bridge applications. Compos Struct 2001;52:441–52.
[40] Chochua G, Shyy W, Moore J. Computational modeling for honeycomb-stator gas annular seal. Int J Heat Mass Transfer 2002;45:1849–63.
[41] Chanteranne J. Use of ultra-light adhesive for the metal honeycomb bonding. ESA Spacecraft Mater Space Environ 1979:287–91.
[42] Abd El-Sayed F, Jones R, Burgess I. A theoretical approach to the deformation of honeycomb based composite materials. Composites 1979;10:209–14.
[43] George J, Onodera J, Miyata T. Biodegradable honeycomb collagen scaffold for dermal tissue engineering. J Biomed Mater Res A 2008;87:1103–11.
[44] Engelmayr Jr GC, Cheng M, Bettinger CJ, Borenstein JT, Langer R, Freed LE. Accordion-like honeycombs for tissue engineering of cardiac anisotropy. Nat Mater 2008;7:1003–10.
[45] Tejavibulya N, Youssef J, Bao B, Ferruccio TM, Morgan JR. Directed self-assembly of large scaffold-free multi-cellular honeycomb structures. Biofabrication 2011;3:034110.
[46] Baggetto L, Danilov D, Notten PH. Honeycomb-structured silicon: remarkable morphological changes induced by electrochemical (de)lithiation. Adv Mater 2011;23:1563–6.
[47] Mishchenko L, Hatton B, Bahadur V, Taylor JA, Krupenkin T, Aizenberg J. Design of ice-free nanostructured surfaces based on repulsion of impacting water droplets. ACS Nano 2010;4:7699–707.
[48] Mukai SR, Nishihara H, Tamon H. Porous microfibers and microhoneycombs synthesized by ice templating. Catal Surv Asia 2006;10:161–71.
[49] Kageyama K, Tamazawa J, Aida T. Extrusion polymerization: catalyzed synthesis of crystalline linear polyethylene nanofibers within a mesoporous silica. Science 1999;285:2113–5.
[50] Ng KY, Lin YA, Ngan AHW. Compression of micron-sized pillars of anodic aluminium oxide nano-honeycomb. J Mech Phys Solids 2011;59:251–64.
[51] Sugiura T, Yoshida T, Minoura H. Designing a TiO_2 nano-honeycomb structure using photoelectrochemical etching. Electrochem Solid-State Lett 1998;1:175–7.
[52] Mao M, He J, Liu Y, Li X, Li D. Ice-template-induced silk fibroin-chitosan scaffolds with predefined microfluidic channels and fully porous structures. Acta Biomater 2011;8:2175–84.
[53] Connal LA, Qiao GG. Preparation of porous poly(dimethylsiloxane)-based honeycomb materials with hierarchal surface features and their use as soft-lithography templates. Adv Mater 2006;18:3024–8.
[54] Kageyama K, Tamazawa J-i, Aida T. Extrusion polymerization: catalyzed synthesis of crystalline linear polyethylene nanofibers within a mesoporous silica. Science 1999;285:2113–5.
[55] Hutmacher DW. Scaffolds in tissue engineering bone and cartilage. Biomaterials 2000;21:2529–43.
[56] Hohe J, Becker W. Effective elastic properties of triangular grid structures. Compos Struct 1999;45:131–45.
[57] Sunami H, Ito E, Tanaka M, Yamamoto S, Shimomura M. Effect of honeycomb film on protein adsorption, cell adhesion and proliferation. Colloids Surf A 2006;284:548–51.
[58] Queheillalt DT, Carbajal G, Peterson GP, Wadley HNG. A multifunctional heat pipe sandwich panel structure. Int J Heat Mass Transfer 2008;51:312–26.
[59] Gu S, Lu TJ, Evans AG. On the design of two-dimensional cellular metals for combined heat dissipation and structural load capacity. Int J Heat Mass Transfer 2001;44:2163–75.

[60] Torquato S, Gibiansky LV, Silva MJ, Gibson LJ. Effective mechanical and transport properties of cellular solids. Int J Mech Sci 1998;40:71–82.
[61] Scarpa F, Burriesci G, Smith F, Chambers B. Mechanical and electromagnetic behaviour of auxetic honeycomb structures. Aeronaut J 2003;107:175.
[62] Buchberg H, Lalude OA, Edwards DK. Performance characteristics of rectangular honeycomb solar-thermal converters. Sol Energy 1971;13:193–221.
[63] Muraoka M, Sanada S. Displacement amplifier for piezoelectric actuator based on honeycomb link mechanism. Sensor Actuat A – Phys 2010;157:84–90.
[64] Chen DH, Yang L. Analysis of equivalent elastic modulus of asymmetrical honeycomb. Compos Struct 2011;93:767–73.
[65] Overaker DW, Cuitino AM, Langrana NA. Elastoplastic micromechanical modeling of two-dimensional irregular convex and nonconvex (re-entrant) hexagonal foams. J Appl Mech – Trans ASME 1998;65:748–57.
[66] Saha GC, Kalamkarov AL, Georglades AV. Asymptotic homogenization modeling and analysis of effective properties of smart composite reinforced and sandwich shells. Int J Mech Sci 2007;49:138–50.
[67] Zhang X, Zhang H. Theoretical and numerical investigation on the crush resistance of rhombic and Kagome honeycombs. Compos Struct 2012;96:143–52.
[68] Bitzer T. Honeycomb marine applications. J Reinf Plast Compos 1994;13:355–60.
[69] Kuo C. Adaptive optics – one meter deformable composite mirror. AIAA J 1991:8–10.
[70] Alderson A, Alderson KL, Attard D, Evans KE, Gatt R, Grima JN, et al. Elastic constants of 3-, 4-and 6-connected chiral and anti-chiral honeycombs subject to uniaxial in-plane loading. Compos Sci Technol 2010;70:1042–8.
[71] Bushby RJ, Lozman OR. Discotic liquid crystals 25 years on. Curr Opin Colloid Interface Sci 2002;7:343–54.
[72] Chen B, Zeng X, Baumeister U, Ungar G, Tschierske C. Liquid crystalline networks composed of pentagonal, square, and triangular cylinders. Science 2005;307:96–9.
[73] Nishikawa T, Nonomura M, Arai K, Hayashi J, Sawadaishi T, Nishiura Y, et al. Micropatterns based on deformation of a viscoelastic honeycomb mesh. Langmuir 2003;19:6193–201.
[74] Wan LS, Ke BB, Zhang J, Xu ZK. Pore shape of honeycomb-patterned films: modulation and interfacial behavior. J Phys Chem B 2012;116:40–7.
[75] Shim J, Shan SC, Kosmrlj A, Kang SH, Chen ER, Weaver JC, et al. Harnessing instabilities for design of soft reconfigurable auxetic/chiral materials. Soft Matter 2013;9:8198–202.
[76] Morgan F. The hexagonal honeycomb conjecture. Trans Am Math Soc 1999;351:1753–63.
[77] Hales TC. Cannonballs and honeycombs. Not-Am Math Soc 2000;47:440–9.
[78] Bezdek K. Isoperimetric inequalities and the dodecahedral conjecture. Int J Math 1997;8:759–80.
[79] Bezdek K, Daroczy-Kiss E. Finding the best face on a Voronoi polyhedron – the strong dodecahedral conjecture revisited. Monatsh Math 2005;145:191–206.
[80] Hales TC, McLaughlin S. The dodecahedral conjecture. J Am Math Soc 2010;23:299–344.
[81] Zhu HX, Mills N. The in-plane non-linear compression of regular honeycombs. Int J Solids Struct 2000;37:1931–49.
[82] Fleck NA, Qiu XM. The damage tolerance of elastic–brittle, two-dimensional isotropic lattices. J Mech Phys Solids 2007;55:562–88.
[83] Wang AJ, McDowell DL. In-plane stiffness and yield strength of periodic metal honeycombs. J Eng Mater 2004;126:137–56.
[84] Wang A, McDowell D. The in-plane mechanical properties of various periodic honeycombs. J Eng Mater Technol 2004;126:137–56.
[85] Wang AJ, McDowell D. Yield surfaces of various periodic metal honeycombs at intermediate relative density. Int J Plast 2005;21:285–320.
[86] Gibson LJ, Ashby MF. Cellular solids: structures and properties. 2nd ed. Cambridge, UK: Cambridge University Press; 1997.
[87] Becker W. The in-plane stiffnesses of a honeycomb core including the thickness effect. Arch Appl Mech 1998;68:334–41.
[88] Becker W. Closed-form analysis of the thickness effect of regular honeycomb core material. Compos Struct 2000;48:67–70.
[89] Triantafyllidis N, Schraad M. Onset of failure in aluminum honeycombs under general in-plane loading. J Mech Phys Solids 1998;46:1089–124.
[90] Zhang J, Ashby M. Buckling of honeycombs under in-plane biaxial stresses. Int J Mech Sci 1992;34:491–509.
[91] Khan M, Baig T, Mirza S. Experimental investigation of in-plane and out-of-plane crushing of aluminum honeycomb. Mater Sci Eng A 2012;539:135–42.
[92] Kim B, Christensen RM. Basic two-dimensional core types for sandwich structures. Int J Mech Sci 2000;42:657–76.
[93] Doyoyo M, Mohr D. Microstructural response of aluminum honeycomb to combined out-of-plane loading. Mech Mater 2003;35:865–76.
[94] Cote F, Deshpande V, Fleck N, Evans A. The out-of-plane compressive behavior of metallic honeycombs. Mater Sci Eng A 2004;380:272–80.
[95] Baker WE, Togami TC, Weydert JC. Static and dynamic properties of high-density metal honeycombs. Int J Impact Eng 1998;21:149–63.
[96] Nia AA, Sadeghi MZ. The effects of foam filling on compressive response of hexagonal cell aluminum honeycombs under axial loading-experimental study. Mater Des 2010;31:1216–30.
[97] Wilbert A, Jang WY, Kyriakides S, Floccari J. Buckling and progressive crushing of laterally loaded honeycomb. Int J Solids Struct 2011;48:803–16.
[98] Yang M, Qiao P. Quasi-static crushing behavior of aluminum honeycomb materials. J Sand Struct Mater 2008;10:133–60.
[99] Côté F, Deshpande VS, Fleck NA, Evans AG. The out-of-plane compressive behavior of metallic honeycombs. Mater Sci Eng A 2004;380:272–80.
[100] Foo CC, Chai GB, Seah LK. Mechanical properties of Nomex material and Nomex honeycomb structure. Compos Struct 2007;80:588–94.
[101] Pan SD, Wu LZ, Sun YG, Zhou ZG, Qu JL. Longitudinal shear strength and failure process of honeycomb cores. Compos Struct 2006;72:42–6.

[102] Pan SD, Wu LZ, Sun YG. Transverse shear modulus and strength of honeycomb cores. Compos Struct 2008;84:369–74.
[103] Grove SM, Popham E, Miles ME. An investigation of the skin/core bond in honeycomb sandwich structures using statistical experimentation techniques. Compos A – Appl Sci 2006;37:804–12.
[104] Alonso IQ, Fleck NA. The damage tolerance of a sandwich panel containing a cracked honeycomb core. J Appl Mech 2009;76:061003.
[105] Petras A, Sutcliffe M. Failure mode maps for honeycomb sandwich panels. Compos Struct 1999;44:237–52.
[106] Hong ST, Pan J, Tyan T, Prasad P. Quasi-static crush behavior of aluminum honeycomb specimens under compression dominant combined loads. Int J Plast 2006;22:73–109.
[107] Chen Z, Yan N, Deng J, Smith G. Flexural creep behavior of sandwich panels containing Kraft paper honeycomb core and wood composite skins. Mater Sci Eng A – Struct 2011;528:5621–6.
[108] Jen YM, Chang LY. Evaluating bending fatigue strength of aluminum honeycomb sandwich beams using local parameters. Int J Fatig 2008;30:1103–14.
[109] Hu L, Yu T. Dynamic crushing strength of hexagonal honeycombs. Int J Impact Eng 2010;37:467–74.
[110] Xu S, Beynon JH, Ruan D, Lu G. Experimental study of the out-of-plane dynamic compression of hexagonal honeycombs. Compos Struct 2012;94:2326–36.
[111] Masters IG, Evans KE. Models for the elastic deformation of honeycombs. Compos Struct 1996;35:403–22.
[112] Moongkhamklang P, Deshpande VS, Wadley HNG. The compressive and shear response of titanium matrix composite lattice structures. Acta Mater 2010;58:2822–35.
[113] Cote F, Deshpande VS, Fleck NA. The shear response of metallic square honeycombs. J Mech Mater Struct 2006;1:1281–99.
[114] Mai SP, Fleck NA, Lu TJ. Optimal design of box-section sandwich beams in three-point bending. Int J Solids Struct 2007;44:4742–69.
[115] Valdevit L, Hutchinson JW, Evans AG. Structurally optimized sandwich panels with prismatic cores. Int J Solids Struct 2004;41:5105–24.
[116] Wei Z, Zok FW, Evans AG. Design of sandwich panels with prismatic cores. J Eng Mater – Trans ASME 2006;128:186–92.
[117] Cote F, Deshpande VS, Fleck NA, Evans AG. The compressive and shear responses of corrugated and diamond lattice materials. Int J Solids Struct 2006;43:6220–42.
[118] Xue ZY, Hutchinson JW. A comparative study of impulse-resistant metal sandwich plates. Int J Impact Eng 2004;30:1283–305.
[119] Mahmoudabadi MZ, Sadighi M. A study on the static and dynamic loading of the foam filled metal hexagonal honeycomb-theoretical and experimental. Mater Sci Eng A 2011;530:333–43.
[120] Yin H, Wen G, Hou S, Chen K. Crushing analysis and multiobjective crashworthiness optimization of honeycomb-filled single and bitubular polygonal tubes. Mater Des 2011;32:4449–60.
[121] Jeong J, Lee Y, Cho M. Sequential multiscale analysis on size-dependent mechanical behavior of micro/nano-sized honeycomb structures. Mech Mater 2012;57:109–33.
[122] Da Silva A, Kyriakides S. Compressive response and failure of balsa wood. Int J Solids Struct 2007;44:8685–717.
[123] Osei-Antwi M, de Castro J, Vassilopoulos AP, Keller T. Shear mechanical characterization of balsa wood as core material of composite sandwich panels. Const Build Mater 2013;41:231–8.
[124] Vural M, Ravichandran G. Dynamic response and energy dissipation characteristics of balsa wood: experiment and analysis. Int J Solids Struct 2003;40:2147–70.
[125] Tagarielli V, Deshpande V, Fleck N. The high strain rate response of PVC foams and end-grain balsa wood. Compos B: Eng 2008;39:83–91.
[126] Ng KY, Lin Y, Ngan AHW. Deformation of anodic aluminum oxide nano-honeycombs during nanoindentation. Acta Mater 2009;57:2710–20.
[127] Ng K, Ngan A. Effects of pore-channel ordering on the mechanical properties of anodic aluminum oxide nano-honeycombs. Scripa Mater 2012;66:439–42.
[128] Jeon J, Lee P, Lee K, Park H, Hwang W. Bending fatigue characteristics of nanohoneycomb structures. Compos Struct 2008;82:28–35.
[129] Choi D, Jeon J, Lee P, Hwang W, Lee K, Park H. Young's modulus measurements of nanohoneycomb structures by flexural testing in atomic force microscopy. Compos Struct 2007;79:548–53.
[130] Knoell AC. Environmental and physical effects on the response of balsa wood as an energy dissipator. JPL technical report no. 32-944. Pasadena, CA: California Institute of Technology; 1966.
[131] Soden P, McLeish R. Variables affecting the strength of balsa wood. J Strain Anal Eng Des 1976;11:225–34.
[132] Easterling KE, Harrysson R, Gibson LJ, Ashby MF. On the mechanics of balsa and other woods. Proc R Soc Lond A: Mater 1982;383:31–41.
[133] Vural M, Ravichandran G. Microstructural aspects and modeling of failure in naturally occurring porous composites. Mech Mater 2003;35:523–36.
[134] Gibson LJ. Biomechanics of cellular solids. J Biomech 2005;38:377–99.
[135] Jeon JH, Hwang W, Lee KH. Measurement of elastic constants of nanohoneycomb structures. J Compos Mater 2009;43:1155–75.
[136] Desplantier-Giscard D, Galarneau A, Di Renzo F, Fajula F. Mechanical strength of nanosized hexagonal silica honeycombs. Mater Sci Eng C – Biol Sci 2003;23:727–32.
[137] Alavinasab A, Jha R, Ahmadi G, Cetinkaya C, Sokolov I. Computational modeling of nano-structured glass fibers. Comput Mater Sci 2008;44:622–7.
[138] Chytil S, Haugland L, Blekkan EA. On the mechanical stability of mesoporous silica SBA-15. Microporous Mesoporous Mater 2008;111:134–42.
[139] Williford RE, Li XS, Addleman RS, Fryxell GE, Baskaran S, Birnbaum JC, et al. Mechanical stability of templated mesoporous silica thin films. Microporous Mesoporous Mater 2005;85:260–6.
[140] Chemin N, Klotz M, Rouessac V, Ayral A, Barthel E. Mechanical properties of mesoporous silica thin films: effect of the surfactant removal processes. Thin Solid Films 2006;495:210–3.

[141] Luo J-T, Wen H-C, Chang Y-M, Wu W-F, Chou C-P. Mesoporous silica reinforced by silica nanoparticles to enhance mechanical performance. J Colloid Interface Sci 2007;305:275–9.
[142] Dubey SP, Dwivedi AD, Sillanpaa M, Gopal K. *Artemisia vulgaris*-derived mesoporous honeycomb-shaped activated carbon for ibuprofen adsorption. Chem Eng J 2010;165:537–44.
[143] Gusev VY, Feng XB, Bu Z, Haller GL, OBrien JA. Mechanical stability of pure silica mesoporous MCM-41 by nitrogen adsorption and small-angle X-ray diffraction measurements. J Phys Chem – US 1996;100:1985–8.
[144] Hartmann M, Bischof C. Mechanical stability of mesoporous molecular sieve MCM-48 studied by adsorption of benzene, n-heptane, and cyclohexane. J Phys Chem B 1999;103:6230–5.
[145] Cassiers K, Linssen T, Mathieu M, Benjelloun M, Schrijnemakers K, Van Der Voort P, et al. A detailed study of thermal, hydrothermal, and mechanical stabilities of a wide range of surfactant assembled mesoporous silicas. Chem Mater 2002;14:2317–24.
[146] Igarashi N, Koyano KA, Tanaka Y, Nakata S, Hashimoto K, Tatsumi T. Investigation of the factors influencing the structural stability of mesoporous silica molecular sieves. Microporous Mesoporous Mater 2003;59:43–52.
[147] Innocenzi P, Falcaro P, Grosso D, Babonneau F. Order-disorder transitions and evolution of silica structure in self-assembled mesostructured silica films studied through FTIR spectroscopy. J Phys Chem B 2003;107:4711–7.
[148] Ryoo R, Jun S. Improvement of hydrothermal stability of MCM-41 using salt effects during the crystallization process. J Phys Chem B 1997;101:317–20.
[149] Dunphy DR, Singer S, Cook AW, Smarsly B, Doshi DA, Brinker CJ. Aqueous stability of mesoporous silica films doped or grafted with aluminum oxide. Langmuir 2003;19:10403–8.
[150] Li X, Birnbaum JC, Williford RE, Fryxell GE, Coyle CA, Dunham GC, et al. Effect of humidity treatments on porosity and mechanical integrity of mesoporous silica films. Chem Commun 2003:2054–5.
[151] Zhu HX. Size-dependent elastic properties of micro- and nano-honeycombs. J Mech Phys Solids 2010;58:696–709.
[152] Bertoldi K, Reis PM, Willshaw S, Mullin T. Negative Poisson's ratio behavior induced by an elastic instability. Adv Mater 2010;22:361–6.
[153] Bertoldi K, Boyce MC. Mechanically triggered transformations of phononic band gaps in periodic elastomeric structures. Phys Rev B 2008;77:052105.
[154] Jang J-H, Koh CY, Bertoldi K, Boyce MC, Thomas EL. Combining pattern instability and shape-memory hysteresis for phononic switching. Nano Lett 2009;9:2113–9.
[155] Kim J, Hanna JA, Byun M, Santangelo CD, Hayward RC. Designing responsive buckled surfaces by halftone gel lithography. Science 2012;335:1201–5.
[156] Mullin T, Deschanel S, Bertoldi K, Boyce M. Pattern transformation triggered by deformation. Phys Rev Lett 2007;99:084301.
[157] Bertoldi K, Boyce MC, Deschanel S, Prange SM, Mullin T. Mechanics of deformation-triggered pattern transformations and superelastic behavior in periodic elastomeric structures. J Mech Phys Solids 2008;56:2642–68.
[158] Krishnan D, Johnson H. Light-induced deformation in a liquid crystal elastomer photonic crystal. J Mech Phys Solids 2014;62:48–56.
[159] Zhang Y, Matsumoto EA, Peter A, Lin P-C, Kamien RD, Yang S. One-step nanoscale assembly of complex structures via harnessing of an elastic instability. Nano Lett 2008;8:1192–6.
[160] Singamaneni S, Bertoldi K, Chang S, Jang JH, Young SL, Thomas EL, et al. Bifurcated mechanical behavior of deformed periodic porous solids. Adv Funct Mater 2009;19:1426–36.
[161] Torquato S, Gibiansky L, Silva M, Gibson L. Effective mechanical and transport properties of cellular solids. Int J Mech Sci 1998;40:71–82.
[162] Lu T, Chen C. Thermal transport and fire retardance properties of cellular aluminium alloys. Acta Mater 1999;47:1469–85.
[163] Yeh C, Chen Y, Wen C, Li K. Measurement of thermal contact resistance of aluminum honeycombs. Exp Therm Fluid Sci 2003;27:271–81.
[164] Groppi G, Tronconi E. Design of novel monolith catalyst supports for gas/solid reactions with heat exchange. Chem Eng Sci 2000;55:2161–71.
[165] Yang XH, Lu TJ, Kim T. Effective thermal conductivity modelling for closed-cell porous media with analytical shape factors. Transp Porous Med 2013;100:211–24.
[166] Hollands K. Honeycomb devices in flat-plate solar collectors. Sol Energy 1965;9:159–64.
[167] Hollands K. Natural convection in horizontal thin-walled honeycomb panels. J Heat Transfer 1973;95:439–42.
[168] Cane RLD, Hollands KGT, Raithby GD, Unny TE. Free convection heat-transfer across inclined honeycomb panels. J Heat Transfer 1977;99:86–91.
[169] Lakhal E, Bilgen E, Vasseur P. Natural convection and conduction in inclined enclosures bounded by a wall with honeycomb structure. Int J Heat Mass Tranfer 1995;38:1397–407.
[170] Wen T. Thermo-fluid characteristics of metallic 2D cellular materials. PhD thesis. University of Cambridge; 2007.
[171] Lu TJ. Heat transfer efficiency of metal honeycombs. Int J Heat Mass Transfer 1999;42:2031–40.
[172] Fairbanks DR. Effective lateral thermal-conductivity of square-cell cores. AIAA J 1982;20:1009–14.
[173] Swann RT, Pittman CM, Aeronautics USN, Administration S. Analysis of effective thermal conductivities of honeycomb-core and corrugated-core sandwich panels. NASA technical note D-714; 1961.
[174] Rajaram S, Tongan W, Nutt S. Sound transmission loss of honeycomb sandwich panels. Noise Control Eng J 2006;54:106–15.
[175] Burton W, Noor A. Assessment of continuum models for sandwich panel honeycomb cores. Comput Method Appl Mech Eng 1997;145:341–60.
[176] Kurtze G, Watters B. New wall design for high transmission loss or high damping. J Acoust Soc Am 1959;31:739–48.
[177] Vipperman J, Li D, Avdeev I, Lane S. Investigation of the sound transmission into an advanced grid-stiffened structure. J Vib Acoust 2003;125:257–66.
[178] Fahy F, Gardonio P. Sound and structural vibration: radiation, transmission and response. 2nd ed. Academic Press; 2007.
[179] Davis E. Designing honeycomb panels for noise control 1999:792–800.

[180] Xin FX, Lu TJ. Analytical modeling of fluid loaded orthogonally rib-stiffened sandwich structures: sound transmission. J Mech Phys Solids 2010;58:1374–96.
[181] Liu Q, Zhao Y. Role of anisotropic core in vibration properties of honeycomb sandwich panels. J Therm Compos Mater 2002;15:23–32.
[182] Ruzzene M. Vibration and sound radiation of sandwich beams with honeycomb truss core. J Sound Vib 2004;277:741–63.
[183] Zhu H. Size-dependent elastic properties of micro-and nano-honeycombs. J Mech Phys Solids 2010;58:696–709.
[184] Wang Q. Wave propagation in carbon nanotubes via nonlocal continuum mechanics. J Appl Phys 2005;98:124301.
[185] Heireche H, Tounsi A, Benzair A, Maachou M, Adda Bedia EA. Sound wave propagation in single-walled carbon nanotubes using nonlocal elasticity. Physica E 2008;40:2791–9.
[186] Spadoni A, Ruzzene M, Gonella S, Scarpa F. Phononic properties of hexagonal chiral lattices. Wave Motion 2009;46:435–50.
[187] Ruzzene M, Tsopelas P. Control of wave propagation in sandwich plate rows with periodic honeycomb core. J Eng Mech 2003;129:975–86.
[188] Phani AS, Woodhouse J, Fleck N. Wave propagation in two-dimensional periodic lattices. J Acoust Soc Am 2006;119:1995.
[189] Sánchez-Pérez J, Caballero D, Martinez-Sala R, Rubio C, Sánchez-Dehesa J, Meseguer F, et al. Sound attenuation by a two-dimensional array of rigid cylinders. Phys Rev Lett 1998;80:5325.
[190] Hsiao F-L, Khelif A, Moubchir H, Choujaa A, Chen C-C, Laude V. Complete band gaps and deaf bands of triangular and honeycomb water-steel phononic crystals. J Appl Phys 2007;101:044903-5.
[191] Sheng P, Zhang X, Liu Z, Chan C. Locally resonant sonic materials. Physica B 2003;338:201–5.
[192] Liu Z, Zhang X, Mao Y, Zhu Y, Yang Z, Chan C, et al. Locally resonant sonic materials. Science 2000;289:1734.
[193] Yang Z, Dai H, Chan N, Ma G, Sheng P. Acoustic metamaterial panels for sound attenuation in the 50–1000 Hz regime. Appl Phys Lett 2010;96:041906.
[194] Mei J, Ma G, Yang M, Yang Z, Wen W, Sheng P. Dark acoustic metamaterials as super absorbers for low-frequency sound. Nat Commun 2012;3:756–63.
[195] Rossing TD. Springer handbook of acoustics. New York: Springer; 2007.
[196] Zhou R, Crocker MJ. Sound transmission loss of foam-filled honeycomb sandwich panels using statistical energy analysis and theoretical and measured dynamic properties. J Sound Vib 2010;329:673–86.
[197] Xin FX, Lu TJ. Transmission loss of orthogonally rib-stiffened double-panel structures with cavity absorption. J Acoust Soc Am 2011;129:1919–34.
[198] Toyoda M, Sakagami K, Takahashi D, Morimoto M. Effect of a honeycomb on the sound absorption characteristics of panel-type absorbers. Appl Acoust 2011;72:943–8.
[199] Maa D-Y. Potential of microperforated panel absorber. J Acoust Soc Am 1998;104:2861.
[200] Miri M, Stark H. Persistent random walk in a honeycomb structure: light transport in foams. Phys Rev E 2003;68:031102-8.
[201] Andrieu G, Panh J, Reineix A, Pelissou P, Girard C, Romeuf X, et al. Homogenization of composite panels from a near-field magnetic shielding effectiveness measurement. IEEE Trans Electromagn Compat 2012;54:700–3.
[202] Hollands K, Iynkaran K. Analytical model for the thermal conductance of compound honeycomb transparent insulation, with experimental validation. Sol Energy 1993;51:223–7.
[203] Suehrcke H, Däldehög D, Harris J, Lowe R. Heat transfer across corrugated sheets and honeycomb transparent insulation. Sol Energy 2004;76:351–8.
[204] Goldsmith W, Sackman JL. An experimental-study of energy-absorption in impact on sandwich plates. Int J Impact Eng 1992;12:241–62.
[205] Wang D. Impact behavior and energy absorption of paper honeycomb sandwich panels. Int J Impact Eng 2009;36:110–4.
[206] Wierzbicki T. Crushing analysis of metal honeycombs. Int J Impact Eng 1983;1:157–74.
[207] Wong IL, Eames PC, Perera R. A review of transparent insulation systems and the evaluation of payback period for building applications. Sol Energy 2007;81:1058–71.
[208] Kaushika N, Sharma P, Padma Priya R. Solar thermal analysis of honeycomb roof cover system for energy conservation in an air-conditioned building. Energy Build 1992;18:45–9.
[209] Rommel M, Wagner A. Application of transparent insulation materials in improved flat-plate collectors and integrated collector storages. Sol Energy 1992;49:371–80.
[210] Manz H, Egolf P, Suter P, Goetzberger A. TIM–PCM external wall system for solar space heating and daylighting. Sol Energy 1997;61:369–79.
[211] Cho JR, Kim KW, Yoo WS, Hong SI. Mesh generation considering detailed tread blocks for reliable 3D tire analysis. Adv Eng Softw 2004;35:105–13.
[212] Rhyne T, Cron SM. Development of a non-pneumatic wheel. Tire Sci Technol 2006;34:150–69.
[213] Ju J, Ananthasayanam B, Summers JD, Joseph P. Design of cellular shear bands of a non-pneumatic tire-investigation of contact pressure. SAE Int J Pass Cars 2010;3:598–606.
[214] Kim K, Kim S, Ju J, Kim D-M. Contact pressure of a non-pneumatic tire with 3D cellular spokes. In: Proc ASME int mech eng cong expo., Denver, CO; 2011.
[215] Ju JY, Summers JD. Compliant hexagonal periodic lattice structures having both high shear strength and high shear strain. Mater Des 2011;32:512–24.
[216] Jang IG, Sung YH, Yoo EJ, Kwak BM. Pattern design of a non-pneumatic tyre for stiffness using topology optimization. Eng Optim 2012;44:119–31.
[217] Radtke T, Charon A, Vodicka R. Hot/wet environmental degradation of honeycomb sandwich structure representative of F/A-18: flatwise tension strength. DTIC document; 1999.
[218] Campbell FC. Manufacturing technology for aerospace structural materials. Amsterdam: Elsevier; 2006.
[219] Choi HS, Jang YH. Bondline strength evaluation of cocure/precured honeycomb sandwich structures under aircraft hygro and repair environments. Compos A – Appl Sci 2010;41:1138–47.
[220] Zinno A, Prota A, Di Maio E, Bakis C. Experimental characterization of phenolic-impregnated honeycomb sandwich structures for transportation vehicles. Compos Struct 2011;93:2910–24.

[221] Park H, Kong C. A study on low velocity impact damage evaluation and repair technique of small aircraft composite structure. Composites Part A 2011;42:1179–88.
[222] Baker AA, Callus PJ, Georgiadis S, Falzon PJ, Dutton SE, Leong KH. An affordable methodology for replacing metallic aircraft panels with advanced composites. Compoites Part A 2002;33:687–96.
[223] Ning H, Janowski GM, Vaidya UK, Husman G. Thermoplastic sandwich structure design and manufacturing for the body panel of mass transit vehicle. Compos Struct 2007;80:82–91.
[224] Heo H, Ju J, Kim D-M. Compliant cellular structures: application to a passive morphing airfoil. Compos Struct 2013;106:560–9.
[225] Bettini P, Airoldi A, Sala G, Di Landro L, Ruzzene M, Spadoni A. Composite chiral structures for morphing airfoils: numerical analyses and development of a manufacturing process. Compos B – Eng 2010;41:133–47.
[226] Radford DD, McShane GJ, Deshpande VS, Fleck NA. Dynamic compressive response of stainless-steel square honeycombs. J Appl Mech 2007;74:658–67.
[227] Cabrera NO, Alcock B, Peijs T. Design and manufacture of all-PP sandwich panels based on co-extruded polypropylene tapes. Compos B – Eng 2008;39:1183–95.
[228] Carlin PS. Lightweight mirror systems for spacecraft – an overview of materials and manufacturing needs. IEEE Aero Conf Proc 2000;4:169–81.
[229] Guo SW, Zhang GY, Li LB, Wang WY, Zhao XZ. Effect of materials and modelling on the design of the space-based lightweight mirror. Mater Des 2009;30:9–14.
[230] Zhang Y, Zhang J, Han J, He X, Yao W. Large-scale fabrication of lightweight Si/SiC ceramic composite optical mirror. Mater Lett 2004;58:1204–8.
[231] Childs DW, Moyer DS. Vibration characteristics of the HPOTP (high-pressure oxygen turbopump) of the SSME (space-shuttle main engine). J Eng Gas Turb Power 1985;107:152–9.
[232] Chupp RE, Hendricks RC, Lattime SB, Steinetz BM. Sealing in turbomachinery. J Propul Power 2006;22:313–49.
[233] Bill RC, Shiembob LT. Some considerations of the performance of 2 honeycomb gas-path seal material systems. Lubr Eng 1981;37:209–17.
[234] Ha TW, Childs DW. Annular honeycomb-stator turbulent gas seal analysis using a new friction-factor model-based on flat-plate tests. J Tribol – Trans ASME 1994;116:352–60.
[235] Ha TW, Childs DW. A rotordynamic analysis of an annular honeycomb seal using a two-control volume model. KSME J 1996;10:332–40.
[236] Li J, Kong SR, Yan X, Obi S, Feng ZP. Numerical investigations on leakage performance of the rotating labyrinth honeycomb seal. J Eng Gas Turb Power 2010;132:062501.
[237] Schramm V, Willenborg K, Kim S, Wittig S. Influence of a honeycomb facing on the flow through a stepped labyrinth seal. J Eng Gas Turb Power 2002;124:140–6.
[238] Smalley AJ, Camatti M, Childs DW, Hollingsworth JR, Vannini G, Carter JJ. Dynamic characteristics of the diverging taper honeycomb-stator seal. J Turbomach 2006;128:717–24.
[239] Soto EA, Childs DW. Experimental rotordynamic coefficient results for (a) a labyrinth seal with and without shunt injection and (b) a honeycomb seal. J Eng Gas Turb Power 1999;121:153–9.
[240] Sprowl TB, Childs DW. A study of the effects of inlet preswirl on the dynamic coefficients of a straight-bore honeycomb gas damper seal. J Eng Gas Turb Power 2007;129:220–9.
[241] Weatherwax M, Childs DW. Theory versus experiment for the rotordynamic characteristics of a high pressure honeycomb annular gas seal at eccentric positions. J Tribol – Trans ASME 2003;125:422–9.
[242] Willenborg K, Schramm V, Kim S, Wittig S. Influence of a honeycomb facing on the heat transfer in a stepped labyrinth seal. J Eng Gas Turb Power 2002;124:133–9.
[243] Yan X, Li J, Feng ZP. Effects of inlet preswirl and cell diameter and depth on honeycomb seal characteristics. J Eng Gas Turb Power 2010;132:122506.
[244] Yu Z, Childs DW. A comparison of experimental rotordynamic coefficients and leakage characteristics between hole-pattern gas damper seals and a honeycomb seal. J Eng Gas Turb Power 1998;120:778–83.
[245] Bondarenko G, Khizhnyak L. Experimental investigation of a honeycomb seal. Chem Petrol Eng 1978;14:793–5.
[246] Chung DDL. Materials for electromagnetic interference shielding. J Mater Eng Perform 2000;9:350–4.
[247] Kopyt P, Damian R, Celuch M, Ciobanu R. Dielectric properties of chiral honeycombs – modelling and experiment. Compos Sci Technol 2010;70:1080–8.
[248] Wen T, Tian J, Lu T, Queheillalt D, Wadley H. Forced convection in metallic honeycomb structures. Int J Heat Mass Transfer 2006;49:3313–24.
[249] Zhou Y, Zuo X, Sun J, Mei J, Sun J. Effects of sintering parameters on the structures of Fe–Cr–Al extruded honeycombs. Mater Sci Eng A 2007;457:329–33.
[250] Martin U, Ehinger D, Kruger L, Martin S, Mottitschka T, Weigelt C, et al. Cellular energy absorbing TRIP-steel/Mg-PSZ composite: honeycomb structures fabricated by a new extrusion powder technology. Adv Mater Sci Eng 2010:1–6.
[251] Muraoka M, Sanada S. Displacement amplifier for piezoelectric actuator based on honeycomb link mechanism. Sens Actuat A 2010;157:84–90.
[252] Zhang QM, Wang H, Zhao J, Fielding JT, Newnham RE, Cross LE. A high sensitivity hydrostatic piezoelectric transducer based on transverse piezoelectric mode honeycomb ceramic composites. IEEE Trans Ultrason Ferr 1996;43:36–43.
[253] Hassan MR, Scarpa F, Mohamed NA. In-plane tensile behavior of shape memory alloy honeycombs with positive and negative Poisson's ratio. J Intel Mater Syst Struct 2009;20:897–905.
[254] You C, Stalculescu D, Martin L, Tentzeris MM. A novel hybrid electrical/mechanical optimization technique using time-domain modeling, finite element method and statistical tools for co-design and optimization of RF-integrated mechanical structures. Int J Numer Model El 2008;21:91–101.
[255] Ewais EMM, Ahmed YMZ, Ameen AMM. Preparation of porous cordierite ceramic using a silica secondary resource (silica fumes) for dust filtration purposes. J Ceram Process Res 2009;10:721–8.
[256] Mei H, Li C, Liu H, Ji S. Simulation of catalytic combustion of methane in a monolith honeycomb reactor1. J Chem Eng 2006;14:56–64.

[257] Kikuchi R, Takeda K, Sekizawa K, Sasaki K, Eguchi K. Thick-film coating of hexaaluminate catalyst on ceramic substrates and its catalytic activity for high-temperature methane combustion. Appl Catal A 2001;218:101–11.
[258] Agrafiotis C, Tsetsekou A, Stournaras CJ, Julbe A, Dalmazio L, Guizard C. Deposition of nanophase doped-ceria systems on ceramic honeycombs for automotive catalytic applications. Solid State Ionics 2000;136:1301–6.
[259] Groppi G, Tronconi E. Honeycomb supports with high thermal conductivity for gas/solid chemical processes. Catal Today 2005;105:297–304.
[260] Plagemann R, Jonas L, Kragl U. Ceramic honeycomb as support for covalent immobilization of laccase from *Trametes versicolor* and transformation of nuclear fast red. Appl Microbiol Biotechnol 2011;90:313–20.
[261] Sepulveda C, Amell A, Cadavid F. Development of a methodology for designing and characterizing honeycomb heat regenerators. Dyna-Colombia 2010;77:200–8.
[262] Yamaguchi T, Shimizu S, Suzuki T, Fujishiro Y, Awano M. Evaluation of extruded cathode honeycomb monolith-supported SOFC under rapid start-up operation. Electro Acta 2009;54:1478–82.
[263] Saha BP, Kumari S, Johnson R, Prasad NE. Effect of relative density on the compressive flow behaviour of cordierite and cordierite: mullite honeycombs. Tran Indian Inst Metals 2010;63:701–6.
[264] Nath Das R, Madhusoodana C, Okada K. Rheological studies on cordierite honeycomb extrusion. J Eur Ceram Soc 2002;22:2893–900.
[265] Amariei D, Amrousse R, Batonneau Y, Brahmi R, Kappenstein C, Cartoixa B. Monolithic catalysts for the decomposition of energetic compounds. In: Proc 10th int symp, vol. 175; 2010. p. 35–42.
[266] Aranzabal A, Iturbe D, Romero-Saez M, Gonzalez-Marcos MP, Gonzalez-Velasco JR, Gonzalez-Marcos JA. Optimization of process parameters on the extrusion of honeycomb shaped monolith of H-ZSM-5 zeolite. Chem Eng J 2010;162:415–23.
[267] Jain V, Johnson R, Ganesh I, Saha B, Mahajan Y. Effect of rubber encapsulation on the comparative mechanical behaviour of ceramic honeycomb and foam. Mater Sci Eng A 2003;347:109–22.
[268] Zeng S, Su H, Liu Y, Wang Y, Wang D. CuO–CeO_2/Al_2O_3/FeCrAl monolithic catalysts prepared by in situ combustion synthesis method for preferential oxidation of carbon monoxide. J Rare Earths 2011;29:69–73.
[269] Davis ME. Ordered porous materials for emerging applications. Nature 2002;417:813–21.
[270] Gourley P, Wendt J, Vawter G, Brennan T, Hammons B. Optical properties of two-dimensional photonic lattices fabricated as honeycomb nanostructures in compound semiconductors. Appl Phys Lett 1994;64:687–9.
[271] Vincetti L, Poli F, Selleri S. Confinement loss and nonlinearity analysis of air-guiding modified honeycomb photonic bandgap fibers. IEEE Photon Technol Lett 2006;18:508–10.
[272] Wang X, Summers CJ, Wang ZL. Large-scale hexagonal-patterned growth of aligned ZnO nanorods for nano-optoelectronics and nanosensor arrays. Nano Lett 2004;4:423–6.
[273] Luo X, Liu Y, Liu W. A honeycomb microchannel cooling system for microelectronics cooling. Heat Transfer Eng 2011;32:616–23.
[274] Hauser H, Michl B, Kübler V, Schwarzkopf S, Müller C, Hermle M, et al. Nanoimprint lithography for honeycomb texturing of multicrystalline silicon. Energy Proc 2011;8:648–53.
[275] Yamamoto T, Shido T, Inagaki S, Fukushima Y, Ichikawa M. Ship-in-bottle synthesis of [Pt15(CO)30] 2-encapsulated in ordered hexagonal mesoporous channels of FSM-16 and their effective catalysis in water-gas shift reaction. J Am Chem Soc 1996;118:5810–1.
[276] Wu Z, Yu K, Zhang S, Xie Y. Hematite hollow spheres with a mesoporous shell: controlled synthesis and applications in gas sensor and lithium ion batteries. J Phys Chem C 2008;112:11307–13.
[277] Selvam P, Bhatia SK, Sonwane CG. Recent advances in processing and characterization of periodic mesoporous MCM-41 silicate molecular sieves. Ind Eng Chem Res 2001;40:3237–61.
[278] Gatica JM, Rodriguez-Izquierdo JM, Sanchez D, Chafik T, Harti S, Zaitan H, et al. Originally prepared carbon-based honeycomb monoliths with potential application as VOCs adsorbents. C R Chim 2006;9:1215–20.
[279] Zhang Z, Dai S, Blom DA, Shen J. Synthesis of ordered metallic nanowires inside ordered mesoporous materials through electroless deposition. Chem Mater 2002;14:965–8.
[280] Avouris P, Lin Y, Xia F, Mueller T, Farmer D, Dimitrakopoulos C, et al. Graphene-based fast electronics and optoelectronics. In: Proceedings of device research conference (DRC); 2010. p. 205–6.
[281] Avouris P, Freitag M, Perebeinos V. Carbon-nanotube photonics and optoelectronics. Nat Photon 2008;2:341–50.
[282] Wang X-Y, Wang L, Wang Z-M, Gao S. Solvent-tuned azido-bridged Co^{2+} layers: square, honeycomb, and kagomé. J Am Chem Soc 2006;128:674–5.
[283] Jani AMM, Losic D, Voelcker NH. Nanoporous anodic aluminium oxide: advances in surface engineering and emerging applications. Prog Mater Sci 2013;58:636–704.
[284] Barela MJ, Brevnov DA, Bauer TM, Lopez GP, Atanassov PB. Fabrication of patterned arrays with alternating regions of aluminum and porous aluminum oxide. Electrochem Solid State Lett 2005;8:4–5.
[285] Karmhag R, Tesfamichael T, Wäckelgård E, Niklasson GA, Nygren M. Oxidation kinetics of nickel particles: comparison between free particles and particles in an oxide matrix. Sol Energy 2000;68:329–33.
[286] Nielsch K, Wehrspohn R, Barthel J, Kirschner J, Gosele U, Fischer S, et al. Hexagonally ordered 100 nm period nickel nanowire arrays. Appl Phys Lett 2001;79:1360–2.
[287] Che G, Lakshmi BB, Martin CR, Fisher ER, Ruoff RS. Chemical vapor deposition based synthesis of carbon nanotubes and nanofibers using a template method. Chem Mater 1998;10:260–7.
[288] Che GL, Lakshmi BB, Fisher ER, Martin CR. Carbon nanotubule membranes for electrochemical energy storage and production. Nature 1998;393:346–9.
[289] Kim Y, Jung B, Lee H, Kim H, Lee K, Park H. Capacitive humidity sensor design based on anodic aluminum oxide. Sens Actuat B – Chem 2009;141:441–6.
[290] Zhang Z, Gekhtman D, Dresselhaus MS, Ying JY. Processing and characterization of single-crystalline ultrafine bismuth nanowires. Chem Mater 1999;11:1659–65.
[291] Sauer G, Brehm G, Schneider S, Nielsch K, Wehrspohn R, Choi J, et al. Highly ordered monocrystalline silver nanowire arrays. J Appl Phys 2002;91:3243.

[292] Yabu H, Tanaka M, Ijiro K, Shimomura M. Preparation of honeycomb-patterned polyimide films by self-organization. Langmuir 2003;19:6297–300.
[293] Ha JM, Wolf JH, Hillmyer MA, Ward MD. Polymorph selectivity under nanoscopic confinement. J Am Chem Soc 2004;126:3382–3.
[294] Kurono N, Shimada R, Ishihara T, Shimomura M. Fabrication and optical property of self-organized honeycomb-patterned films. Mol Cryst Liquid Cryst 2002;377:285–8.
[295] Yabu H, Shimomura M. Single-step fabrication of transparent superhydrophobic porous polymer films. Chem Mater 2005;17:5231–4.
[296] Körstgens V, Hsu CC, Paneque D, Wiedersich J, Müller-Buschbaum P. Improvement of quantum efficiency of photomultiplier tubes by humidity controlled coatings based on porous polymer structures. Appl Phys Lett 2008;93:041916.
[297] Widawski G, Rawiso M, François B. Self-organized honeycomb morphology of star-polymer polystyrene films. Nature 1994;369:387–9.
[298] Han S, Briseno AL, Shi X, Mah DA, Zhou F. Polyelectrolyte-coated nanosphere lithographic patterning of surfaces: fabrication and characterization of electropolymerized thin polyaniline honeycomb films. J Phys Chem B 2002;106:6465–72.
[299] Bolognesi A, Mercogliano C, Yunus S, Civardi M, Comoretto D, Turturro A. Self-organization of polystyrenes into ordered microstructured films and their replication by soft lithography. Langmuir 2005;21:3480–5.
[300] Jenekhe SA, Chen XL. Self-assembly of ordered microporous materials from rod-coil block copolymers. Science 1999;283:372–5.
[301] Uraki Y, Nemoto J, Otsuka H, Tamai Y, Sugiyama J, Kishimoto T, et al. Honeycomb-like architecture produced by living bacteria, *Gluconacetobacter xylinus*. Carbohyd Polym 2007;69:1–6.
[302] Nemoto J, Uraki Y, Kishimoto T, Sano Y, Funada R, Obata N, et al. Production of mesoscopically patterned cellulose film. Biores Technol 2005;96:1955–8.
[303] Yabu H, Shimomura M. Simple fabrication of micro lens arrays. Langmuir 2005;21:1709–11.
[304] Bunz UHF. Breath figures as a dynamic templating method for polymers and nanomaterials. Adv Mater 2006;18:973–89.
[305] Escalé P, Rubatat L, Billon L, Save M. Recent advances in honeycomb-structured porous polymer films prepared via breath figures. Eur Polym J 2012;48:1001–25.
[306] Jung S-B, Ha T-J, Park H-H. Investigation of the properties of organically modified ordered mesoporous silica films. J Colloid Interface Sci 2008;320:527–34.
[307] Reddy KM, Wei B, Song C. Mesoporous molecular sieve MCM-41 supported Co–Mo catalyst for hydrodesulfurization of petroleum resids. Catal Today 1998;43:261–72.
[308] Ye Y, Sun W, Wang Y, Shao X, Xu X, Cheng F, et al. A unified model: self-assembly of trimesic acid on gold. J Phys Chem C 2007;111:10138–41.
[309] Chae HK, Siberio-Perez DY, Kim J, Go Y, Eddaoudi M, Matzger AJ, et al. A route to high surface area, porosity and inclusion of large molecules in crystals. Nature 2004;427:523–7.
[310] Thandavamoorthy S, Gopinath N, Ramkumar S. Self-assembled honeycomb polyurethane nanofibers. J Appl Polym Sci 2006;101:3121–4.
[311] Geim AK, Novoselov KS. The rise of graphene. Nat Mater 2007;6:183–91.
[312] Knight JC, Broeng J, Birks TA, Russell PSJ. Photonic band gap guidance in optical fibers. Science 1998;282:1476–8.
[313] Coffey VC. Novel fibers use space to extend capacity limits. Photon Spectra 2013;47:52–5.
[314] Kievsky Y, Sokolov I. Self-assembly of uniform nanoporous silica fibers. IEEE Trans Nanotechnol 2005;4:490–4.
[315] Singh MK, Titus E, Gonçalves G, Marques PA, Bdikin I, Kholkin AL, et al. Atomic-scale observation of rotational misorientation in suspended few-layer graphene sheets. Nanoscale 2010;2:700–8.
[316] Mishchenko L, Hatton B, Bahadur V, Taylor JA, Krupenkin T, Aizenberg J. Design of ice-free nanostructured surfaces based on repulsion of impacting water droplets. ACS Nano 2010;4:7699–707.
[317] Wang L, Li Y. Controlled synthesis and luminescence of lanthanide doped NaYF4 nanocrystals. Chem Mater 2007;19:727–34.
[318] Liu K, Zhang M, Zhai J, Wang J, Jiang L. Bioinspired construction of Mg–Li alloys surfaces with stable superhydrophobicity and improved corrosion resistance. Appl Phys Lett 2008;92. 183103-3.
[319] Sun TL, Feng L, Gao XF, Jiang L. Bioinspired surfaces with special wettability. Acc Chem Res 2005;38:644–52.
[320] Cassie ABD, Baxter S. Wettability of porous surfaces. Trans Faraday Soc 1944;40:0546-50.
[321] Li S, Li H, Wang X, Song Y, Liu Y, Jiang L, et al. Super-hydrophobicity of large-area honeycomb-like aligned carbon nanotubes. J Phys Chem B 2002;106:9274–6.
[322] Yin S, Niu Z, Chen X. Assembly of graphene sheets into 3D macroscopic structures. Small 2012;8:2458–63.
[323] Yin S, Goldovsky Y, Herzberg M, Liu L, Sun H, Zhang Y, et al. Functional free-standing graphene honeycomb films. Adv Funct Mater 2013;23:2972–8.
[324] Kotobuki M, Suzuki Y, Munakata H, Kanamura K, Sato Y, Yamamoto K, et al. Fabrication of three-dimensional battery using ceramic electrolyte with honeycomb structure by sol-gel process. J Electrochem Soc 2010;157:493–8.
[325] Li N, Mitchell DT, Lee KP, Martin CR. A nanostructured honeycomb carbon anode. J Electrochem Soc 2003;150:979–84.
[326] François B, Pitois O, François J. Polymer films with a self-organized honeycomb morphology. Adv Mater 1995;7:1041–4.
[327] Oekermann T, Yoshida T, Nakazawa J, Yasuno S, Sugiura T, Minoura H. Wall thickness and charge transport properties of nano-honeycomb TiO_2 structures prepared by photoetching. Electrochim Acta 2007;52:4325–33.
[328] Liu H, Chen F, Yang Q, Qu P, He S, Wang X, et al. Fabrication of bioinspired omnidirectional and gapless microlens array for wide field-of-view detections. Appl Phys Lett 2012;100:133701-3.
[329] Meade RD, Brommer KD, Rappe AM, Joannopoulos J. Existence of a photonic band gap in two dimensions. Appl Phys Lett 1992;61:495–7.
[330] Zhou L, Smith D, McCartney MR, Katzer D, Storm D. Observation of vertical honeycomb structure in InAlN/GaN heterostructures due to lateral phase separation. Appl Phys Lett 2007;90. 081917-3.

[331] Honda K, Rao TN, Tryk D, Fujishima A, Watanabe M, Yasui K, et al. Electrochemical characterization of the nanoporous honeycomb diamond electrode as an electrical double-layer capacitor. J Electrochem Soc 2000;147:659–64.
[332] Ragonese E, Girlando G, Palmisano G. A very accurate design of monolithic inductors in a 2D EM simulator. In: 9th International conference on electronics, circuits and systems. IEEE; 2002. p. 1199–202.
[333] Zhang K, Rossi C, Alphonse P, Tenailleau C. NiO nanostructured honeycomb realized by annealing Ni film deposited on silicon. J Nanosci Nanotechnol 2008;8:5903–7.
[334] Sazio PJ, Amezcua-Correa A, Finlayson CE, Hayes JR, Scheidemantel TJ, Baril NF, et al. Microstructured optical fibers as high-pressure microfluidic reactors. Science 2006;311:1583–6.
[335] Weissmüller J, Viswanath RN, Kramer D, Zimmer P, Würschum R, Gleiter H. Charge-induced reversible strain in a metal. Science 2003;300:312–5.
[336] Kramer D, Viswanath RN, Weissmüller J. Surface-stress induced macroscopic bending of nanoporous gold cantilevers. Nano Lett 2004;4:793–6.
[337] Chen PC, Wan LS, Ke BB, Xu ZK. Honeycomb-patterned film segregated with phenylboronic acid for glucose sensing. Langmuir 2011;27:12597–605.
[338] Kumeria T, Parkinson L, Losic D. A nanoporous interferometric micro-sensor for biomedical detection of volatile sulphur compounds. Nanoscale Res Lett 2011;6:1–7.
[339] Albert KJ, Walt DR, Gill DS, Pearce TC. Optical multibead arrays for simple and complex odor discrimination. Anal Chem 2001;73:2501–8.
[340] Dickinson TA, White J, Kauer JS, Walt DR. A chemical-detecting system based on a cross-reactive optical sensor array. Nature 1996;382:697–700.
[341] Kosynkin DV, Higginbotham AL, Sinitskii A, Lomeda JR, Dimiev A, Price BK, et al. Longitudinal unzipping of carbon nanotubes to form graphene nanoribbons. Nature 2009;458:872–6.
[342] Zhang K, Kemp KC, Chandra V. Homogeneous anchoring of TiO_2 nanoparticles on graphene sheets for waste water treatment. Mater Lett 2012;81:127–30.
[343] Xu Y, Bai H, Lu G, Li C, Shi G. Flexible graphene films via the filtration of water-soluble noncovalent functionalized graphene sheets. J Am Chem Soc 2008;130:5856–7.
[344] Nishikawa T, Ookura R, Nishida J, Arai K, Hayashi J, Kurono N, et al. Fabrication of honeycomb film of an amphiphilic copolymer at the air-water interface. Langmuir 2002;18:5734–40.
[345] May S, Ben-Shaul A. DNA-lipid complexes: stability of honeycomb-like and spaghetti-like structures. Biophys J 1997;73:2427–40.
[346] Tanaka M, Nishikawa K, Okubo H, Kamachi H, Kawai T, Matsushita M, et al. Control of hepatocyte adhesion and function on self-organized honeycomb-patterned polymer film. Colloid Surf A 2006;284:464–9.
[347] Fang Y, Gu D, Zou Y, Wu Z, Li F, Che R, et al. A low-concentrationhydrothermal synthesis of biocompatible ordered mesoporous carbon nanospheres with tunable and uniform size. Angew Chem Int Ed Engl 2010;49:7987–91.
[348] Pawin G, Wong KL, Kwon KY, Bartels L. A homomolecular porous network at a Cu(1 1 1) surface. Science 2006;313:961–2.
[349] Tanaka M. Design of novel 2D and 3D biointerfaces using self-organization to control cell behavior. Bba-Gen Subj 2011;1810:251–8.
[350] Xiu Y, Zhu L, Hess D, Wong C. Superhydrophobic silicone/PTFE films for biocompatible application in encapsulation of implantable microelectronics devices. In: 56th Electronic components and technology conference, San Diego; 2006. p. 686–92.
[351] Nyström D, Malmström E, Hult A, Blakey I, Boyer C, Davis TP, et al. Biomimetic surface modification of honeycomb films via a "grafting from" approach. Langmuir 2010;26:12748–54.
[352] Nishikawa T, Nishida J, Ookura R, Nishimura S-I, Wada S, Karino T, et al. Honeycomb-patterned thin films of amphiphilic polymers as cell culture substrates. Mater Sci Eng C 1999;8:495–500.
[353] Nishikawa T, Nishida J, Ookura R, Nishimura S-I, Wada S, Karino T, et al. Mesoscopic patterning of cell adhesive substrates as novel biofunctional interfaces. Mater Sci Eng C 1999;10:141–6.
[354] Tanaka M, Takebayashi M, Miyama M, Nishida J, Shimomura M. Design of novel biointerfaces (II). Fabrication of self-organized porous polymer film with highly uniform pores. Biomed Mater Eng 2004;14:439–46.
[355] Zhang Y, Wang C. Micropatterning of proteins on 3D porous polymer film fabricated by using the breath-figure method. Adv Mater 2007;19:913–6.
[356] Yao X, Yao H, Li Y, Chen G. Preparation of honeycomb scaffold with hierarchical porous structures by core-crosslinked core-corona nanoparticles. J Colloid Interface Sci 2009;332:165–72.
[357] Shi S, Wang XH, Guo G, Fan M, Huang MJ, Qian ZY. Preparation and characterization of microporous poly(D,L-lactic acid) film for tissue engineering scaffold. Int J Nanomed 2010;5:1049–55.
[358] Zhang Z, Hughes TC, Gurr PA, Blencowe A, Hao X, Qiao GG. Influence of polymer elasticity on the formation of non-cracking honeycomb films. Adv Mater 2012;24:4327–30.
[359] Tanaka M, Takayama A, Ito E, Sunami H, Yamamoto S, Shimomura M. Effect of pore size of self-organized honeycomb-patterned polymer films on spreading, focal adhesion, proliferation, and function of endothelial cells. J Nanosci Nanotechnol 2007;7:763–72.
[360] Fukuhira Y, Kitazono E, Hayashi T, Kaneko H, Tanaka M, Shimomura M, et al. Biodegradable honeycomb-patterned film composed of poly(lactic acid) and dioleoylphosphatidylethanolamine. Biomaterials 2006;27:1797–802.
[361] Abbott A. Cell culture: biology's new dimension. Nature 2003;424:870–2.
[362] Li Y, Huang G, Zhang X, Wang L, Du Y, Lu TJ, et al. Engineering cell alignment in vitro. Biotechnol Adv 2014;32:347–65.
[363] Huang G, Wang L, Wang S, Han Y, Wu J, Zhang Q, et al. Engineering three-dimensional cell mechanical microenvironment with hydrogels. Biofabrication 2012;4:042001.
[364] Han YL, Wang S, Zhang X, Li Y, Huang G, Qi H, et al. Engineering physical microenvironment for stem cell based regenerative medicine. Drug Discov Today 2014;19:763–73.
[365] Huang GY, Zhou LH, Zhang QC, Chen YM, Sun W, Xu F, et al. Microfluidic hydrogels for tissue engineering. Biofabrication 2011;3:012001.

[366] Hutmacher DW. Scaffold design and fabrication technologies for engineering tissues—state of the art and future perspectives. J Biomater Sci 2001;12:107–24.
[367] Hutmacher DW, Schantz T, Zein I, Ng KW, Teoh SH, Tan KC. Mechanical properties and cell cultural response of polycaprolactone scaffolds designed and fabricated via fused deposition modeling. J Biomed Mater Res 2001;55:203–16.
[368] Zein I, Hutmacher DW, Tan KC, Teoh SH. Fused deposition modeling of novel scaffold architectures for tissue engineering applications. Biomaterials 2002;23:1169–85.
[369] Hollister SJ. Porous scaffold design for tissue engineering. Nat Mater 2005;4:518–24.
[370] Peltola SM, Melchels FP, Grijpma DW, Kellomäki M. A review of rapid prototyping techniques for tissue engineering purposes. Ann Med 2008;40:268–80.
[371] Abdelaal OA, Darwish SM. Review of rapid prototyping techniques for tissue engineering scaffolds fabrication. Charact Develop Biosys Biomater 2013:33–54.
[372] Bidan CM, Kommareddy KP, Rumpler M, Kollmannsberger P, Brechet YJM, Fratzl P, et al. How linear tension converts to curvature: geometric control of bone tissue growth. PLoS ONE 2012;7:36336.
[373] Bidan CM, Kommareddy KP, Rumpler M, Kollmannsberger P, Fratzl P, Dunlop JWC. Geometry as a factor for tissue growth: towards shape optimization of tissue engineering scaffolds. Adv Health Mater 2013;2:186–94.
[374] Hanson Shepherd JN, Parker ST, Shepherd RF, Gillette MU, Lewis JA, Nuzzo RG. 3D microperiodic hydrogel scaffolds for robust neuronal cultures. Adv Funct Mater 2011;21:47–54.
[375] Miyagawa Y, Okita H, Hiroyama M, Sakamoto R, Kobayashi M, Nakajima H, et al. A microfabricated scaffold induces the spheroid formation of human bone marrow-derived mesenchymal progenitor cells and promotes efficient adipogenic differentiation. Tissue Eng Part A 2010;17:513–21.
[376] Engelmayr GC, Cheng M, Bettinger CJ, Borenstein JT, Langer R, Freed LE. Accordion-like honeycombs for tissue engineering of cardiac anisotropy. Nat Mater 2008;7:1003–10.
[377] Park H, Larson BL, Guillemette MD, Jain SR, Hua C, Engelmayr GC, et al. The significance of pore microarchitecture in a multi-layered elastomeric scaffold for contractile cardiac muscle constructs. Biomaterials 2011;32:1856–64.
[378] Schantz JT, Ng MML, Netto P, Chong Lai Ming J, Wong KM, Hutmacher DW, et al. Application of an X-ray microscopy technique to evaluate tissue-engineered bone-scaffold constructs. Mater Sci Eng C 2002;20:9–17.
[379] da Silva J, Lautenschläger F, Sivaniah E, Guck JR. The cavity-to-cavity migration of leukaemic cells through 3D honeycombed hydrogels with adjustable internal dimension and stiffness. Biomaterials 2010;31:2201–8.
[380] Gao B, Wang L, Han S, Pingguan-Murphy B, Zhang X, Xu F. Engineering of microscale three-dimensional pancreatic islet models in vitro and their biomedical applications. Crit Rev Biotechnol 2015:1–11.
[381] Wang L, Li Y, Huang G, Zhang X, Pingguan-Murphy B, Gao B, et al. Hydrogel-based methods for engineering cellular microenvironment with spatiotemporal gradients. Crit Rev Biotechnol 2015:1–13.
[382] Wang L, Huang G, Sha B, Wang S, Han Y, Wu J, et al. Engineering three-dimensional cardiac microtissues for potential drug screening applications. Curr Med Chem 2014;21:2497–509.
[383] Hutmacher DW, Sittinger M, Risbud MV. Scaffold-based tissue engineering: rationale for computer-aided design and solid free-form fabrication systems. Trends Biotechnol 2004;22:354–62.
[384] Zhang H, Burdet E, Hutmacher DW, Poo A-N, Bellouard Y, Clavel R, et al. Robotic micro-assembly of scaffold/cell constructs with a shape memory alloy gripper. Proc ICRA IEEE Int Conf 2002:1483–8.
[385] Zhang H, Hutmacher DW, Chollet F, Poo AN, Burdet E. Microrobotics and MEMS-based fabrication techniques for scaffold-based tissue engineering. Macromol Biosci 2005;5:477–89.
[386] Li Y, Huang G, Zhang X, Li B, Chen Y, Lu T, et al. Magnetic hydrogels and their potential biomedical applications. Adv Funct Mater 2013;23:660–72.
[387] Huang G, Zhang X, Xiao Z, Zhang Q, Zhou J, Xu F, et al. Cell-encapsulating microfluidic hydrogels with enhanced mechanical stability. Soft Matter 2012;8:10687–94.
[388] Xu F, Inci F, Mullick O, Gurkan UA, Sung Y, Kavaz D, et al. Release of magnetic nanoparticles from cell-encapsulating biodegradable nanobiomaterials. ACS Nano 2012;6:6640–9.
[389] Xu F, Finley TD, Turkaydin M, Sung YR, Gurkan UA, Yavuz AS, et al. The assembly of cell-encapsulating microscale hydrogels using acoustic waves. Biomaterials 2011;32:7847–55.
[390] Han YL, Yang YS, Liu SB, Wu JH, Chen YM, Lu TJ, et al. Directed self-assembly of microscale hydrogels by electrostatic interaction. Biofabrication 2013;5:035004.
[391] Xu F, Sridharan B, Wang S, Gurkan UA, Syverud B, Demirci U. Embryonic stem cell bioprinting for uniform and controlled size embryoid body formation. Biomicrofluidics 2011;5:022207.
[392] Xu F, Celli J, Rizvi I, Moon S, Hasan T, Demirci U. A three-dimensional in vitro ovarian cancer coculture model using a high-throughput cell patterning platform. Biotechnol J 2011;6:204–12.
[393] Xu F, Moon S, Emre A, Turali E, Song Y, Hacking S, et al. A droplet-based building block approach for bladder smooth muscle cell (SMC) proliferation. Biofabrication 2010;2:014105.
[394] Zhou L, Huang G, Wang S, Wu J, Lee WG, Chen Y, et al. Advances in cell-based biosensors using three-dimensional cell-encapsulating hydrogels. Biotechnol J 2011;6:1466–76.
[395] Fulati A, Ali SMU, Asif MH, Alvi NU, Willander M, Brannmark C, et al. An intracellular glucose biosensor based on nanoflake ZnO. Sens Actuat B – Chem 2010;150:673–80.
[396] Suneesh PV, Chandhini K, Ramachandran T, Nair BG, Babu TGS. Tantalum oxide honeycomb architectures for the development of a non-enzymatic glucose sensor with wide detection range. Biosens Bioelect 2013;50:472–7.
[397] Patel AC, Li SX, Yuan JM, Wei Y. In situ encapsulation of horseradish peroxidase in electrospun porous silica fibers for potential biosensor applications. Nano Lett 2006;6:1042–6.
[398] Ang PK, Jaiswal M, Lim CHYX, Wang Y, Sankaran J, Li A, et al. A bioelectronic platform using a graphene–lipid bilayer interface. ACS Nano 2010;4:7387–94.
[399] Seo DH, Pineda S, Yick S, Bell J, Han ZJ, Ostrikov KK. Plasma-enabled sustainable elemental lifecycles: honeycomb-derived graphenes for next-generation biosensors and supercapacitors. Green Chem 2015;16:4772–9.
[400] Feng M, Morales AB, Beugeling T, Bantjes A, vanderWerf K, Gosselink G, et al. Adsorption of high density lipoproteins (HDL) on solid surfaces. J Colloid Interface Sci 1996;177:364–71.

[401] Hubbell JA. Biomaterials in tissue engineering. Bio-Technology 1995;13:565–76.
[402] Hartmann M. Ordered mesoporous materials for bioadsorption and biocatalysis. Chem Mater 2005;17:4577–93.
[403] Popat A, Hartono SB, Stahr F, Liu J, Qiao SZ, Lu GQM. Mesoporous silica nanoparticles for bioadsorption, enzyme immobilisation, and delivery carriers. Nanoscale 2011;3:2801–18.
[404] Yue YH, Gédéon A, Bonardet JL, Melosh N, Espinosea JB, Fraissarda J. Direct synthesis of AlSBA mesoporous molecular sieves: characterization and catalytic activities. Chem Commun 1999;19:1967–8.
[405] Vinu A, Murugesan V, Bohlmann W, Hartmann M. An optimized procedure for the synthesis of alsba-15 with large pore diameter and high aluminum content. J Phys Chem B 2004;108:11496–505.
[406] Slowing II, Vivero-Escoto JL, Wu C-W, Lin VS-Y. Mesoporous silica nanoparticles as controlled release drug delivery and gene transfection carriers. Adv Drug Deliv Rev 2008;60:1278–88.
[407] Vallet-Regí M, Balas F, Arcos D. Mesoporous materials for drug delivery. Angew Chem Int Ed 2007;46:7548–58.
[408] Vallet-Regi M, Ramila A, Del Real R, Pérez-Pariente J. A new property of MCM-41: drug delivery system. Chem Mater 2001;13:308–11.
[409] Salonen J, Laitinen L, Kaukonen AM, Tuura J, Bjorkqvist M, Heikkila T, et al. Mesoporous silicon microparticles for oral drug delivery: loading and release of five model drugs. J Control Release 2005;108:362–74.
[410] Vallet-Regi M, Doadrio JC, Doadrio AL, Izquierdo-Barba I, Perez-Pariente J. Hexagonal ordered mesoporous material as a matrix for the controlled release of amoxicillin. Solid State Ionics 2004;172:435–9.
[411] Balas F, Manzano M, Horcajada P, Vallet-Regi M. Confinement and controlled release of bisphosphonates on ordered mesoporous silica-based materials. J Am Chem Soc 2006;128:8116–7.
[412] Doadrio JC, Sousa EMB, Izquierdo-Barba I, Doadrio AL, Perez-Pariente J, Vallet-Regi M. Functionalization of mesoporous materials with long alkyl chains as a strategy for controlling drug delivery pattern. J Mater Chem 2006;16:462–6.
[413] Doadrio AL, Sousa EM, Doadrio JC, Perez Pariente J, Izquierdo-Barba I, Vallet-Regi M. Mesoporous SBA-15 HPLC evaluation for controlled gentamicin drug delivery. J Control Release 2004;97:125–32.
[414] Wang G, Otuonye AN, Blair EA, Denton K, Tao ZM, Asefa T. Functionalized mesoporous materials for adsorption and release of different drug molecules: a comparative study. J Solid State Chem 2009;182:1649–60.
[415] Cavallaro G, Pierro P, Palumbo FS, Testa F, Pasqua L, Aiello R. Drug delivery devices based on mesoporous silicate. Drug Deliv 2004;11:41–6.
[416] Yu H, Zhai QZ. Mesoporous SBA-15 molecular sieve as a carrier for controlled release of nimodipine. Microporous Mesoporous Mater 2009;123:298–305.
[417] Hata H, Saeki S, Kimura T, Sugahara Y, Kuroda K. Adsorption of taxol into ordered mesoporous silicas with various pore diameters. Chem Mater 1999;11:1110–9.
[418] Doadrio AL, Doadrio JC, Sanchez-Montero JM, Salinas AJ, Vallet-Regi M. A rational explanation of the vancomycin release from SBA-15 and its derivative by molecular modelling. Microporous Mesoporous Mater 2010;132:559–66.
[419] Lee KT, Oh SM. Novel synthesis of porous carbons with tunable pore size by surfactant-templated sol-gel process and carbonisation. Chem Commun 2002:2722–3.
[420] Saha D, Contescu CI, Gallego NC. Bimodal mesoporous carbon synthesized from large organic precursor and amphiphilic tri-block copolymer by self-assembly. Microporous Mesoporous Mater 2012;155:71–4.
[421] Gultepe E, Nagesha D, Sridhar S, Amiji M. Nanoporous inorganic membranes or coatings for sustained drug delivery in implantable devices. Adv Drug Deliv Rev 2010;62:305–15.
[422] Gultepe E, Nagesha D, Casse BD, Banyal R, Fitchorov T, Karma A, et al. Sustained drug release from non-eroding nanoporous templates. Small 2010;6:213–6.
[423] Gibson LJ, Ashby MF. Cellular solids: structure and properties. Cambridge University Press; 1999.
[424] Han B, Qin KK, Yu B, Wang B, Zhang QC, Lu TJ. Honeycomb-corrugation hybrid as a novel sandwich core for significantly enhanced compressive performance. Mater Des 2015, submitted for publication.
[425] Hepburn H, Kurstjens S. The combs of honeybees as composite materials. Apidologie 1988;19:25–36.
[426] Zhang K, Duan H, Karihaloo BL, Wang J. From the cover: hierarchical, multilayered cell walls reinforced by recycled silk cocoons enhance the structural integrity of honeybee combs. PNAS 2010;107:9502–6.
[427] Kamat S, Su X, Ballarini R, Heuer A. Structural basis for the fracture toughness of the shell of the conch *Strombus gigas*. Nature 2000;405:1036–40.
[428] Buehler MJ, Ackbarow T. Fracture mechanics of protein materials. Mater Today 2007;10:46–58.
[429] Wan Y, Cui X, Wen Z. Ordered mesoporous carbon coating on cordierite: synthesis and application as an efficient adsorbent. J Hazard Mater. 2011;198:216–23.
[430] Song F, Su HL, Chen JJ, Moon WJ, Lau WM, Zhang D. 3D hierarchical porous SnO_2 derived from self-assembled biological systems for superior gas sensing application. J Mater Chem 2012;22:1121–6.
[431] Compton BG, Lewis JA. 3D-printing of lightweight cellular composites. Adv Mater 2014;26:5930–5.
[432] Bauer J, Hengsbach S, Tesari I, Schwaiger R, Kraft O. High-strength cellular ceramic composites with 3D microarchitecture. Proc Natl Acad Sci 2014;111:2453–8.
[433] Brockmann A, Groh C, Fröhlich B. Wax perception in honeybees: contact is not necessary. Naturwissenschaften 2003;90:424–7.
[434] D'Ettorre P, Wenseleers T, Dawson J, Hutchinson S, Boswell T, Ratnieks FLW. Wax combs mediate nestmate recognition by guard honeybees. Animal Behav 2006;71:773–9.
[435] Seeley T, Morse R. The nest of the honey bee (*Apis mellifera* L.). Insectes Soc 1976;23:495–512.
[436] Berry JA, Delaplane KS. Effects of comb age on honey bee colony growth and brood survivorship. J Apicult Res 2001;40:3–8.
[437] Rho JY, Kuhn-Spearing L, Zioupos P. Mechanical properties and the hierarchical structure of bone. Med Eng Phys 1998;20:92–102.
[438] Lee N, Horstemeyer MF, Rhee H, Nabors B, Liao J, Williams LN. Hierarchical multiscale structure-property relationships of the red-bellied woodpecker (*Melanerpes carolinus*) beak. J R Soc Interface 2014;11. 20140274-13.
[439] Hao GY, Wheeler JK, Holbrook NM, Goldstein G. Investigating xylem embolism formation, refilling and water storage in tree trunks using frequency domain reflectometry. J Exp Bot 2013;64:2321–32.

[440] Miyako E, Sugino T, Okazaki T, Bianco A, Yudasaka M, Iijima S. Self-assembled carbon nanotube honeycomb networks using a butterfly wing template as a multifunctional nanobiohybrid. ACS Nano 2013;7:8736–42.
[441] Scarpa F, Tomlinson G. Theoretical characteristics of the vibration of sandwich plates with in-plane negative Poisson's ratio values. J Sound Vib 2000;230:45–67.
[442] Evans KE. The design of doubly curved sandwich panels with honeycomb-cores. Compos Struct 1991;17:95–111.
[443] Fan T-X, Chow S-K, Zhang D. Biomorphic mineralization: from biology to materials. Prog Mater Sci 2009;54:542–659.
[444] Gauvin R, Chen YC, Lee JW, Soman P, Zorlutuna P, Nichol JW, et al. Microfabrication of complex porous tissue engineering scaffolds using 3D projection stereolithography. Biomaterials 2012;33:3824–34.
[445] Murphy SV, Atala A. 3D bioprinting of tissues and organs. Nat Biotechnol 2014;32:773–85.
[446] Xu F, Inci F, Mullick O, Gurkan UA, Sung Y, Kavaz D, et al. Release of magnetic nanoparticles from cell-encapsulating biodegradable nanobiomaterials. ACS Nano 2012;6:6640–9.
[447] Han YL, Yang Y, Liu S, Wu J, Chen Y, Lu TJ, et al. Directed self-assembly of microscale hydrogels by electrostatic interaction. Biofabrication 2013;5:035004.
[448] Huang G, Wang S, He X, Zhang X, Lu TJ, Xu F. Helical spring template fabrication of cell-laden microfluidic hydrogels for tissue engineering. Biotechnol Bioeng 2013;110:980–9.
[449] Abramovitch H, Burgard M, Edery-Azulay L, Evans KE, Hoffmeister M, Miller W, et al. Smart tetrachiral and hexachiral honeycomb: sensing and impact detection. Compos Sci Technol 2010;70:1072–9.
[450] Hum JEY, Hollands KGT, Wright JL. Analytical model for the thermal conductance of double-compound honeycomb transparent insulation, with validation. Sol Energy 2004;76:85–91.
[451] Wang X, Zhi L, Mullen K. Transparent, conductive graphene electrodes for dye-sensitized solar cells. Nano Lett 2008;8:323–7.
[452] Hu YH, Wang H, Hu B. Thinnest two-dimensional nanomaterial-graphene for solar energy. Chem Sus Chem. 2010;3:782–96.